UNIVERSITY OF HAWAII
LIBRARY
SEP 16 '53

The PHILOSOPHICAL MAGAZINE

FIRST PUBLISHED IN 1798

. 44 SEVENTH SERIES No. 355 August 1953

A Journal of Theoretical Experimental and Applied Physics

EDITOR
PROFESSOR N. F. MOTT, M.A., D.Sc., F.R.S.

EDITORIAL BOARD
SIR LAWRENCE BRAGG, O.B.E., M.C., M.A., D.Sc., F.R.S.
SIR GEORGE THOMSON, M.A., D.Sc., F.R.S.
PROFESSOR A. M. TYNDALL, C.B.E., D.Sc., F.R.S.

PRICE 15s. 0d.
Annual Subscription £8 0s. 0d. payable in advance

AND PUBLISHED BY TAYLOR & FRANCIS LTD., RED LION COURT, FLEET ST., LONDON, E.C.4.

Early Scientific Publications

ALERE FLAMMAM

DIARY OF ROBERT HOOKE, M.A., M.D., F.R.S.
1672-1680

25/-
net

Edited by **H. W. ROBINSON** and **W. ADAMS**
Recommended for publication by the Royal Society, London

"This vivid record of the scientific, artistic and social activities of a remarkable man during remarkable years has too long remained in obscurity."—Extract from foreword by Sir Frederick Gowland Hopkins, O.M., President of the Royal Society.

MATHEMATICAL WORK OF JOHN WALLIS, D.D., F.R.S.

12/6
net

By **J. F. SCOTT, Ph.D., B.A.**

"His work will be indispensable to those interested in the early history of The Royal Society. I commend to all students of the Seventeenth Century, whether scientific or humane, this learned and lucid book."—Extract from foreword by Prof. E. N. da C. Andrade, D.Sc., Ph.D., F.R.S.
Recommended for publication by University of London

CORRESPONDENCE AND PAPERS OF EDMOND HALLEY

21/-
net

Arranged and Edited by **EUGENE FAIRFIELD MACPIKE**

First published on behalf of The History of Science Society by Oxford University Press. Now re-issued by Taylor & Francis, Ltd.

MEMOIRS OF SIR ISAAC NEWTON'S LIFE

5/-
net

By **WILLIAM STUKELEY, M.D., F.R.S., 1752**
From an Original Manuscript
Now in the possession of the Royal Society, London

HEVELIUS, FLAMSTEED AND HALLEY

12/6
net

Three Contemporary Astronomers and their Mutual Relations
By **EUGENE FAIRFIELD MACPIKE**
Published by arrangement with The History of Science Society

Established over 150 years

TAYLOR & FRANCIS, LTD.
RED LION COURT, FLEET ST., LONDON E.C.
PRINTERS & PUBLISHERS OF SCIENTIFIC BOOKS

LXXXIV. *Cosmic Rays at* 60 m.w.e. *Underground : I. The Knock-on Electrons and Nuclear Interactions Produced by Relativistic μ-Mesons*

By M. L. T. KANNANGARA* and M. ZIVKOVIC†
The Physical Laboratories, The University, Manchester‡

[Received April 25, 1953]

ABSTRACT

A length of 126·6 m of minimum ionization track has been examined in Ilford G5 plates, coated, exposed, and processed at 60 m.w.e. underground, and a detailed study of knock-on electrons of energy greater than 50 MeV has been made. After making suitable corrections for scanning efficiency, it is found that the theoretical cross section, as derived by Bhabha, fits the data well for knock-on energies greater than 100 MeV. The mean free path for the production of these knock-on electrons is $(4{\cdot}5 \pm 1)$ m of emulsion corresponding to a cross section of $(20 \pm 4) \times 10^{-28}$ cm^2/electron. The theoretical cross section for the μ-meson spectrum at 60 m.w.e. is $18{\cdot}4 \times 10^{-28}$ cm^2/electron. A typical μ-meson star has been found. It is shown that the number of small stars with less than three dark tracks produced by μ-mesons is not very different from the number of larger stars with three or more dark tracks. No evidence for or against the existence of pairs of associated penetrating particles has been obtained.

§ 1. INTRODUCTION

SEVERAL groups of workers have recently reported observations which point to the possible existence of new forms of interaction of μ-mesons with matter. Perhaps the most striking is the preliminary report that Menon (private communication) has found two cases of slow μ-mesons, which subsequently decay, emerging from stars in a photographic emulsion (see also Perkins 1952, Rochester Conference). Shutt (1946), Sahiar (1951), Whittemore and Shutt (1952), and Leontic and Wolfendale (1953, private communication), have found anomalous large-angle scatterings among μ-mesons ; and Braddick and his co-workers (1951) have found several examples of pairs of associated penetrating particles. Both of the latter phenomena have so far only been observed with cloud chambers and in no case has the actual scattering or creation of a pair of associated penetrating particles been directly observed. For this reason it was thought of interest to look for such events in photographic emulsions which had been poured, exposed, and processed underground. Some Ilford G5 plates, of thicknesses 400 μ and 600 μ, which fulfilled these criteria, and which had been exposed for 120 days at 60 m.w.e. underground, were made available to us through the kindness of Dr. E. P. George. Further plates were exposed by us for the same period and at the same depth, under a lead shield of 10 cm in thickness, in order to reduce the background of slow electrons. The lead reduced the background by a factor of seven.

---

* On leave from the University of Ceylon.
† On leave from the University of Zagreb, Yugoslavia.
‡ Communicated by Dr. G. D. Rochester.

The examination of the plates involved the following of 126·6 m of track, at approximately minimum ionization, by two scanners working from December 1951 to November 1952. Of the full length, 92 m occurred on plates with no lead and 34·6 m on the plates surrounded by lead. The events observed included knock-on electrons, tridents, electron pairs, stars, and large-angle scatterings. In the present paper (I) knock-on electrons, stars, and pairs of associated penetrating particles are considered ; in paper II, electron pairs, tridents, and the equilibrium of the hard and soft components underground will be dealt with ; and in paper III an account will be given of the observations made on the anomalous scattering of μ-mesons.

§ 2. EXPERIMENTAL DETAILS

Beck microscopes with binocular eyepieces were used for scanning the plates. After preliminary tests of the efficiency of scanning under different magnifications, the plates were scanned with ×45 oil immersion objectives and ×10 eyepieces. Each microscope was provided with a stage having an X motion of 6 cm and a Y motion of 2·5 cm ; the plates were 5 cm square, so that each plate had to be scanned in two positions. In each of these positions, the edges of the plate which were vertical during the exposure were placed parallel to the X movement of the microscope, and the plate was scanned along seven traverses parallel to the Y movement of the stage. These traverses were 5 mm apart.

Only those tracks which were approximately at minimum ionization and which were not obviously multiply-scattered were followed. The scanned tracks were mapped on a sheet of graph paper in such a manner as to give a track the same orientation on the graph as seen through the microscope. The maps helped the scanners to exclude tracks already followed. The coordinates of every straight section of track were noted at three points, viz. the point on the traverse at which the track was first noticed, and the coordinates of each end. These three points were then plotted on the map. If they were collinear to within about 0·2 mm, the track was accepted. If not, the track was rejected as not being straight enough. A track thus rejected would almost certainly be an electron track of energy less than 70 MeV. A meson track which has the appearance of a minimum ionization track would usually be straight enough to be accepted. A typical track length distribution is given in fig. 1. The types of events recorded are shown in fig. 2.

The events were divided into two classes, designated ‘ single ’ and ‘ double ’ respectively. A ‘ single ’ event was one found in normal scanning along single tracks, while a 'double' event was one found because it happened to be in the field of view at the same time as the track being followed. In order to find out what weight should be given to a 'double' event in evaluating cross sections, it is important to know the probability that a particular track will be followed. The flatness of a track in the field of view determines whether it will be followed or not. This quantity is a function of its length. Let the probability of following a track of length L which cuts a single traverse be P_L. Then if the track cuts n traverses, the probability of its being followed will be

Fig. 1

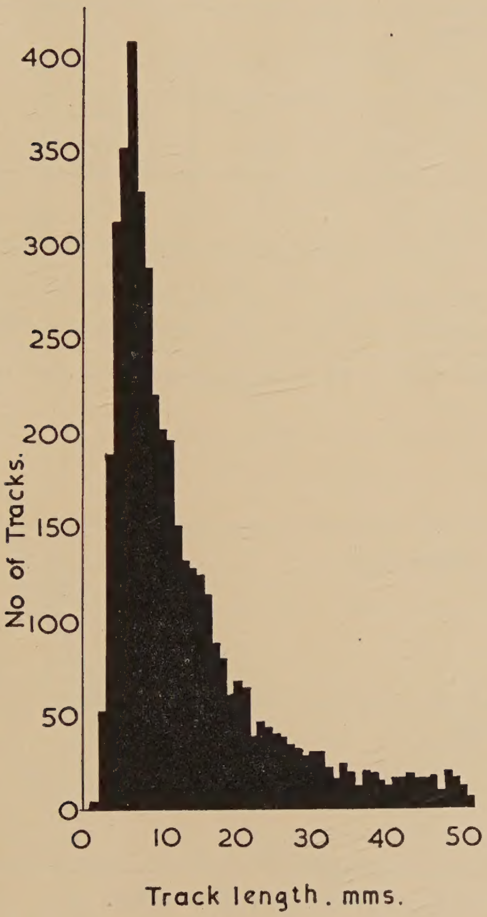

Track length distribution for 400 μ 'no-lead' plates.

$$\pi(L)=(1-Q_L{}^n),$$

where $Q_L=(1-P_L)$.

The depth of focus of the ×45 objective is about 2 μ, or 4·5 μ of an unprocessed emulsion. The diameter of a field of view is about 200 μ.

Thus a track of length L greater than 20 mm in either a 400 μ or 600 μ plate will be in focus over almost the entire diameter of a field of view. Hence, all these tracks will have sensibly the same flatness and thus the same value of P_L. As L falls below 20 mm, P_L will be expected to decrease. For tracks less than 5 mm long, the track length distributions (see fig. 1) show that P_L drops sharply to zero. P_L has been estimated in the manner described in Appendix I and is tabulated in table 1.

Fig. 2

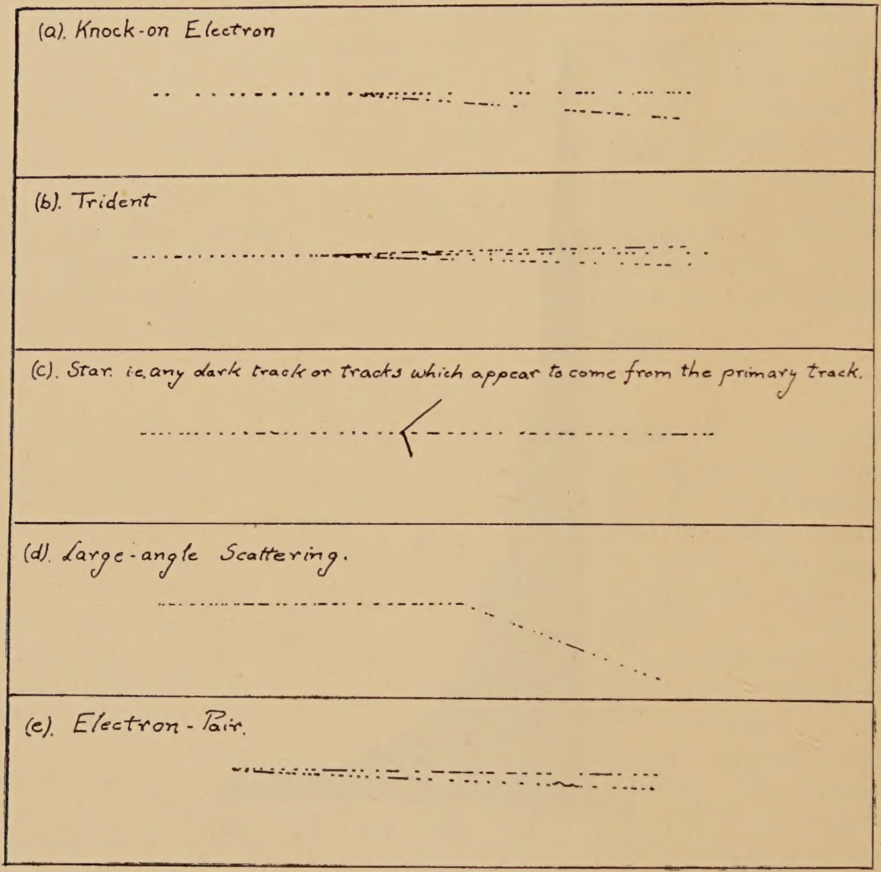
(a). Knock-on Electron
(b). Trident
(c). Star. i.e. any dark track or tracks which appear to come from the primary track.
(d). Large-angle Scattering.
(e). Electron-Pair.

Types of event recorded.

§ 3. KNOCK-ON ELECTRONS (EVENTS OF TYPE 2 (*a*))

3.1. *Dynamics of the Event*

Application of the conservation laws yields eqn. (1)—(Rossi and Greisen 1941) :

$$W=\frac{2\mu_e p^2\cos^2\alpha}{[\mu_e+(p^2+\mu^2)^{1/2}]^2-p^2\cos^2\alpha}, \qquad \ldots \quad (1)$$

where μ_e and μ are the masses of the electron and the primary particle in

MeV/c^2, W is the kinetic energy of the knock-on electron in MeV, p is the momentum of the primary in MeV/c and α is the angle of emission of the electron with respect to the primary.

Table 1

L mm	P_L	
	400 μ	600 μ
>20	0·44	0·44
15–20	0·42	0·40
10–15	0·39	0·33
5–10	0·37	0·32

In fig. 3, curves are plotted giving W as a function of α, for μ-meson primaries of different energies. For a given primary energy, W is a

Fig. 3

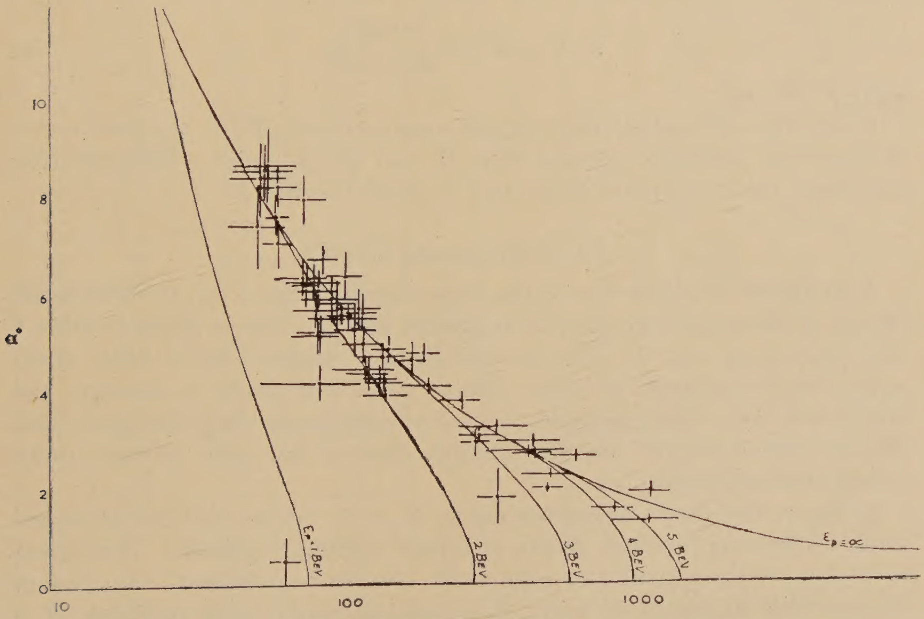

W MeV.

Angle of emission vs. energy of knock-on electron.

maximum when $\alpha=0$, i.e. for a ‘ head-on ’ collision. Thus, if E_p is the total energy of the primary, $W_{\max}$ is given by eqn. (2) :

$$W_{\max}=\frac{(E_p{}^2-\mu^2)2\mu_e}{(\mu_e{}^2+\mu^2)+2\mu_e E_p}. \qquad (2)$$

Thus if $\mu \gg \mu_e$, and $\mu_e \sim 0{\cdot}5$ MeV/c², we have

$$W_{\max}=\frac{E_p{}^2-\mu^2}{E_p+\mu^2}=\frac{p^2}{E_p+\mu^2}. \qquad \ldots\ldots \qquad (2\,a)$$

3.2. *The Cross Section for the Production of Knock-on Electrons by μ-mesons*

The differential cross section $\chi(E_p, W)\,dW$ cm² per electron for the production of a knock-on electron of kinetic energy W in the range dW by a primary singly charged particle with total energy E_p and spin $(\frac{1}{2})$ is given by (3)—(Bhabha 1938, Massey and Corben 1939) :

$$\chi(E_p, W)\,dW=\frac{\pi r_0{}^2}{1000\beta^2}\left[\left(1-\beta^2\frac{W}{W_{\max}}\right)+\frac{1}{2}\left(\frac{W}{E_p}\right)^2\right]\frac{dW}{W^2}, \quad . \quad (3)$$

where E_p and W are in Bev, β is the velocity of the primary in units of c, r_0 is the electron radius, and $W_{\max}$ in Bev is given by (2 *b*) for $\mu=0{\cdot}11$ Bev/c² :

$$W_{\max}=\frac{E_p{}^2}{(E_p+12{\cdot}1)}\ \text{Bev}. \qquad \ldots\ldots \qquad (2\,b)$$

According to George (1951) the normalized differential μ-meson spectrum at a depth of 60 m.w.e. is given by (4) :

$$N(E_p)\,dE_p=\frac{392\,dE_p}{(E_p+14)^3}, \qquad \ldots\ldots \qquad (4)$$

with E_p in Bev.

Using eqns. (3) and (4), the integral cross section $\phi(W)$ for the production of knock-on electrons greater than W can be obtained. This function has been computed graphically and is plotted in fig. 4.

3.3. *Experimental Results*

A complete list of events of the type shown in fig. 2 (*a*), for which the energy of the secondary electron is greater than 50 Mev, is given in table 2 and plotted in fig. 3. The events found ‘ double ’ have been given appropriate statistical weights. No attempt was made to measure the energies of the primary particles, because distortion in the plates prevented reliable estimation of energies greater than a few Bev, except under exceptional circumstances.

In fig. 3, the curve corresponding to $E_p=\infty$, is seen to form an upper limit to the experimental points in a most striking manner. The agreement between theory and experiment is seen to be excellent. In view of the possible existence of pairs of associated penetrating particles, it is important to enquire what would be indicated by a point not on one of the curves defined by eqn. (1). Such a point may be due to one of the following causes :

(*a*) An event which is not a knock-on electron.

(*b*) An error in the measurement of α. The chief sources of such an error are (i) the single and multiple scattering of the knock-on electron, and (ii) the uncertainty of depth measurements in the emulsion. These errors have been estimated and are shown in fig. 3.

Table 2

Event number.	Length of primary in mm.	Length of 'Knock-on' on which scatter measurements were made, in mm.	Distance of the origin of the event from the glass backing expressed as a fraction of the emulsion thickness.	Event-found 'single' or 'double'—S or D	No. of traverses cut by the primary of 'double' events.	Statistical weight of the event.	$p \frac{\text{MeV}}{c}$ of the Knock-on electron.	Angle of ejection in degrees.
1	7·8	2·3	0·39	D	1	0·3	1150±300	1·36±0·07
2	6·1	1·3	0·76	S	–	1	440±160	2·75±0·15
3	31·3	2·4	0·50	S	–	1	73±15	6·36±0·4
4	4·0	2·0	0·47	D	0	0	82±16	5·18±0·4
5	7·8	1·7	0·30	S	–	1	340±100	3·25±0·1
6	10·0	1·7	0·57	S	–	1	80±17	6·28±0·5
7	6·0	4·2	0·25	D	1	0·3	460±90	2·7 ±0·1
8	18·5	6·1	0·57	S	–	1	510±115	2·25±0·1
9	28·5	5·4	0·11	S	–	1	140±25	3·94±0·1
10	7·0	5·4	0·38	S	–	1	80±14	5·68±0·4
11	21·1	0·7	0·06	S	–	1	>1000	0·73±0·15
12	6·4	3·1	0·41	S	–	1	59±5	7·6 ±0·5
13	4·0	1·2	0·53	S	–	1	104±30	5·53±0·3
14	13·0	3·1	0·74	S	–	1	122±20	4·27±0·3
15	30·3	2·4	0·86	S	–	1	137±25	4·68±0·3
16	21·0	9·6	0·23	S	–	1	640±110	2·7 ±0·08
17	8·8	3·5	0·41	S	–	1	86±10	6·74±0·3
18	1·5	0·8	0·62	D	0	0	198±40	4·05±0·2
19	4·3	6·6	0·30	D	1	0·3	99±10	5·56±0·2
20	14·0	21·0	0·86	D	1	0·35	510±60	2·0 ±0·1
21	6·5	1·9	0·52	S	–	1	190±25	4·8 ±0·2
22	16·3	2·6	0·81	S	–	1	122±25	5·7 ±0·4
23	18·3	3·5	0·47	S	–	1	137±15	4·4 ±0·3
24	10·5	2·2	0·43	D	1	0·35	143±20	4·83±0·3
25	34·6	1·8	0·43	S	–	1	74±15	8·0 ±0·5
26	6·8	0·4	0·11	S	–	1	83±35	4·2 ±0·4
27	19·8	3·0	0·53	S	–	1	255±40	3·8 ±0·2
28	3·1	1·5	0·08	D	0	0	99±15	5·7 ±0·6
29	5·0	4·6	0·65	S	–	1	75±8	6·2 ±0·6
30	14·9	5·8	0·10	S	–	1	170±20	4·7 ±0·4
31	10·6	9·3	0·73	S	–	1	875±140	1·54±0·1
32	14·9	1·4	0·23	S	–	1	102±15	6·33±0·5
33	17·0	11·4	0·30	S	–	1	1160±170	1·9 ±0·16
34	24·8	6·6	0·48	S	–	1	118±20	5·0 ±0·4
35	6·0	5·3	0·25	D	1	0·3	116±15	5·76±0·4
36	6·5	0·2	0·02	S	–	1	too short	3·7 ±0·2
37	17·6	6·2	0·48	S	–	1	285±35	2·9 ±0·3
38	18·0	0·8	0·93	S	–	1	120±30	4·4 ±0·3
39	48·0	3·6	0·85	S		1	340±55	1·8 ±0·6
40	2·8	2·1	0·83	D	0	0	52±11	8·45±0·9
41	43·4	0·9	0·57	S	–	1	54±13	8·6 ±0·6
42	23·2	3·4	0·68	S	–	1	82±13	6·1 ±0·6
43	19·2	4·5	0·31	S	–	1	136±27	4·3 ±0·2
44	2·0	1·1	0·32	D	0	0	>500	2·3 ±0·5
45	13·6	4·5	0·66	S	–	1	60±9	8·3 ±0·4
46	48·0	2·0	0·91	S	–	1	455±120	2·85±0·2
47	6·4	2·2	0·32	S	–	1	92±20	5·9 ±0·6
48	10·5	1·1	0·26	S	–	1	82±16	5·2 ±0·7
49	11·5	3·3	0·37	S	–	1	295±47	3·1 ±0·25
50	17·5	2·0	0·38	S	–	1	59±7	7·1 ±0·6
51	20·5	3·0	0·70	D	4	0·9	114±20	5·3 ±0·6
52	34·4	5·0	0·78	S	–	1	63±8	0·5 ±0·4
53	4·1	1·1	0·33	D	1	0·2	55±15	8·65±0·8
54	27·2	0·6	0·18	S	–	1	52±12	7·5 ±1

(*c*) The scattering of the knock-on electron by its parent nucleus. It can be shown that less than 1 in 500 knock-on electrons with energy greater than 50 MeV will be scattered by more than 1° by this process.

(*d*) A false value of the energy of the knock-on electron because of loss by radiation. Such losses usually occur in sudden large jumps, and if the electron were to lose energy suddenly within 500 μ of its origin, the loss would usually not be detected. If the loss took place beyond 500 μ from the origin, there is a chance of detection from the scattering measurements. Rossi and Greisen (1941) have shown that the rate of loss of energy per radiation length through radiation from an electron of energy about 250 MeV is approximately $0{\cdot}8\,W$, where W is the energy of the electron. There are 50 events recorded in table 2 with an average energy W of approximately 250 MeV. Hence, taking the radiation length in G5 emulsion to be 2·9 cm, the total energy loss by all these knock-on electrons during the first 500 μ of their path would be approximately $(50\times 0{\cdot}8\times 250\times 500/29\,000)\simeq 170$ MeV. This loss would not be shared by all the knock-on electrons, but would occur in only a few of the tracks. Thus due to this cause three or four points would be expected to be displaced towards the left of their true curves in fig. 3.

These considerations seem to indicate that all the events listed in table 2 are consistent with the assumption that they are knock-on electrons.

3.4. *The Cross Section for the Production of Knock-on Electrons by μ-mesons (Experimental)*

The energy distribution of the knock-on electrons is plotted as a histogram in fig. 5. The distribution expected from the cross sections given in fig. 4 is also given in fig. 5. The experimental distribution agrees with the theoretical distribution for $W > 100$ MeV. In the region $50 < W < 100$, the expected number of events is significantly greater than the observed number, indicating that the efficiency of finding low energy events is not high. This is probably connected with the fact that these electrons are difficult to distinguish from the background obtained during the 120-day exposure. A high-energy, knock-on electron is ejected at a very small angle to the primary, and in consequence both the primary and the knock-on electron travel together for a relatively large distance. Such an event is therefore very unlikely to be missed. It is also reasonable to expect a bias towards high energy events. The system of classifying the events as ‘ single ’ and ‘ double ’ tends to minimize this bias. As the energy of the knock-on electron is reduced its angle of ejection and its scattering increases. It is possible that a relatively low energy knock-on event will be missed if it is formed near the surface, on the glass backing of the emulsion and ejected or scattered so as to move steeply out of the emulsion. It is important to ascertain at what energy the probability of missing a knock-on electron becomes appreciable.

If there are no losses, the points of origin of the knock-on electrons should be distributed uniformly over the depth of the emulsion. To test this point, the emulsion thickness has been divided into five equal layers, and the numbers of knock-on electrons having their origins in each of these layers plotted for various energy ranges. (The appropriate weighting factors were given to the events found ‘double’.) It was found that the points were more or less uniformly distributed over the five layers for knock-on electrons >100 Mev, whereas for the energy range $50<W<100$ the top and the bottom layers were almost empty (see fig. 6).

Fig. 4

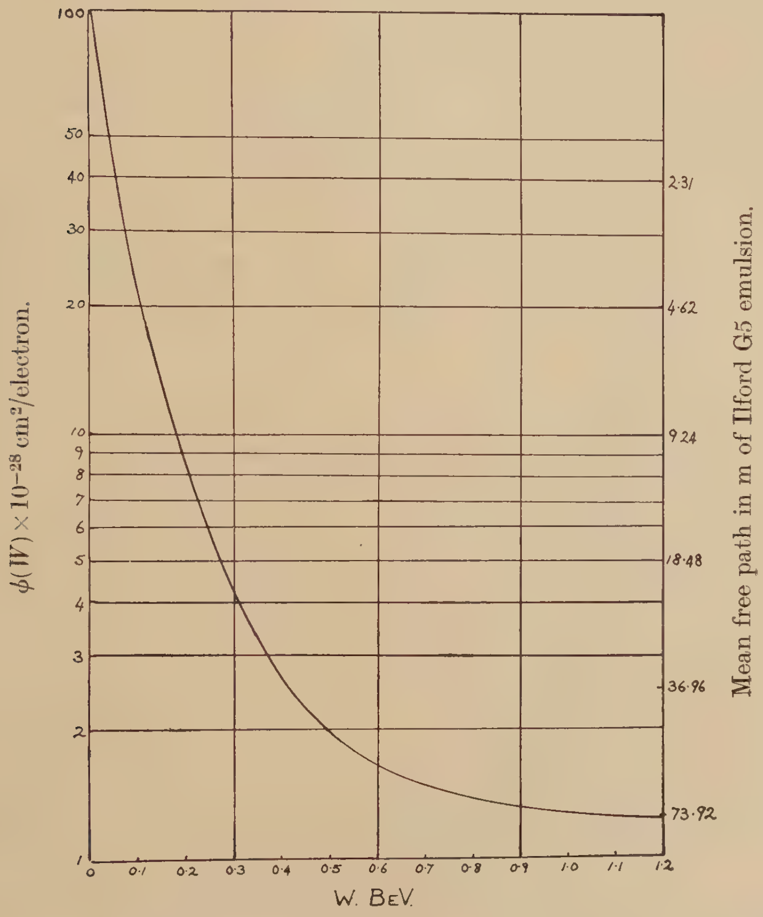

Theoretical integral cross section for the production of knock-on electrons.

The reliability of the scanning has also been tested by having two plates rescanned with the scanners interchanged. In the common tracks followed by both scanners, there are four recorded knock-on electrons of energy greater than 50 Mev. These events have been found by both scanners.

Thus it seems reasonable to assume that the losses for knock-on electrons greater than 100 MeV are negligible. For this reason, the cross section has been evaluated for these events. The results are given in table 3, where the errors quoted are purely statistical.

Fig. 5

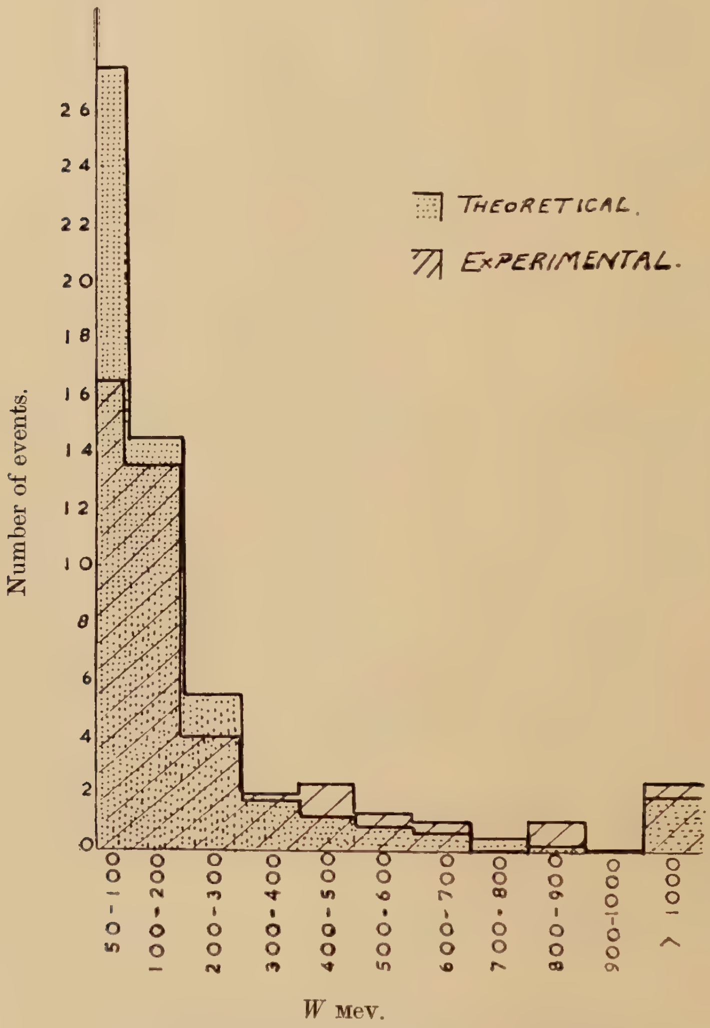

Energy distribution of knock-on electrons.

The agreement with theory is seen to be very satisfactory. Recently, Walker (private communication), using a cloud chamber operated in a magnetic field, measured the energy spectrum of knock-on electrons from a carbon plate by high energy μ-mesons, over a wide range of energies, and found good agreement with Bhabha's cross section for knock-on energies of a few MeV, up to energies of the order of a BeV.

§4. NUCLEAR DISINTEGRATIONS

One star of the type 6+1p (according to the notation used by Brown *et al.* 1949) was found in the 126·6 m of track examined. The parts of the track of the primary before and after the star are both about 12 mm long and have a value of $p\beta$ greater than 10 BeV/c. The angle between them is 0·16°±0·1°. The star is a typical 1p, μ-meson star of the type found by George and Evans (1951), who gave a cross section of 5×10^{-30} cm²/nucleon for (1, 2, . . . n)p stars with three or more dark tracks. The latest results of George (private communication), indicate that the cross section is probably about 10^{-29} cm²/nucleon, corresponding to a mean free path of about 400 m of emulsion. Thus our results are not inconsistent with those of George and Evans.

Table 3

Track length (m)	Total statistical weight of events with $W>100$ MeV	Mean free path in Ilford G5 emulsion (m)	Experimental cross section in cm²/electron	Theoretical cross section in cm²/electron
126·6	27·5	4·5±1	$(20\pm4)\times10^{-28}$	$18{\cdot}4\times10^{-28}$

Fig. 6

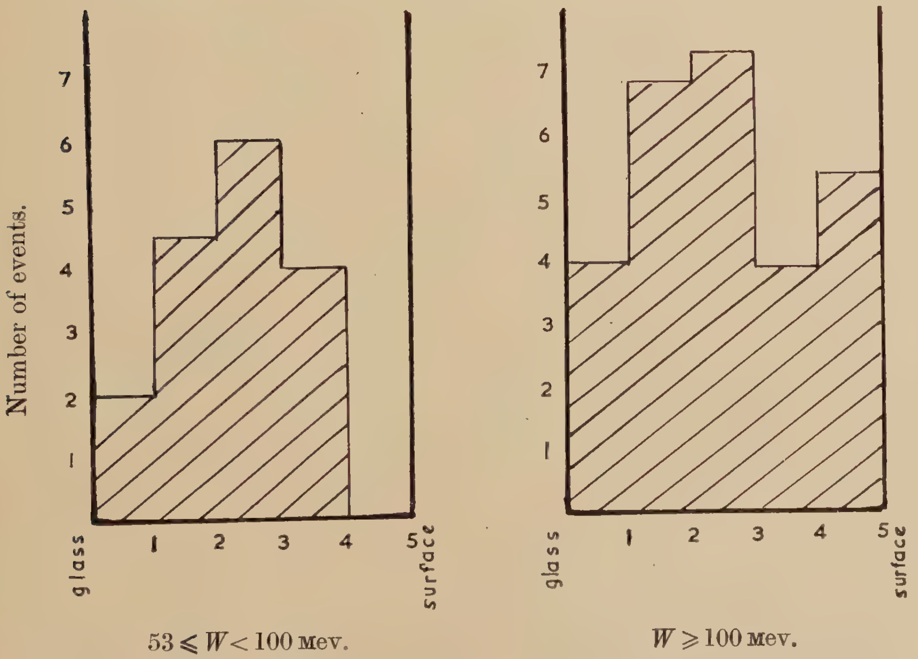

The distribution of the points of origin of the knock-on electrons through the depth of the emulsion.

In the present experiment any star with one or more dark tracks would have been detected. We therefore conclude that the number of stars with less than three dark tracks is not very much larger than the number of larger stars with three or more dark tracks.

§ 5. PAIRS OF ASSOCIATED PENETRATING PARTICLES

Braddick *et al.* (1951) gave a cross section of 5×10^{-29} cm²/nucleon for the production of pairs of associated penetrating particles. This corresponds to a mean free path of 83 m of Ilford G5 emulsion. It was estimated that the secondary particle usually had an energy greater than 1 BEV, and the pair-angle was greater than 2° for at least two-thirds of the events and greater than 6° for about one-quarter. The results reported in the present paper refer to a track length of 126·6 m. It is important to consider what was the effective path length scanned for the detection of the creation of a pair of associated penetrating particles. If the event is associated with one or more dark tracks, then the effective length scanned is the actual length followed (i.e. 126·6 m) because the probability of missing a dark track in these plates, which contain almost entirely light tracks, is very small. On the other hand, if there are no associated dark tracks, the event will have the appearance of a knock-on electron. It was hoped to distinguish these events from knock-on electrons by means of fig. 3, since a point well above the curve marked $E_p=\infty$, could not be a knock-on electron. Using the data given by Braddick *et al.*, and assuming that the secondary particle has an energy of the order of 1 BEV, it is seen from fig. 3 that the event will be identified if the angle of emission is greater than 2°—which, according to Braddick *et al.* is true for at least two-thirds of the events. In the analysis of knock-on electrons, however, it was shown that when the angle of ejection exceeds 6°, the efficiency of finding the event drops to about two-thirds. Thus the total efficiency of finding a pair of associated penetrating particles having no dark tracks associated with it is only $[1-\frac{1}{3}-(\frac{1}{3})(\frac{1}{4})]\simeq0{\cdot}6$. This makes the effective path length scanned only 76 m. We are therefore not in a position to infer much from the absence of an event attributable to a pair of associated penetrating particles after scanning 126·6 m. It will certainly be necessary to scan a length considerably greater than 126 m in order to make certain of detecting such an event.

Moreover, if the cross section given by Braddick *et al.* is too high, e.g. by a factor of two or more, as is suggested by recent experiments of Amaldi *et al.* (1952), Lovati (private communication), and Walker (private communication), the problem becomes even more formidable.

ACKNOWLEDGMENTS

We wish to express our thanks to Dr. G. D. Rochester for suggesting the experiment and for valuable discussion and advice. We also wish to thank Mrs. J. Cunliffe and Mrs. E. Birchall, who scanned the plates, for devoting themselves diligently to a painstaking task.

APPENDIX I

ESTIMATION OF THE PROBABILITY OF FOLLOWING A TRACK OF LENGTH L (SEE § 2)

An estimate of P_L was made by asking the scanners to put a cross on the graph every time they saw a particular track and thought of following it. The following example will illustrate the procedure. A track was found on the traverse $X=25$ mm at the point ($Y=13{\cdot}5$, $X=25{\cdot}0$). It was followed from end to end, and its end coordinates were ($Y=7{\cdot}7$, $X=50{\cdot}7$) and ($Y=18{\cdot}5$, $X=2{\cdot}5$) respectively. This track was also seen on traverses $X=30$, 15 and 10. Thus four crosses were marked on the track. It will be observed that this track crossed all seven traverses but was observed on only four of them. Every track followed in two plates was analysed in this manner.

The tracks were divided into four groups: (1) $L\geqslant 20$; (2) $15\leqslant L<20$; (2) $10\leqslant L<15$; (4) $5\leqslant L<10$ mm. Since P_L is primarily a function of the flatness of the track, it was necessary to include in the above analysis only those tracks which have a true length L—i.e. tracks which went out at the surface and the glass respectively. The tracks which went out at the edge of a plate at either end were excluded from groups 2, 3 and 4. Let P_{L1}, P_{L2}, P_{L3} and P_{L4} be the values of P_L applicable to each of the four groups defined above. The way in which these probabilities were calculated is illustrated in the example given below.

The total number of traverses cut by the recorded tracks with $L\geqslant 20$ mm was 236. The number of crosses marked on the graph for these tracks was 110. Assume that very few tracks of this length would be missed altogether. Thus a first estimate of P_{L1} (P_{L1}^* say) is obtained immediately by putting $P_{L1}^*=110/236=0{\cdot}47$. P_{L1}^* is now used to calculate a more accurate value of P_{L1} in the following way. Let the number of tracks each of which cuts x traverses be n. Then table 4 gives a complete analysis of the tracks in this group.

Table 4

x	n	Probability of completely missing track cutting x traverses, i.e. $(1-P_{L1}^*)^x$	Probable number of tracks cutting x traverses missed	Contribution to Number of traverses cut
1	0	0·53	—	—
2	0	0·29	—	—
3	14	0·15	2·54	7·6
4	14	0·082	1·25	5·0
5	7	0·044	0·32	1·6
6	7	0·024	0·17	1·0
7	8	0·0125	0·1	0·7
			Total	15·9

In this table an estimate has been made of the number of tracks missed altogether and the total number of traverses (15·9) which those tracks would have cut. P_{L1} is then obtained by putting

$$P_{L1}=110/(236+15\cdot9)=0\cdot44.$$

To compute P_{L2}, P_{L1} is taken as a first estimate of P_{L2} and the analysis is made exactly as before. Similarly for P_{L3} and P_{L4}.

REFERENCES

AMALDI, E., CASTAGNOLI, C., GIGLI, A., and SCIUTI, S., 1952, *Nuovo Cim.*, **9,** 969.
BHABHA, H. J., 1938, *Proc. Roy. Soc.* A, **164,** 257.
BRADDICK, H. J. J., NASH, W., and WOLFENDALE, A., 1951, *Phil. Mag.*, **42,** 1277.
BROWN, R. H., CAMERINI, U., FOWLER, P., HEITLER, H., KING, D., and POWELL, C. F., 1949, *Phil. Mag.*, **40,** 862.
GEORGE, E. P., and EVANS, J., 1951, *Proc. Phys. Soc.* A, **64,** 243.
MASSEY, H. S. W., and CORBEN, H. C., 1939, *Proc. Camb. Phil. Soc.*, **35,** 84.
ROSSI, B., and GREISEN, K., 1941, *Rev. Mod. Phys.*, **13,** 240.
SAHIAR, A. B., 1951, *Proc. Indian Acad. Sci., Bangalore*, **34,** No. 3, A, 201.
SHUTT, R. P., 1946, *Phys. Rev.*, **69,** 261.
WHITTEMORE, W. L., and SHUTT, R. P., 1952, *Phys. Rev.*, **88,** 1312.

LXXXV. *Cosmic Rays at* 60 m.w.e. *Underground* *II : The Hard and Soft Components*

By S. J. GOLDSACK and M. L. T. KANNANGARA*
The Physical Laboratories, The University, Manchester†

[Received April 25, 1953]

ABSTRACT

The tracks of the relativistic charged particles, which have been found and examined by the methods described in I, are used to estimate the total vertical intensity and the electron component at 60 m.w.e. The total vertical intensity is found to be $(6{\cdot}8 \pm 1)10^{-4}$ particles/cm^2/sec/steradian. About 0·5% of the relativistic charged particles with momenta greater than 100 MeV/c are electrons. The possible sources of these electrons are examined and it is found that they consist almost entirely of knock-on electrons and their cascade progeny. Both the absolute rate and the spectrum of the electron pairs which are found on the plates indicate an electron component whose magnitude is rather greater than can be accounted for by known sources.

A detailed analysis is also made of 20 tridents and it is shown that they consist of 9 electron and 11 μ-meson tridents. The μ-meson tridents are classified further into the various cases covered by Bhabha's theory. It is again found that rather more electron tridents occur than are expected. The discrepancy may be due to a fluctuation.

§ 1. INTRODUCTION

IN this paper, the tracks of the relativistic particles at 60 m.w.e., which have been found and examined by the method described in I (Kannangara and Zivkovic 1953), are used to calculate the total vertical intensity, and to analyse the soft component. As already shown by many other workers (cf. George 1951), the relativistic particles at this depth consist almost entirely of μ-mesons and electrons. Most of these electrons are the knock-on electrons described in I and their cascade progeny. Electron pairs and electron and meson tridents have also been found and examined in detail.

---

* On leave from the University of Ceylon.

† Communicated by Dr. G. D. Rochester.

§ 2. THE VERTICAL INTENSITY

2.1. *The Total Intensity (Hard and Soft Components)*

The data required for the calculation of the vertical intensity are given in table 1.

The plates were 5 cm square, and were scanned in two independent halves: thus the tracks used were effectively those on a plate $5 \times 2{\cdot}5$ cm^2. Let fig. 1 represent the emulsion of a plate. The tracks considered are those which pass through both rectangles ABCD and A′B′C′D′, entering an area $2{\cdot}5d$ cm^2 into a solid angle which is approximately $2{\cdot}5d/5^2$ steradian. Thus, if I is the vertical intensity, the number of tracks formed per ‘half’ plate per second should be $(2{\cdot}5)^2d^2I/5^2$. The total number of tracks on all plates during an exposure of t seconds is $(2{\cdot}5)^2It\Sigma d^2/5^2$. Setting $\Sigma d^2 = 10{\cdot}18 \times 10^{-2}$ cm^2 (cf. table 1) and $t = 120$ days, we find

Table 1

Plates	No. of ‘half’ plates	No. of tracks	Average per ‘half’ plate
600 micron	16	38	2·33
400 micron	27	45	1·65

Fig. 1

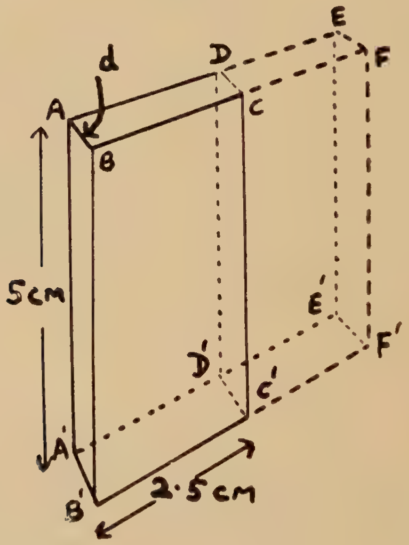

Three dimensional drawing of the emulsion of a plate.

$$I \simeq 3 \times 10^{-4} \text{ particles/cm}^2\text{/sec/steradian.}$$

This value must be too small, since all tracks are lost which are scattered in a distance of 5 cm by an amount greater than the emulsion thickness. The effect of scattering is to lead to a low energy cut-off at about 1 BeV. According to George (1951), about 20% of the mesons at 60 m.w.e. should have energies less than this value. An alternative treatment which uses tracks of a wide range of track-length is given in the Appendix I, leading to a value for the total vertical intensity of

$$(6{\cdot}8 \pm 1) \times 10^{-4} \text{ particles/cm}^2\text{/sec/steradian.}$$

This result is in good agreement with the value of about

$$6 \times 10^{-4} \text{ particles/cm}^2\text{/sec/steradian,}$$

deduced by George (1951) from the experiments of Follet and Crawshaw (1936), Ehmert (1937) and Greisen (1942).

2.2. *The Soft Component*

The soft component underground is secondary to the μ-meson beam, and must therefore be in equilibrium with it. The electron-photon component may arise in one or more of the following processes :

(1) Knock-on electrons and their cascades.
(2) Tridents and their cascades.
(3) Bremsstrahlung of μ-mesons and the subsequent cascades.
(4) Decay of μ-mesons and the subsequent cascades.
(5) Nuclear interaction of the μ-meson with formation of neutral π-mesons leading to photons by decay.

It is easily shown (cf. George 1951) that the first source is the only one of any importance.

Let the cascade length in the material above the plates be λ cm, and let the number of electrons in λ cm³ of the material be n_λ. Let an electron of energy W_0 produce on the average at a depth x cascade units $\pi(W_0, W, x)dW$ electrons with energy W in the range dW. Then, using the differential cross section given by Bhabha for the production of knock-on electrons (I, eqn. (3)), the average number of electrons with energy W in the range dW accompanying a μ-meson of total energy E_p is given by

$$N(W, E_p)\, dW = n_\lambda\, dW \int_{x=0}^{\infty} \int_{W}^{W_{\max}} \chi(E_p, W_0)\pi(W_0, W, x)\, dW_0\, dx. \quad . \quad (1)$$

Rossi and Greisen (1941), using their approximation A, showed that the differential track length

$$dW \int_0^\infty \pi(W_0, W, x)\, dx$$

is given by

$$dW \int_0^\infty \pi(W_0, W, x)\, dx = 0{\cdot}4347(W_0/W^2)\, dW. \quad . \quad . \quad . \quad (2)$$

By substituting (2) in (1) and integrating, we obtain, with energies expressed in BeV,

$$N(W, E_p)\, dW = (0{\cdot}4347 n_\lambda \pi r_0^2/1000)(dW/W^2)\{\log(W_{\max}/W)$$
$$-[(W_{\max} - W)/W_{\max}] + (1/4)(W_{\max} - W^2)/E_p^2\},$$

where $W_{\max}$ is the maximum transferable energy, and is given by eqn. (2 *b*) of I.

Using the differential energy spectrum for μ-mesons given by George (cf. I, eqn. (4)), the total number of electrons of energy W in the range dW per meson at 60 m.w.e. is then given by

$$S(W)\,dW=(0{\cdot}4347 n_{\lambda}\pi r_0^{\,2}\,392/1000)(dW/W^2)I, \quad . \quad . \quad . \quad (3)$$

where I is the integral

$$I=\int_{(1/2)[W+\sqrt{(W^2+48{\cdot}4W)}]}^{\infty}\left\{\frac{\log_e[E_p^{\,2}/W(E_p+12{\cdot}1)]-[E_p^{\,2}-W(E_p+12{\cdot}1)]}{E_p^{\,2}}\right.$$
$$\left.+\frac{[E_p^{\,2}/(E_p+12{\cdot}1)^2]-W}{4}\right\}\frac{dE_p}{E_p^{\,2}(E_p+14)^3}.$$

The lower limit is that value of E_p which makes $W_{\max}=W$.

Fig. 2

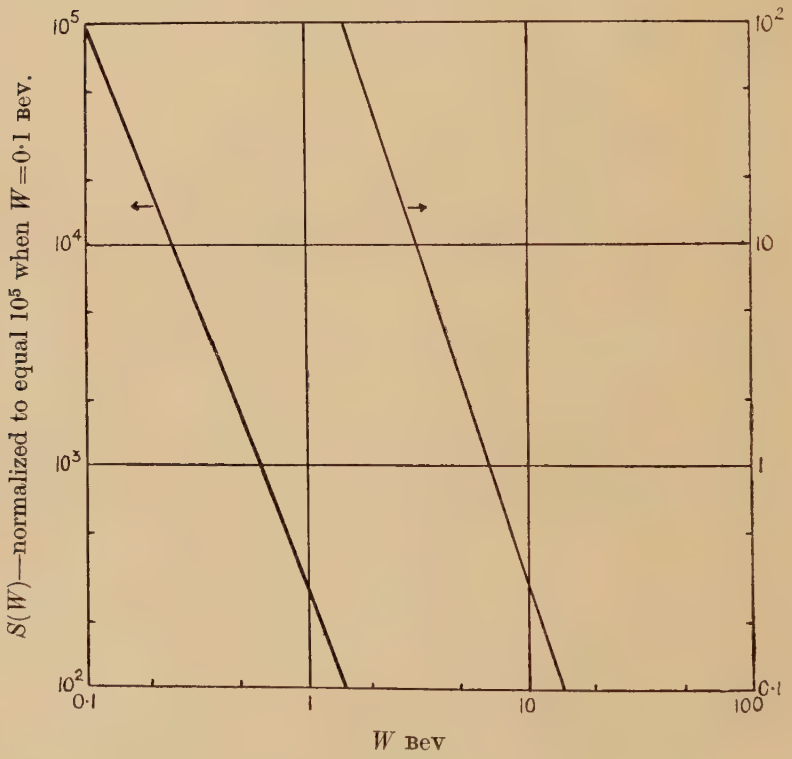

Differential energy spectrum of electrons at 60 m.w.e.

$S(W)$ is given as a function of W in fig. 2. In the energy region $W<1$ Bev, it can be represented approximately by $S(W)dW=K\,dW/W^{2{\cdot}5}$, while in the region $1<W$ Bev<20, it becomes approximately

$$S(W)\,dW=K^1\,dW/W^{3{\cdot}3}.$$

After substituting the values of n_λ for rock and lead, and integrating graphically, the values of the total flux of electrons of energy greater than 70 Mev and greater than 100 Mev per primary meson are obtained as

$$\int_{0\cdot07}^{\infty} S(W)\,dW=0\cdot009 \qquad \text{and} \qquad \int_{0\cdot1}^{\infty} S(W)\,dW=0\cdot006,$$

for plates without lead, and

$$\int_{0\cdot07}^{\infty} S(W)\,dW=0\cdot004 \qquad \text{and} \qquad \int_{0\cdot1}^{\infty} S(W)\,dW=0\cdot0025,$$

for plates surrounded by lead. It follows that out of the total of 126·6 m of relativistic track examined, nearly 1 m should be due to fast electrons, with about 70 cm of track from electrons greater than 100 Mev (cf. I, § 2).

According to the cascade theory, photons have the same spectrum as the electrons, but are more numerous in the ratio 9/7.

§ 3. Electron Pairs

3.1. *Experimental Results*

Forty of the tracks followed proved to be arms of electron pairs. In addition, thirty electron pairs were found ' double ', i.e. they were recorded because they were visible as a pair of associated tracks in the field of view, not because they were found in the course of following a track. These pairs have been taken into account in estimating the relative intensity of the soft component by allotting to each a ' weight ', i.e. a probability that it would have been found ' single ' if only one of the tracks had been visible at a time. The method of assessing this probability follows exactly the method described in I for knock-on electrons.

Fig. 3

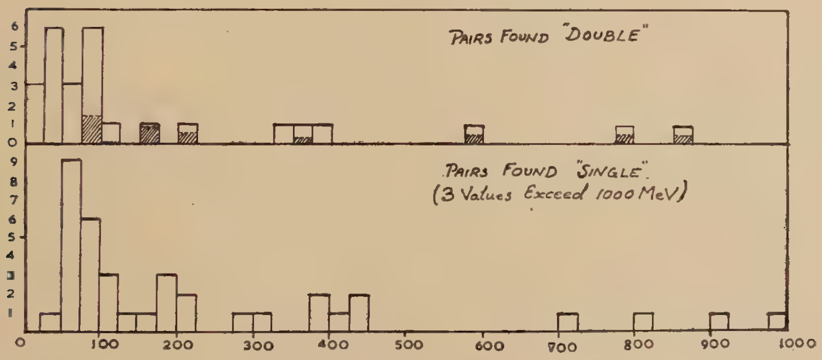

Energy Mev

Energy distributions of electron pairs.

The energy of the photon which gave rise to each pair has been measured by the scattering method, and the distributions are given in fig. 3 for the two types of pair. The shaded portions of the histogram for the ‘ double ’ pairs indicate the statistical weights attached to them.

The spectra of the ‘ single ’ and ‘ double ’ pairs may be expected to differ from the true spectrum of the photons for the following reasons. A pair is most easily found ‘ double ’ if the energy is high, since the tracks are then more nearly parallel : thus, there is a steadily increasing loss of ‘ double ’ pairs as the energy decreases. A sharper low energy cut-off operates on the ‘ single ’ pair spectrum, since scattered tracks are not followed. However, if the photon energy is greater than 100 MeV, at least one of the tracks is usually of sufficient energy to be followed (see I, § 2), while both tracks are usually sufficiently straight if the energy exceeds 200 MeV. For these reasons only photons of energy greater than 100 MeV have been considered. Of all the pairs recorded 24 were ‘ single ’ and

Fig. 4

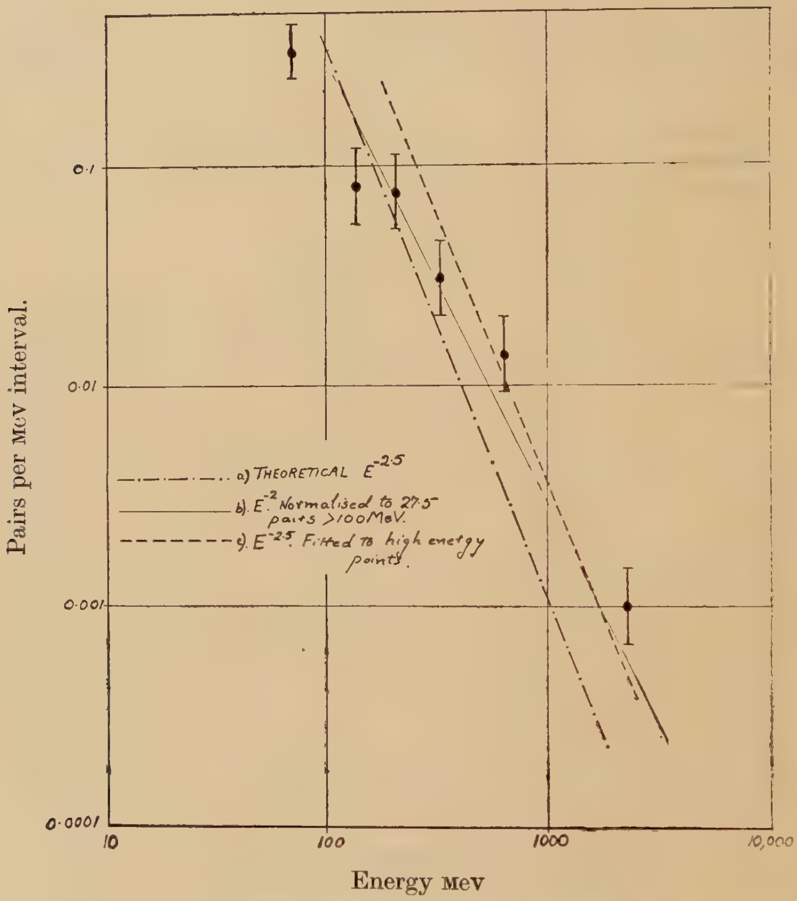

Energy spectrum of electron pairs.

8 ' double ', but to the 8 double events a statistical weight of 3·7 was allotted, giving an effective total of 27·7 single pairs. In this total, 23·3 pairs came from the plates with no lead shield, while 4·4 occurred on the plates surrounded by 10 cm of lead. The energy spectrum is given in fig. 4.

The angular distribution of the single tracks is strongly affected by the scanner's tendency to follow tracks parallel to the X movement of the microscope stage, which was arranged to be the same as the vertical for the tracks recorded in the plates (cf. I, § 2). The angular distribution of the pairs is likewise affected. The distribution for pairs and single tracks is given in fig. 5, and it is clear that there is no significant difference. Single tracks are rather strongly grouped around the vertical, and the empirical distribution fits closely to a $\cos^6 \theta$ distribution.

Fig. 5

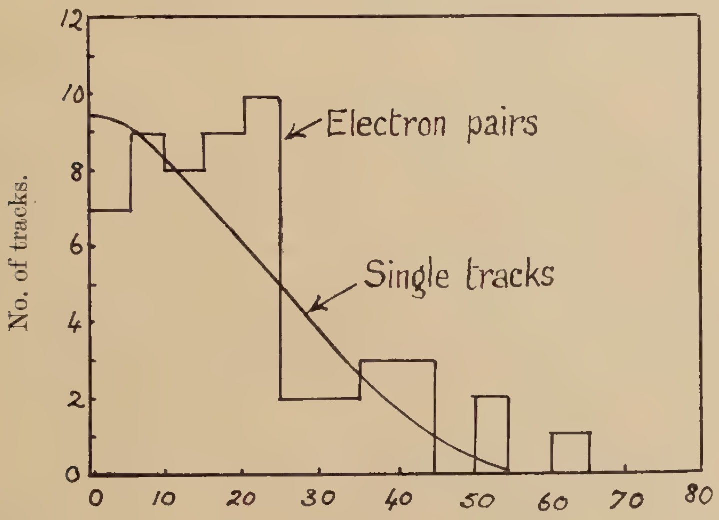

Inclination to vertical in degrees.
Angular distribution of the electron pairs.

3.2. *The Expected Number of Electron Pairs*

The expected number of electron pairs can be calculated in the following way.

Consider N_L μ-mesons which cross the emulsion with track length L. Suppose that in equilibrium f photons accompany each μ-meson. Then there are in all $N_L f$ photons at each depth with ' potential path length ' or ' gate length ' L in the emulsion : i.e. if one of the photons materializes, it will form a pair whose tracks have such an inclination to the surface that they would have length L if they crossed the emulsion from surface to glass. Suppose the actual length of each track of the pair is x. (The finite angle of emission of the pair tracks can be neglected for energies greater than 100 MeV.)

The number of pairs with tracks of length x in the range dx, and having a gate length L is $N_L f\, dx/\lambda^1$, where λ^1 is the pair-production length. From the scanning procedure described in I, § 2, it will be seen that the average number of traverses cut by a track of length L mm is L/γ where $\gamma=5$ if all the tracks were vertical, but $\gamma=5\cdot9$ for a $\cos^2\theta$ distribution. The angular distribution of the tracks followed by the scanners was found to be $\cos^6\theta$. The results of the following calculation are not at all sensitive to the exact value, and a value of $\gamma=5\cdot5$ has been adopted for convenience. It follows that the total probability of a track of length L being followed is $\pi(L)=(1-Q_L^{L/5\cdot5})$, where Q_L is defined in I, § 2. The corresponding probability of any one arm of the electron pair being followed is $(1-Q_L^{x/5\cdot5})$, and the chance of the pair being found on either arm is $(1-Q_L^{2x/5\cdot5})$. The number of pairs m_L found with gate length L is therefore

$$m_L=N_L f\int_0^L(1-Q_L^{2x/5\cdot5})\,dx/\lambda'=N_L f\{(1/\lambda')-(5\cdot5/2\lambda'\log_e Q_L)(Q_L^{2L/5\cdot5}-1)\}.$$

However, for a total number, N_L, of mesons crossing the emulsion with track length L, only $N_L{}^1=N_L\pi(L)$ tracks are followed. Thus the number of pairs found with gate length L is given by $m_L=N_L{}^1R_L f$, where

$$R_L=[L/\lambda^1\pi(L)][1-(5\cdot5/2L\log_e Q_L)(Q_L^{2L/5\cdot5}-1)].$$

We have so far assumed that a pair can be found on either arm. This leads to an overestimate in the case of low energy pairs where one arm is frequently too scattered to be followed. As a lower limit we can suppose that only one track is sufficiently straight to be followed. In this case the formula for m_L is $m_L=N_L{}^1R_L{}^1f$, where

$$R_L{}^1=(L/\lambda^1)\{[1/\pi(L)]+(5\cdot5/L\log_e Q_L)\}.$$

R_L and $R_L{}^1$ are plotted against L in fig. 6 with $\lambda^1=3\cdot5$ cm. These two assumptions lead to the extreme values. Thus if N^1 is the total number of tracks of all lengths followed, the expected number of pairs should lie between N^1fR and N^1fR^1 where R and R^1 are the mean values of R_L and $R_L{}^1$ taken over all the tracks followed. Using the track length distributions given in fig. 1 of I, we arrive at the mean values $R=0\cdot36$, and $R^1=0\cdot28$. With these values and the photon intensities given in the last section we obtain the results given in table 2.

In table 2, appropriate statistical weights have been given to ' double ' pairs. There seems to be reasonable agreement with the theory. The spectral distribution which is shown in fig. 4 is however less satisfactory since there are too many high energy pairs. Thus for pairs greater than 200 MeV, 8·5 are expected as against an observed number of 18·5. The slope of the spectrum may be brought into agreement with the theoretical value by assuming that the low energy pairs suffer losses from the effects discussed in § 3.1, but then the total number has to be increased, and the apparent agreement in table 2 is lost. However, it is well known that cascade phenomena are subject to violent fluctuations. Thus, if a single high energy electron has been ejected in the vicinity of the stack of plates it could easily have produced a large number of pairs in the plates. It is interesting to notice that such a shower would make a large contribution to the number of pairs, and that the energy spectrum of these pairs would be $E^{-2}dE$, compared with the average $E^{-2\cdot5}dE$, thus making the effective spectrum of all the pairs harder.

Fig. 6

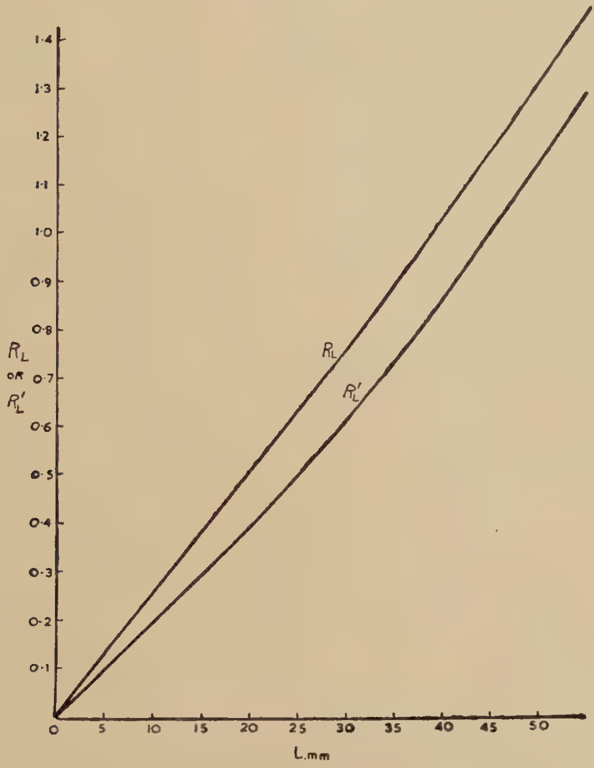

Probability of finding electron pairs as a function of the ‘ gate length ’ *L*.

Table 2

Absorber above plates	Track length followed m	Expected No. of pairs with energy >100 Mev	No. of pairs with energy >100 Mev found experimentally
None	92·0	13–18	23·3
10 cm lead	34·6	3–5	4·4

§ 4. TRIDENTS

4.1. *General*

During a collision with a nucleus a fast charged particle can create an electron pair through the interaction of the electromagnetic field of the two particles with an electron in a negative energy state. Such an electron is raised to an intermediate virtual state by interaction with one of the particles and then goes into the final state by interaction with the other. The event which is produced appears to consist of a charged relativistic primary particle, and three relativistic secondaries, the primary and the pair of electrons.

Such events have been previously described by Occhialini (1949), Powell (1949), and Hooper *et al.* (1951, 1952). In the present experiment 35 such events were found, of which 13 were found ‘ single ’ and 22 ‘ double ’. To the 22 ‘ double ’ events a total statistical weight of 3·3 has been allotted. Two of the ‘ double ’ tridents were formed on arms of electron pairs, and are therefore certainly produced by electrons : one ‘ single ’ event (No. 8 of table 3) was formed on the arm of a knock-on electron. Apart from these three cases there is no direct evidence as to the nature of the primary particles. However, it will be shown in what follows that at least a considerable proportion of the rest of the examples must have formed by meson primaries.

4.2. *Experimental Results*

A full list of the tridents to which statistical weights were given is tabulated in table 3. In addition, there were 15 tridents (including two found on the arms of electron pairs) which were found ‘ double ’ and to which no statistical weight could be given. These tridents were mostly too short for measurement. In table 3, the particles of the pair are denoted by 1 and 2, where 1 refers to the higher energy particle. The angles of ejection of the two particles are α_1 and α_2 respectively. An attempt has been made to measure the primary energy of each trident, but because of distortion it has frequently only been possible to give a lower limit when $p\beta$ exceeded 1 BEV.

4.3. *Theoretical Considerations*

The theory of the production of electron pairs by fast charged particles in the field of a nucleus has been treated by Bhabha (1935). Ravenhall (1950) has considered the effect of screening on the cross section for pair production by electrons. Hooper *et al.* (1951, 1952) have shown that Bhabha's theory explains satisfactorily the main features of the production of tridents by electrons. They have also found one event which seems to fit better with the Bhabha theory if it is assumed that the primary was a meson : the event described by Occhialini was probably also due to a meson primary.

Adopting Bhabha's notation, let E and E_+ be the total energy of the electron and the positron and $E_T = E + E_+$ the total pair energy. Let E_p

Table 3

Event No.	Length of primary (mm)	Values of $p\beta$ for primary (Mev/c)	Measurement on secondaries				‘ Single ’ or ‘ Double ’ S or D	Statistical weight	Type of trident
			$p\beta_1$ (Mev/c)	$p\beta_2$ (Mev/c)	α_1 (deg)	α_2 (deg)			
1	15·0	>3000	225±50	100±2	0·6±0·2	1·4±0·1	S	1	Meson (*c*)
2	31·1	>5000	28±7	13±5	No measure	ment possible	S	1	Meson (*b*)
3	5·3	>2000	15±5	13±5	2 ±1·5	6 ±3	S	1	Meson (*b*)
4	12·2	>6000	52±7	15±2	1·6±0·4	2·6±1·5	S	1	Meson (*b*)
5	9·5	>4000	290±74	210±30	0·5±0·05	0·5±0·05	S	1	Meson (*c*)
6	15·7	>1000	77±10	24±4	No measure	ment possible	S	1	Electron
7	12·0	650±130	47±9	<10	No measure	ment possible	S	1	Electron
8	47·0	550±50	40±10	8±5	0·7±0·2	7 ±3	S	1	Electron
9	34·3	>8000	210±40	<10	1·3±1	11 ±0·6	S	1	Meson (*b*)
10	24·0	>12000	<10	<10	~17	7·4±2	S	1	Meson (*b*)
11	34·3	>10000	100±90	90±18	0·9±0·1	1·4±0·1	S	1	Meson (*c*)
12	7·2	>1000	210±46	130±23	Too small	to measure	S	1	Electron
13	31·1	200±40	~25	~10	2·5±1	4 ±1·5	S	1	Electron
14	20·5	>12000	~700	680±170	Too small	to measure	D	0·9	Meson (*c*)
15	11·4	>1000	76±15	31±6	No measure	ment possible	D	0·6	Electron
16	8·2	>2000	27±4	10±2	1 ±1	3·5±2	D	0·5	Meson (*b*)
17	13·4	400±50	80±15	80±15	0·4±0·1	2 ±0·3	D	0·35	Electron
18	5·4	1000±130	26±7	20±7	1·7±7	3·1±1	D	0·3	Electron
19	6·8	>1000	88±18	58±14	1·5±1	3 ±1·5	D	0·3	Meson (*c*)
20	5·2	600±130	50±9	38±8	2·4±0·1	4·4±0·4	D	0·3	Electron

be the total energy of the primary particle, M its mass and β its velocity, in units of c. The electron mass is represented by m and $\gamma=[\sqrt{(1-\beta^2)}]^{-1}$.

Bhabha discusses three different cases :

(*a*) $E, E_+ \sim mc^2$; (*b*) $mc^2 \ll E, E_+ \ll mc^2\gamma$; (*c*) $mc^2\gamma \ll E, E_+ \ll Mc^2\gamma$.

Clearly the last case does not exist for electron primaries, where $m=M$. This separation into three energy regions is not essential in the mathematical formulation of the problem. However to obtain an understanding of the different types of angular distribution it is convenient to picture the three cases in the following way.

In Case (*a*), an electron in the negative energy state is raised into a positive energy state by interaction with the primary particle, in a manner similar to the knock-on process, except that the electron is not free but moves in the Coulomb field or screened field of the nucleus. The nucleus must be present to conserve momentum.

Case (*c*) is analogous to Case (*a*) with the roles of the primary and the secondary particles interchanged. A Case (*a*) trident, produced in the rest frame of the primary particle becomes a high energy pair when it is transferred into the laboratory frame of reference.

Case (*b*) can be conveniently treated as a pair production by the virtual quanta of the quantized electromagnetic field of a charged particle moving with relativistic velocity, following the Williams–Weiszäcker picture.

Because of the background of slow electrons, and the difficulty of observing tracks at a wide angle to the primary, Case (*a*) tridents have not been observed in this experiment. Cases (*b*) and (*c*) will now be considered in detail.

Case (*b*)

The differential cross section per nucleus of charge Ze for the production of tridents of this type with E_T in the range dE_T is given by Bhabha as

$$dQ_b=(56/9\pi)(Z^2r_0^2/137^2)\log_e(E_T/mc^2)\log_e(mc^2\gamma/E_T)(dE_T/E_T)\ \text{cm}^2/\text{nucleus}.$$

This formula takes no account of screening, and is valid for the energy region $(\gamma) < 2\times137\times Z^{-1/3}$. The cross section is given by

$$Q_b=(28/27\pi)(Z^2r_0^2/137^2)\log_e^3(\gamma)\ \text{cm}^2/\text{nucleus}.$$

When the inequality is not satisfied, the effects of screening reduce the total cross section. These screening effects are negligible for low energy pairs, which are created near the nucleus (i.e. a low energy photon requires a larger electric field for materialization) while the number of pairs with energy near the upper limit decreases.

Using the appropriate constants for Ilford G5 emulsion, and allowing for screening, the total cross section has been calculated and is given in fig. 7 as a function of the energy in Bev of a primary meson. The same curve gives the cross section for electrons when referred to the scale at the top of the graph.

The important properties of tridents of this type are the following:

(1) At high energies ($E_T > 100mc^2$) the energy received by the two electrons of the pair is often widely different. At lower energies the particles tend to receive about equal energies. The maximum value of E_T is of the order of $mc^2\gamma = E_p(m/M)$.

Fig. 7

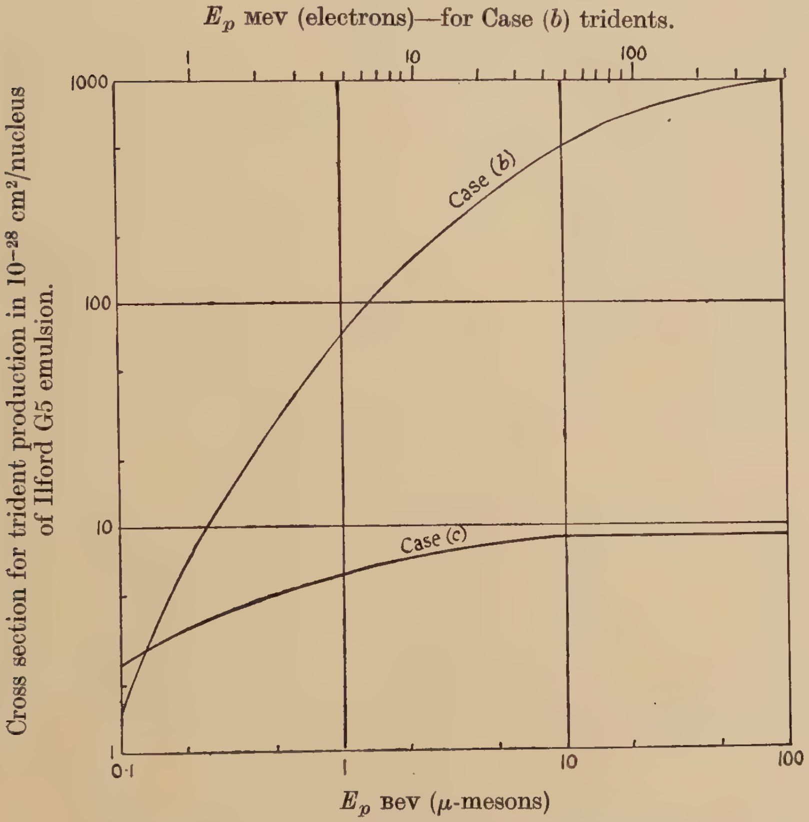

Cross section for trident production by μ-mesons and electrons.

(2) The mean angles of ejection are of the order of mc^2/E and mc^2/E_+ as in the case of pair production by photons. The two particles are usually ejected on opposite sides of the primary.

Case (*c*)

The differential cross section without screening in this case is given by Bhabha as

$$dQ_c = (8/\pi)(Z^2 r_0^2/137^2)(\gamma^2 mc^2/E_T^3) \log_e (2\gamma) dE_T \text{ cm}^2/\text{nucleus}.$$

The integral cross section is then

$$Q_c = (1/3\pi)(Z^2 r_0^2/137^2) \log_e (2\gamma) \text{ cm}^2/\text{nucleus}.$$

Screening effects enter when $(\gamma)>137Z^{-1/3}$ and affect pairs near the lower energy limit, while high energy pairs are unaffected, being produced near the nucleus where screening is unimportant. The calculated total cross section per nucleus of emulsion is also given in fig. 7 for this case. The properties of the pair in this case are the following : (1) The electrons tend to receive about equal energies, and the total pair energy is greater than $E_p(m/M)$. (2) The mean angle at which the particle of the pair are ejected is of the order of $1/\gamma$ radians.

In the present experiment tridents of the following three types should be observed : meson Case (*b*), meson Case (*c*), and electron Case (*b*). These may in principle be distinguished in the following way. The energy of the primary and secondaries can be measured, and the angle of ejection of the secondaries. If the angles satisfy the condition $\alpha_{E,E+}\sim mc^2/E, E_+$, the trident is of Case (*b*) ; if the condition $\alpha_{E,E+}\sim 1/\gamma$ is fulfilled it is of Case (*c*), when $mc^2/E, E_+$ is quite different from $1/\gamma$. If it is of Case (*c*), the energy will also satisfy $E_T>E_p/M$, whereas if it is of Case (*b*) and satisfies this condition it is necessarily an electron primary : if it is of Case (*b*) but does not satisfy the condition, it may be either a meson or an electron primary. In practice, the discrimination is not at all certain, especially as it has frequently only been possible to give a lower limit to the energy of a high energy primary. However, an attempt at a classification into the three types has been made with the tridents listed in table 3.

4.4. *Cross Section for Trident Production Underground*

The average cross section σ_{el} for tridents produced by fast electrons (>70 MeV) has been calculated from the differential electron spectrum given in eqn. (3). The result is that $\sigma_{el}=1{\cdot}03\times10^{-25}$ cm²/nucleus, corresponding to a mean free path of 1·08 m of emulsion.

The average cross section for tridents of Cases (*b*) and (*c*) produced by μ-mesons has been calculated from the differential spectrum of μ-mesons given by eqn. (4) of I. The results are shown in fig. 8.

4.5. *Expected Number of Tridents*

A trident is a relatively conspicuous event, because the tracks of the pair are usually formed at a rather small angle to the primary, and there are three tracks in all. They are consequently found very efficiently even at quite low energies. The lower limit is really set by the slow electron background. It is estimated that tridents with E_T greater than 20 MeV are efficiently found. For this reason, rather a large number of ‘ double ’ tridents were found.

From fig. 8, the mean free path for the production of Case (*b*) and Case (*c*) tridents with E_T greater than 20 MeV can be found, and hence the number of tridents expected. The results are given in table 4.

For the reasons given in § 4.3 it must be stressed that the classification of the observed tridents into the three cases is only tentative. To illustrate the method of classification consider the case of trident number 12, which is classified as having an electron primary. The energy of the pair is a large fraction of the primary energy, and the angles are very small.

Fig. 8

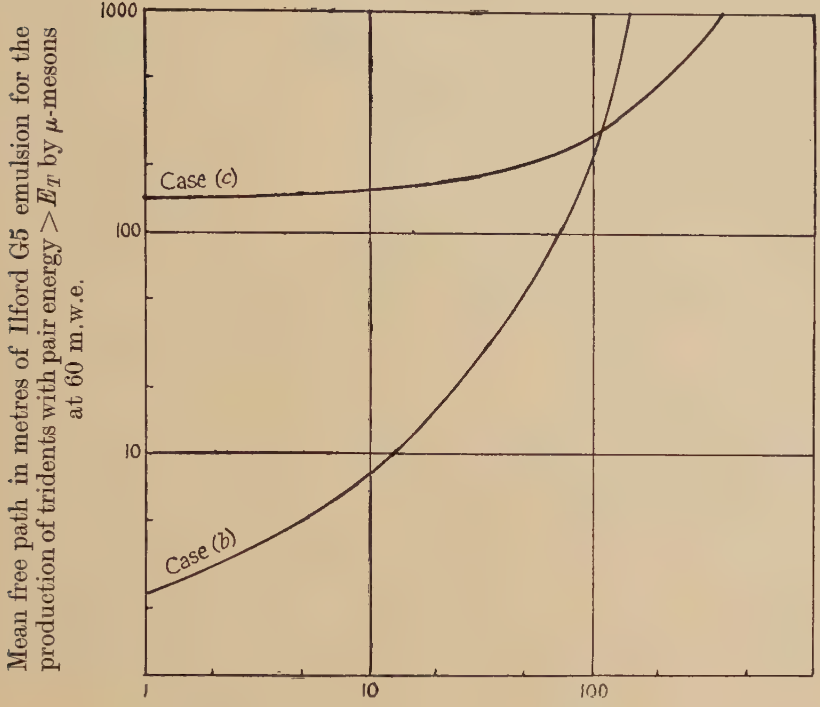

E_T MeV.

Mean free path in Ilford G5 emulsion for trident production with pair energies E_T by μ-mesons at 60 m.w.e.

Table 4

Primary particle and trident type	Observed No.	Expected No.
μ-meson Case (*b*)	5·5	8
μ-meson Case (*c*)	4·2	1
electron Case (*b*)	5·5	1
Total	16·2	10

A Case (*b*) meson trident is ruled out, since the primary would need 340 × 220 MeV = 70 BeV. On the other hand, a Case (*c*) trident is ruled out from considerations of angle : a one BeV meson primary would require a pair angle of about $2/\gamma$ or 10°, and the angle would not be too small to measure (as in the present case) unless the primary energy was greater than 60 Bev.

According to the classification given in table 3, there are four electron primaries with energies greater than 1 Bev. Such a requirement does not seem to be in good agreement with the spectrum of the electrons underground given in eqn. (3), according to which not more than 10 cm of the track length examined should be due to electrons with energy greater than 1 Bev. It is possible that some of the tridents have been wrongly classified. However, it is interesting to note that an excess of high energy electrons would be in agreement with the results on high energy photons given in § 3.2.

The total number of tridents observed affords a more definite comparison with theory. Remembering that Bhabha estimated that his cross sections are probably correct only to within a factor of two, the total observed number of tridents compares favourably with the total expected number.

ACKNOWLEDGMENTS

We wish to express our thanks to Dr. G. D. Rochester for his interest in the experiment. We are grateful to Professor M. Schönberg for valuable discussion on the theoretical aspects of trident formation, and to Mr. J. V. Major for checking some of the calculations.

APPENDIX I

THE TOTAL INTENSITY OF THE COSMIC RAY BEAM

(*a*) *Track Length Distribution*

Suppose the flux of cosmic ray particles can be represented by $I\cos^n\theta$ particles per cut area normal to the beam per second per unit solid angle, at an angle θ to the vertical. It is easily shown that the integral track length distribution in an infinite vertical plate should be given by

$$n(L)=I(d^2/L^2)\int_{-\pi/2}^{\pi/2}\cos^n\theta\,d\theta, \qquad \text{for } L \gg d,$$

where $n(L)$ is the number of tracks per second with length greater than L per unit area of a plate of thickness d.

The observers followed tracks belonging to a distribution fitting closely to a $\cos^6\theta$ distribution, for which the integral is 0·96. Thus for unit area of an infinite plate the track length distribution should be approximately

$$n(L)=I(d^2/L^2).$$

The number of tracks with length L in the range dL is therefore $2I(d^2/L^3)\,dL$.

(*b*) *Plate of Finite Dimensions*

It can be shown that the total effect of the edges of a plate is the following. Tracks which would have had length L in dL (L being less than either edge of the plate), if the plate had been infinite, but are cut short by the edge of the plate, are just compensated by those tracks which would have been longer but are reduced to a length L in dL by the edge effect.

Fig. 9

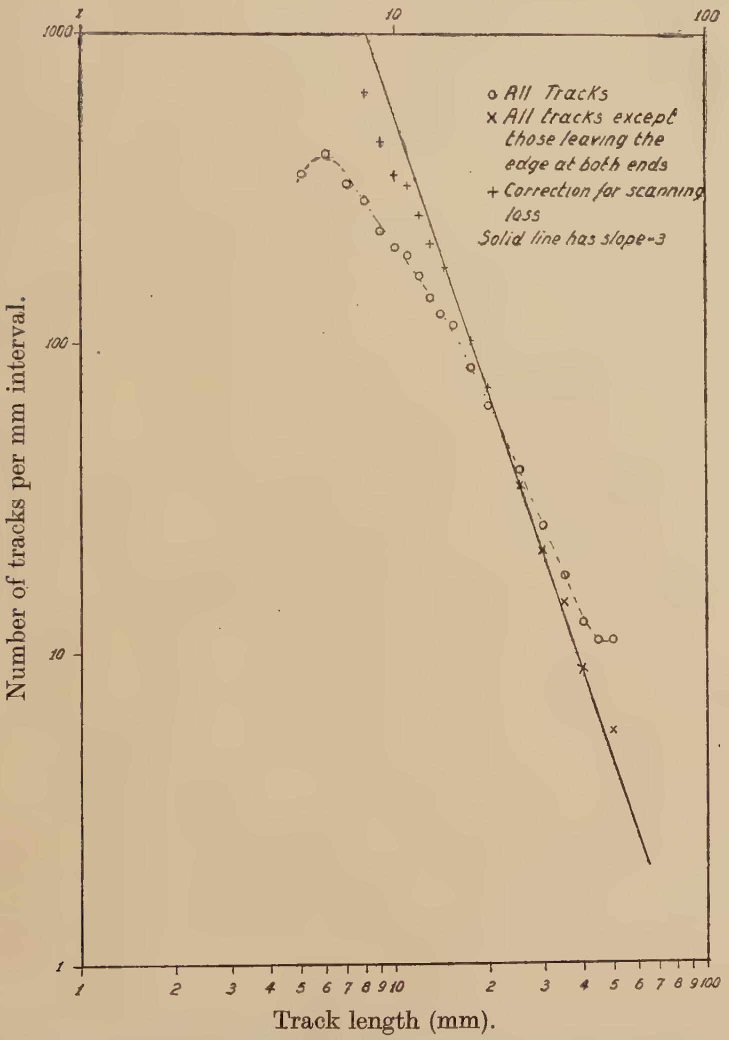

Corrections to the track-length distribution from the geometry of the plate, and scanning effects.

The track length distribution is therefore unaffected up to this value of L provided all tracks which reach an edge at both ends are eliminated. This compensation strictly ceases when the track length is equal to the length of the shorter side, but with an angular distribution strongly collimated round the longer side it effectively continues up to the length of the larger side.

(c) *Experimental Results*

Figure 9 shows the track length distribution for all the 400 μ plates of the no-lead group. The circles represent all tracks, the crosses represent all tracks except those which leave the edge of the emulsion at both ends (either crossing from end to end or from edge to edge or across a corner). When a correction is applied for the proportion of tracks of length L followed by the scanners according to Appendix I of I the series of points marked with a dagger is obtained. The line is the best line of slope $\tan \alpha = -3$ fitting those results where the two sources of correction are least. It corresponds to a value of $I = 6{\cdot}8 \times 10^{-4}$ particles/cm^2/sec/sterad.

REFERENCES

Bhabha, H. J., 1935, *Proc. Roy. Soc.* A, **152,** 559.
Ehmert, A., 1937, *Zeits. für Physik*, **106,** 751.
Follett, D. H., and Crawshaw, J. D., 1936, *Proc. Roy. Soc.* A, **155,** 546.
George, E. P., 1951, *Progress in Cosmic Ray Physics* (North Holland Publishing Co.), p. 395.
Greisen, K., 1942, *Phys. Rev.*, **61,** 212.
Hooper, J. E., King, D. T., and Morrish, A. H., 1951, *Phil. Mag.*, **42,** 304 ; 1952, *Ibid.*, **43,** 853.
Kannangara, M. L. T., and Zivkovic, M., 1953, *Phil. Mag.*, **44,** 797.
Occhialini, G. P. S., 1949, Report on the Como Conference, *Nuovo Cim.*, **6,** 420.
Powell, C. F., 1949, Report on the Como Conference, *Nuovo Cim.*, **6,** 380.
Ravenhall, D. G., 1950, *Proc. Phys. Soc.* A, **63,** 1177.
Rossi, B., and Greisen, K., 1941, *Rev. Mod. Phys.*, **13,** 240.

LXXXVI. *A Note on the Portevin–Le Chatelier Effect*

By A. H. Cottrell
Metallurgy Department, University of Birmingham*

[Received April 1, 1953]

Summary

Substitutional solute atoms in aluminium usually diffuse too slowly to cause appreciable strain ageing at room temperature. However, if the concentration of vacancies is increased by plastic deformation or by quenching, the rate of diffusion may increase sufficiently to cause strain ageing during plastic deformation. A serrated stress–strain curve should then result. These ideas are used to explain the Portevin–Le Chatelier effect.

§ 1. The Portevin–Le Chatelier Effect

It is well known that the stress–strain curve of an aluminium alloy at room temperature often begins smoothly but develops numerous serrations after a small plastic deformation. In ' hard ' testing machines, where sudden plastic deformation causes stress relaxation, the serrations appear as repeated oscillations of the applied stress of up to about 5% of its average value. In ' soft ' machines, where the stress cannot relax, they appear as alternate vertical and horizontal steps on the curve, corresponding to periods where the rate of plastic flow is either practically zero or very large. At each oscillation a wave of plastic deformation runs along the specimen.

These phenomena have been observed many times, but mainly in freshly quenched commercial age-hardening alloys containing a few per cent of copper or magnesium, and smaller amounts of silicon, chromium, and manganese. The first systematic study of them was made by Portevin and Le Chatelier (1923), in recognition of whom the name ' Portevin–Le Chatelier effect ' is now often used.

Serrations are often observed in stress–strain curves on soft iron at temperatures around 200°c. In this case they are due to repeated yielding which occurs because nitrogen and carbon atoms can diffuse fast enough to allow strain ageing while plastic deformation is in progress (Fettweiss 1919, Nabarro 1948, Hall 1952). It is attractive to suppose that the Portevin–Le Chatelier effect has a similar cause, with copper, and magnesium, etc., as the active solute atoms, since

(1) it does not appear in pure aluminium (McReynolds 1949, Masing and Raffelsieper 1950, Kawada 1950, 1952);

---

* Communicated by the Author.

(2) it appears most prominently in freshly-quenched alloys, where the alloying elements are retained in solution, and becomes less noticeable after precipitation has occurred (Portevin and Le Chatelier 1923, Lubahn 1949, Berghezan 1952) ;

(3) it appears only in a certain range of temperature, usually around room temperature (McReynolds 1949, Lubahn 1949).

However, this theory of the Portevin–Le Chatelier effect has previously always met with two difficulties :

(1) the serrations usually do not begin until some plastic deformation has taken place ;

(2) the rates of diffusion of alloying elements in aluminium at room temperature, deduced by extrapolating measurements at high temperatures, are far too small to account for the necessary rates of strain ageing.

The purpose of this note is to suggest that, when due consideration is given to the factors involved in diffusion, these two effects no longer appear as difficulties in the theory.

§ 2. RATES OF DIFFUSION DURING PLASTIC DEFORMATION

We can estimate the rate of strain ageing necessary for the Portevin–Le Chatelier effect from known information on soft iron. From the experiments of Manjoine (1944) we deduce the minimum temperatures for repeated yielding in iron at various rates of strain as follows :

Rate of strain, $\dot{\epsilon}$, sec^{-1}:	$1{\cdot}4\times10^{-5}$	$8{\cdot}3\times10^{-3}$	5·0
Temperature, T, °K:	330	410	620

These data satisfy the relation $\dot{\epsilon}=C\exp(-Q/RT)$, with $C=10^7$ sec^{-1} and an activation energy Q close to that (18 200 cal mol.$^{-1}$) for diffusion of nitrogen in α-iron. Since there is other evidence that strain ageing in iron is usually caused by nitrogen (Fast 1950, Cottrell and Leak 1952), we shall use the known value (Wert 1950) of the diffusion coefficient of nitrogen, $3\times10^{-3}\exp(-18200/RT)$ cm^2 sec^{-1}, to deduce that the minimum rate of diffusion for repeated yielding is of order $10^{-9}\,\dot{\epsilon}$ cm^2 sec^{-1}.

Before applying this result to aluminium alloys, an allowance must be made for some other factors. The atomic concentration of solute in a freshly quenched aluminium alloy is generally of order 10^{-2}, whereas that of nitrogen in iron is of order 10^{-4}, so that the aluminium alloys should age 100 times faster than iron, for the same diffusion coefficient. To set against this, the weaker interaction energy between solute atoms and dislocations in aluminium, about one-third that of nitrogen in iron, will result in both a smaller drift velocity of the atoms to dislocations, for the same diffusion coefficient, and a smaller yield point ; together, these effects should reduce the rate of strain ageing by a factor of about 10. Thus we expect the Portevin–Le Chatelier effect to appear in aluminium alloys when the diffusion coefficient reaches the value

$$D\simeq10^{-10}\,\dot{\epsilon}\ \text{cm}^2\ \text{sec}^{-1}. \qquad (1)$$

The data analysed by Nowick (1951) show that the diffusion coefficients of several metals in aluminium in equilibrium at room temperature are of order 10^{-23} cm^2 sec^{-1}, which is far too small to satisfy eqn. (1) at practical rates of strain. This, we suggest, is why the Portevin–Le Chatelier effect is normally absent at the start of plastic deformation.

However, this plastic deformation should create vacancies and other atomic defects (Seitz 1952, Mott 1952, 1953), and these will speed up the diffusion of substitutional atoms while having practically no effect on that of interstitial atoms such as nitrogen in iron. According to Seitz and Mott the atomic concentration, c, of vacancies created by plastic deformation should be about $10^{-4}\epsilon$, where ϵ is the strain. The diffusion coefficient of substitutional atoms should then be of order $ca^2\nu \exp(-U/RT)$, where a is the interatomic spacing, ν is the frequency of atomic vibrations, and U is the activation energy to move a vacancy. Hence, with $a^2=10^{-15}$ cm^2 and $\nu=10^{13}$ sec^{-1}, the diffusion coefficient should depend on the strain ϵ as

$$D\simeq 10^{-6}\,\epsilon \exp(-U/RT) \text{ cm}^2 \text{ sec}^{-1}. \quad \ldots \quad (2)$$

The activation energy U is difficult to estimate. The experiments of Manintveld (1952) suggest that, for copper, silver, and gold, U is about one-third of the activation energy of diffusion. The latter is typically 30 000 cal mol.$^{-1}$ in aluminium alloys so that, if the same ratio applies to these, $U\simeq 10\,000$ cal mol.$^{-1}$. At room temperature this value gives

$$D\simeq 10^{-13}\,\epsilon \text{ cm}^2 \text{ sec}^{-1}. \quad \ldots \quad (3)$$

§ 3. COMPARISONS WITH EXPERIMENT

Experiments on serrated stress–strain curves in commercial aluminium and aluminium–copper alloys were made by McReynolds (1949), using a rate of strain $\dot{\epsilon}\simeq 10^{-5}$ sec^{-1}. Thus, according to eqn. (1), the Portevin–Le Chatelier effect should be observed when $D\simeq 10^{-15}$ cm^2 sec^{-1}, i.e. when $\epsilon\simeq 10^{-2}$ at room temperature, according to eqn. (3). In fact, serrations were first observed at room temperature when $\epsilon\simeq 10^{-3}$. In similar experiments Lubahn (1949) used a strain rate $\dot{\epsilon}\simeq 2\times 10^{-5}$ and observed serrations first at $\epsilon\simeq 5\times 10^{-3}$. These values give $D\simeq 2\times 10^{-15}$ cm^2 sec^{-1} in eqn. (1) and $D\simeq 5\times 10^{-16}$ cm^2 sec^{-1} in eqn. (3).

McReynolds (1949) also studied the effect of temperature on the stress–strain curve. From his results we deduce the strains at which serrations first appeared as follows :

Temperature, T°K :	263	268	273	293	313	323
Strain, ϵ :	7×10^{-3}	$3{\cdot}5\times 10^{-3}$	4×10^{-3}	10^{-3}	7×10^{-4}	5×10^{-4}

These data fit the relation

$$\epsilon=5\times 10^{-9}\exp(7500/RT) \quad \ldots \quad (4)$$

reasonably well, which implies on our interpretation that $U=7500$ cal mol.$^{-1}$ for aluminium. Substituting these values for ϵ and U in eqn. (2) we find that the diffusion coefficient at which serrations begin is about 5×10^{-15} cm^2 sec^{-1}, in fair agreement with the value, about 10^{-15} cm^2 sec^{-1}, predicted by eqn. (1) for McReynolds rate of strain.

That 7500 cal mol.$^{-1}$ is a reasonable value for U in aluminium alloys is also suggested by the experiments of Sherby, Anderson, and Dorn (1951), who showed that a lightly strained aluminium–magnesium alloy undergoes strain ageing, indicated by the development of a sharp yield point, at temperatures in the range 194°K to 310°K, and that the activation energy for the beginning of strain ageing is 8000 cal mol.$^{-1}$.

In interpreting the above experiments we have considered the vacancies produced by plastic deformation as responsible for strain ageing. However, it is also possible to retain, temporarily, large numbers of vacancies by quenching from high temperatures. This, we suggest, explains an observation of Lubahn (1949) that, if his specimen was tested directly after quenching from 520°C, serrations appeared immediately.

ACKNOWLEDGMENTS

I am grateful to Dr. F. R. N. Nabarro, Dr. M. J. Dumbleton and Mr. T. Broom for useful discussions on this subject.

REFERENCES

BERGHEZAN, A., 1952, *Rev. Met.*, **49,** 99.

COTTRELL, A. H., and LEAK, G. M., 1952, *J. Iron Steel Inst.*, **172,** 301.

FAST, J. D., 1950, *Iron and Coal Trades Review*, **160,** 837.

FETTWEISS, F., 1919, *Stahl und Eisen*, **39,** 1, 34.

HALL, E. O., 1952, *J. Iron Steel Inst.*, **170,** 331.

LUBAHN, J. D., 1949, *Trans. Amer. Inst. Min. Met. Engrs.*, **185,** 702.

KAWADA, T., 1950, *J. Phys. Soc., Japan*, **5,** 60, 64, 68 ; 1952, *Ibid.*, **7,** 240.

McREYNOLDS, A. W., 1949, *Trans. Amer. Inst. Min. Met. Engrs.*, **185,** 32.

MANJOINE, M. J., 1944, *Trans. Amer. Soc. Mech. Engrs.*, **66,** 221A.

MANINTVELD, I., 1952, *Nature, Lond.*, **169,** 623.

MASING, G., and RAFFELSIEPER, J., 1950, *Zeit. Metall.*, **41,** 65.

MOTT, N. F., 1952, *Phil. Mag.*, **43,** 1151 ; 1953, *Ibid.*, **44,** 187, 742.

NABARRO, F. R. N., 1948, *Report on Strength of Solids* (London : Physical Society), p. 38.

NOWICK, A. S., 1951, *J. Appl. Phys.*, **22,** 1182.

PORTEVIN, A., and LE CHATELIER, F., 1923, *C. R. Acad. Sci.*, **176,** 507.

SHERBY, O. D., ANDERSON, R. A., and DORN, J. E., 1951, *Trans. Amer. Inst. Min. Met. Engrs.*, **191,** 643.

SEITZ, F., 1952, *Advances in Physics*, **1,** 43.

WERT, C. A., 1950, *J. Appl. Phys.*, **21,** 1196.

LXXXVII. *A Study of Individual Radio Atmospherics Received Simultaneously at Two Places*

By P. W. A. Bowe*
Cavendish Laboratory, Cambridge†

[Received April 1, 1953]

Summary

A previous paper (Bowe 1951) described a method of studying the propagation of radio waves of frequency 2 kc/s to 10 kc/s over the surface of the earth, by observing the responses of narrow-band receivers to individual radio atmospherics. The present paper describes an extension of these observations in which the same method was used simultaneously at two places, Cambridge and Aberdeen, 550 km apart. The narrow band receivers at both places were tuned to frequencies 7·5, 5·0, 3·5 and 0·6 kc/s. By comparing the responses at the two places, the attenuation factors for each frequency could be found. The sources of the atmospherics were located by the 'Sferic' direction finding system of the Meteorological Office, supplemented by a direction finder at Cambridge. Most of the observations were made at about noon. The results are presented as tables giving the propagation factor for 1000 km path, for the four frequencies studied. It was found that waves of frequency 0·6 kc/s are less attenuated than waves of frequency 3·5 kc/s. The results for 7·5 and 5·0 kc/s appear to indicate that the attenuation is less in winter than in summer.

§ 1. Introduction

Two methods have already been described for investigating the propagation of radio waves of frequency less than 16 kc/s where long-wave transmitters are not available. Both used lightning discharges as the source of radiation. In one method Gardner (1950) recorded the 'integrated level of atmospherics' at certain fixed frequencies and, by comparing the magnitude of this 'level', by day and by night and when close storms were present, he showed that, during daytime, waves of frequency 3·5 and 5 kc/s were more heavily attenuated than waves of frequency greater than about 8 kc/s. He showed also that the attenuation was much less at night. These results were confirmed and extended by Bowe (1951) who used a second method in which he observed the responses of narrow-band receivers to individual atmospherics coming from distances of 200 to 3000 km. He deduced the relative attenuation at fixed frequencies.

In the present paper experiments are described in which individual atmospherics were received simultaneously at two different places.

---

* Communicated by J. A. Ratcliffe, F.R.S.

† Now in Australia.

The observations were made in Great Britain at Cambridge and Aberdeen which are separated by a distance of 550 km. The method used at each station was the same as that previously used for single station observations (Bowe 1951). The atmospherics were received on four narrow-band receivers tuned to frequencies of 7·5, 5·0, 3·5 and 0·6 kc/s. By comparing the responses at the two places, it was possible to determine the attenuation factors for each frequency separately.

The sources of the atmospherics were located by radio direction finding methods by the 'Sferic' section of the Meteorological Office. This method was supplemented by a direction finder installed at the Cambridge station as described later.

In § 2 a brief description of the apparatus is given. The method of identification of atmospherics recorded at both stations and methods of location of the sources of atmospherics are described. The method of analysis of results is given in § 3. In § 4 the results are described. § 5 is concerned with conclusions and discussion of the results.

§ 2. Experimental Method

2.1. *Recording Apparatus*

The two sets of receiving apparatus were the same as that described by Bowe (1951). At each station the output from a vertical aerial was applied to four tuned receivers. The outputs were displayed on four cathode-ray tubes and the traces of these tubes were photographed together. The receiver bandwidths were 120 c/s on 7·5 and 5 kc/s, 60 c/s on 3·5 kc/s and 20 c/s on 0·6 kc/s. A wide-band amplifier and cathode-ray tube were also included to display the transient waveform.

2.2. *Identification of Atmospherics Recorded at Both Stations*

At each observing station the strongest atmospherics were recorded and it was then necessary to decide which of these had been recorded simultaneously. To assist in this identification, a simple record of the B.B.C. 'Light' programme was made at the two stations and a mark was put on the record to show when an atmospheric had been recorded. It was then possible to decide, afterwards, by inspection of the records, which atmospherics had been received simultaneously. It proved sufficient to record the B.B.C. programme by inserting a small neon lamp in the audio output from a receiver. The lamp was then photographed on moving film to give a record of the type shown in fig. 1. A second neon lamp was brightened when an atmospheric was recorded and produced the marks shown on the lower portions of the records.

Two typical sections of record for the two stations are shown in fig. 1 and it can be seen that the resolution, about 0·05 sec, is adequate to establish identification.

In order to relate the atmospherics recorded simultaneously at both stations to those whose positions were determined by the Meteorological Office 'Sferics' organization, direct telephonic connection was established between the observing station at Cambridge and the operator of the ‘ Sferics ’ system. It proved that about 60% of the atmospherics recorded simultaneously at the two stations were also located by the ‘ Sferics ’ system, if it was in operation. Since, however, it was not operating on all occasions, an auxiliary arrangement was set up, as follows, to assist in the location of the sources.

A cathode-ray direction finder installed at Cambridge provided a photographic trace which indicated the direction of arrival of each strong atmospheric. By combining a knowledge of this recorded direction with a knowledge of the location of the chief thunderstorm regions, known from the ‘ Sferics ’ observations made a few hours before and after the experiment, it was often possible to specify a region from which a given atmospheric came. It will be shown, in the next section, that, provided the distance of the source was greater than about 1000 km it was not necessary to know the distance exactly: an accurate knowledge of the direction was all that was required.

Fig. 1

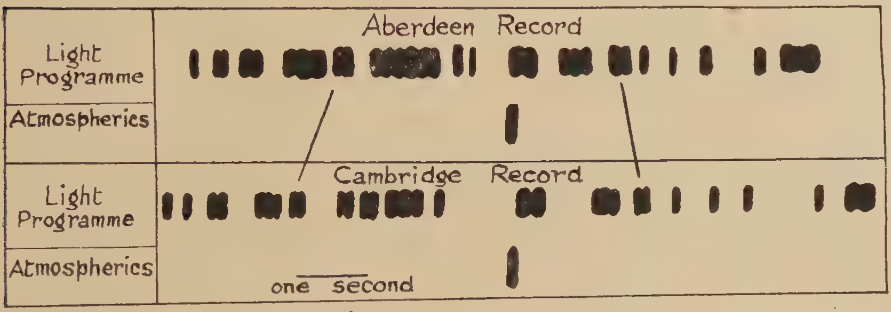

Nature of records used to identify atmospherics recorded at the two stations.

§ 3. ANALYSIS OF RESULTS

Suppose that a given lightning discharge radiating a wave in free space produces in a narrow-band receiver an e.m.f. $E(f, r)$ given by

$$E(f, r) = KA\phi(f)r^{-1}$$

where f is the frequency to which the receiver is tuned,
r is the distance,
A is determined by the magnitude of the current in the discharge,
$\phi(f)$ describes the spectrum of the atmospheric at the source, and
K is a constant of the apparatus.

If now the same lightning discharge radiates a wave which travels between the ground and the ionosphere, as in a waveguide, an analysis such as that of Budden (1951) shows that the factor r^{-1} is replaced by a factor $r^{-1/2} \exp \{-\alpha(f) . r\}$, where $\alpha(f)$ depends on frequency. The e.m.f. $E(f, r)$ produced in the narrow band receiver is now given by

$$E(f, r) = KA\phi(f)r^{-1/2} \exp \{-\alpha(f) . r\}. \quad . \quad . \quad . \quad . \quad (1)$$

Fig. 2

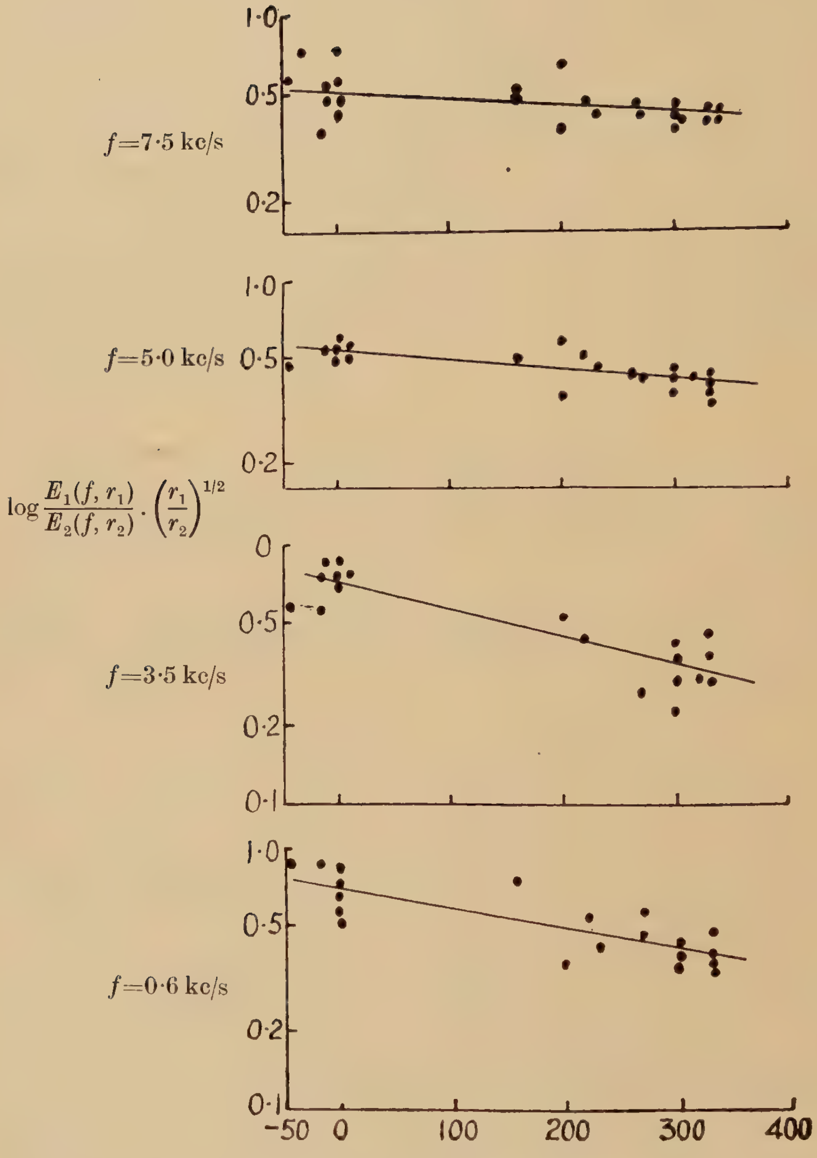

(r_1-r_2) km

Example of results deduced from a single summer daytime experiment. The same horizontal scale applies to each graph.

If now quantities appropriate to the two receiving stations are denoted by subscripts 1 and 2, it follows that

$$E_1(f, r_1)/E_2(f, r_2)=(K_1/K_2)(r_1/r_2)^{-1/2}\exp\{-\alpha(f)(r_1-r_2)\}.$$

This equation applies for atmospherics from all bearings provided the attenuation does not depend on bearing. In what follows

$\alpha(f)$ will be called the attenuation exponent,

$\exp\{-\alpha(f)r\}$ will be called the propagation factor, and

$\exp\{-\alpha(f)\,.\,r_0\}$, where $r_0=1000$ km, will be called the propagation factor for 1000 km.

In presenting the results it will be convenient to plot the quantity

$$\{E_1(f, r_1)/E_2(f, r_2)\}(r_1/r_2)^{1/2}$$

on a logarithmic scale as a function of (r_1-r_2).

The difference (r_1-r_2) of the two distances depends primarily on the *direction* of the source, and only secondarily on its distance. If the *distance* is greater than about 1000 km the difference (r_1-r_2) is almost independent of the distance and the ratio r_1/r_2 is not usually far from unity. This provides the justification for the use of the cathode-ray direction finder mentioned in the previous section.

§ 4. RESULTS

The observations were made between June and November 1951. They were spaced throughout the period so that seasonal changes could be examined. Most of the observations were made about noon although a few were made in the evening and at night.

4.1. *Results for Daytime*

A total of 22 experiments, each of ten minutes duration, was made within two hours of noon. Of these, twelve were such that useful results could be obtained, and in ten there was insufficient variation in the quantity (r_1-r_2). An example of the results is shown in fig. 2. For each atmospheric the four values of

$$\{E_1(f, r_1)/E_2(f, r_2)\}(r_1/r_2)^{1/2},$$

corresponding to the four frequencies, were deduced and plotted on a logarithmic scale against (r_1-r_2). If a straight line could be fitted to the points its slope would give a value for the attenuation exponent. For all useful experiments it was found that atmospherics fell naturally into two groups, one corresponding to (r_1-r_2) between -100 km and $+200$ km and the other corresponding to (r_1-r_2) between $+200$ km and $+500$ km. For each group a mean point was derived with respect to both variables and the straight line was drawn through these two mean points. The attenuation exponent was deduced from the slope of this line and the propagation factor for 1000 km was deduced. The values of this factor for the 12 daytime experiments are shown in table 1.

The measurements show that the propagation factor for waves of frequency 0·6 kc/s is about twice that for waves of frequency 3·5 kc/s. The results for 7·5 kc/s and 5 kc/s are plotted in fig. 3 against time of year and they appear to indicate that the propagation factor is greater in winter than in summer. The results for 3·5 and 0·6 kc/s are insufficient to reveal seasonal changes.

Table 1. Propagation Factor for 1000 km for Daytime Experiments

Date	Time	Propagation factor for 1000 km path			
1951	G.M.T.	7·5 kc/s	5 kc/s	3·5 kc/s	0·6 kc/s
23 June	14.00	0·61	0·39	0·07	0·13
23 June	15.00	0·50	0·30	—	—
26 June	14.00	0·53	0·29	0·07	—
19 July	14.00	0·71	0·38	—	—
24 July	13.00	0·52	0·36	0·05	0·10
24 July	14.00	0·60	0·37	0·09	0·18
23 Aug.	14.30	0·58	0·25	—	—
23 Aug.	15.30	0·58	0·23	—	—
1 Oct.	14·00	0·70	0·35	—	—
1 Oct.	15.00	0·66	0·51	—	—
18 Oct.	15.00	0·85	0·60	—	—
5 Nov.	12.00	0·80	0·49	0·07	0·29

Fig. 3

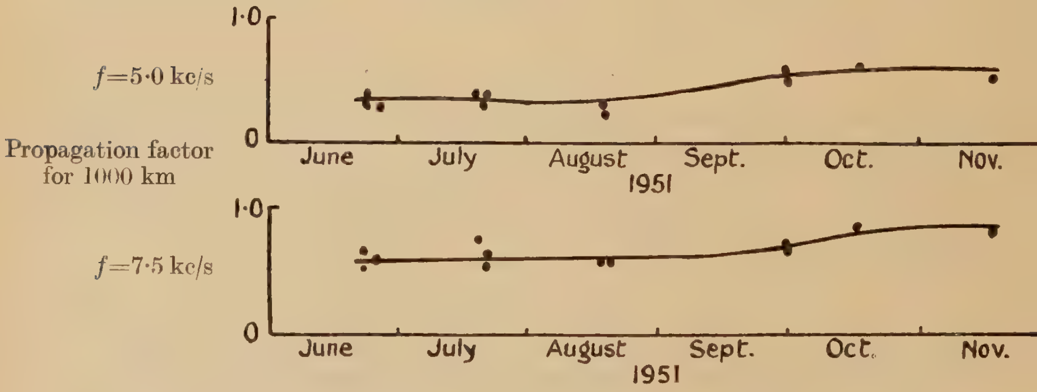

Seasonal change of propagation factor for 1000 km.

4.2. *Results for Evening and Night Time*

Eleven experiments were made at night, of which four were suitable for analysis. The results of one of these experiments are given in table 2. For the other three the results did not fit the exponential behaviour assumed in eqn. (1). In one case the points for different atmospherics were scattered and in two the results seemed to indicate that the field increased with distance. In view of the fact that only a small number of experiments was available, the detailed interpretation of these results cannot be attempted. The experiments did generally indicate, however, that the attenuation at night was small.

Table 2. Propagation Factor for 1000 km for Night-time Experiments

Date	Time	Propagation factor for 1000 km path			
1951	G.M.T.	7·5 kc/s	5 kc/s	3·5 kc/s	0·6 kc/s
23 Aug.	20.00	0·75	0·75	0·23	0·50

§ 5. CONCLUSIONS

The results of experiments made during the day in summer are summarized in fig. 4. The points for 7·5, 5, 3·5, and 0·6 kc/s represent the results of the present series of experiments. That for 16 kc/s was provided by Dr. K. Weekes from the results of measurements made on the Hollingworth interference pattern produced by the Post Office sender G.B.R. (Weekes 1950). The results shown in fig. 4 are summarized in table 3, in which the tabulated accuracy has been deduced from the scatter of the individual experiments.

Fig. 4

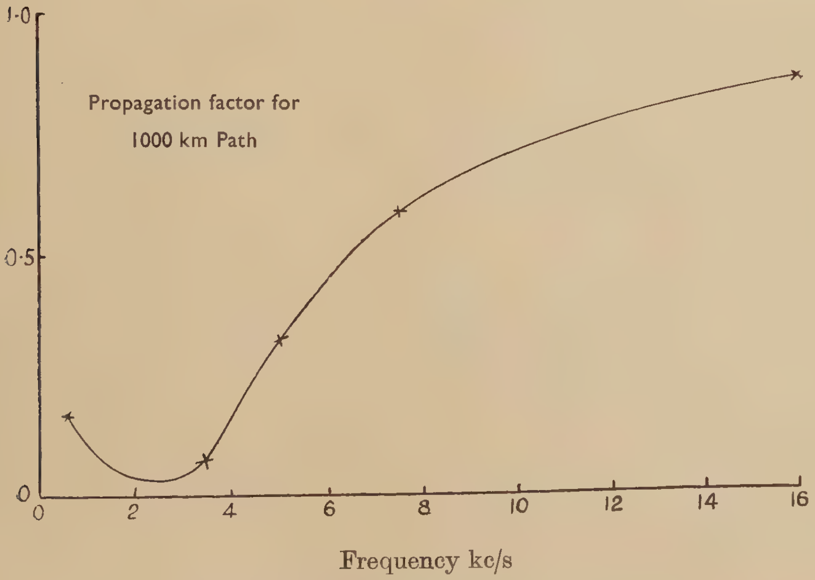

Plot of propagation factor for 1000 km.
[exp $\{-\alpha(f), r_0\}$, $r_0=1000$ km] against frequency.
x . . . . experimental points.

The investigation has revealed the fact that waves of frequency 0·6 kc/s are less attenuated than waves of frequency 3·5 kc/s. This was predicted by Budden (1951) and may be of importance in explaining the ' slow tail ' part of the waveforms of radio-atmospherics.

Table 3. Mean Daytime Values of the Propagation Factor for 1000 km

Frequency	Propagation factor for 1000 km path	
kc/s	Summer Day	Winter Day
7·5	0·58 ± 0·03	0·82 ± 0·04
5	0·32 ± 0·02	0·55 ± 0·03
3·5	0·07 ± 0·01	
0·6	0·17 ± 0·03	

ACKNOWLEDGMENTS

The author wishes to thank the following people and organizations for help given with this experiment : Professor R. V. Jones for providing the facilities at the University of Aberdeen, Dr. C. B. I. Glass for maintaining and operating the equipment at Aberdeen, the Director of the Meteorological Office and the workers of the ' Sferics ' section for help in locating the sources of the atmospherics, the Australian Department of Supply for enabling the author to work at the Cavendish Laboratory, the D.S.I.R. for supporting the work which was done at the Radio Section of the Cavendish Laboratory, Cambridge.

REFERENCES

Bowe, P. W. A., 1951, *Phil. Mag.*, **42,** 121.
Budden, K. G., 1951, *Phil. Mag.*, **42,** 1.
Gardner, F. F., 1950, *Phil. Mag.*, **41,** 1259.
Weekes, K., 1950, *J.I.E.E.*, **97** (3), 100.

LXXXVIII. *The Thermal Etching of Uranium*

By B. W. Mott and J. Williams
Atomic Energy Research Establishment, Harwell*

[Received April 17, 1953]

Summary

A description is given of the thermal etching characteristics of uranium with particular reference to the formation of steps on beads of metal produced by melting the powder.

§ 1. Introduction

Many workers have observed the thermal etching of a variety of metals and a review of the phenomenon was made by Shuttleworth (1948). The only reference in the literature to the thermal etching characteristics of uranium is that by Mott and Haines (1952) who described the results obtained at temperatures below about 800°c. The rate of oxidation of uranium at elevated temperatures, is too rapid for useful results to be obtained in air although heat tinting, i.e. variation of the rate of oxidation with orientation, occurs at about 100°c on polished surfaces. For electrolytically polished specimens heated *in vacuo* or in sealed silica containers, thermal etching begins at about 300°c, at which temperature boundaries appear between grains of markedly different orientations. With further rise in temperature, the grain boundary grooves increase in width and twins and boundaries between other grains are revealed. Unlike the grooves in silver observed by Chalmers, King and Shuttleworth (1948), those in uranium appear to be locked in position and do not move forward with the boundary on recrystallization. If recrystallized uranium, with fine polygonal grains, is transformed to the beta-form by heating above 665°c, the grain structure becomes coarse with irregular grain boundaries, so that examination after cooling reveals thermal etching grooves corresponding to both the initial and final structures. This is illustrated in fig. 1 (figs. 1–6, Plate 30) in which the twins of the coarse grains are superimposed on the fine network of the original grains. More recently, a different type of effect has been observed and is described below.

§ 2. Experimental

During experiments on the vacuum sintering of uranium powder, the temperature temporarily exceeded the melting point and fused uranium globules were formed. After four hours sintering at a temperature just below the melting point, the specimens were slowly cooled to room temperature in the furnace over a period of 21 hours. Subsequent examination showed that the globules which had exuded from the loosely sintered mass, had bright surfaces which remained untarnished for several weeks in air instead of acquiring in a few hours the more usual discoloration.

---

*Communicated by Mr. A. D. LeClaire.

The bright beads were carefully examined under a metallurgical microscope to determine the nature of the surface and striking effects were observed. Numerous facets were present which gave a striated appearance at low powers and typical areas are shown in figs. 2 and 3. On first examination, it appeared possible that the area marked by the arrow in fig. 3 contained three dislocation growth spirals of the type recently described in the literature (Griffin 1950, Verma 1951, Amelinckx 1952 and Forty 1952). It was however difficult to correlate the appearance of the rest of the structure with this assumption. For a more complete examination, the specimen was attached to a small goniometer head so that its orientation with respect to the optical axis of the microscope could be varied. This revealed that spirals were not present but that the effect was due to steps running in three directions and meeting at the centres of the ‘ spiral ’ areas. This is shown in fig. 4, in which the three series of steps are clearly evident. Furthermore, the depth of the steps varied from about 10 000 to 80 000 Å. These figures are considerably greater than those normally observed for dislocation spirals but of the same order as those for steps observed on thermally etched silver (Chalmers, King and Shuttleworth 1948).

Several peculiarities were noted. The appearance varied considerably ; the step systems were such that a peak was formed in some cases and a hollow in others. There was no regular variation in the height of the steps in any given system as can be observed in figs. 2–4. Occasionally where the surface was stepped in two different directions as in fig. 2, two edges amalgamated to form a single edge as indicated by the arrow A and cases were observed in which a new step appeared as shown by arrow B. The broad faces of the steps were not perfectly plane and minor steps were observed at higher magnification. Although no precise goniometric measurements were made, the angles between the different series of steps appeared to be consistently 90°.

The thermal etching occurred in the temperature range in which uranium has a body-centred cubic structure for which the most densely-packed plane is the (110). It would be expected therefore that if thermal etching occurred by evaporation from a pure uranium surface without interference from the atmosphere or oxide film, the surfaces retained would be the (110) faces which make a 90° angle between each other, as observed. There is a marked diversity of opinion on which crystal planes are involved in other metals, e.g. for silver, Graf (1945) identified the faces as (100) planes and Chalmers, King and Shuttleworth (1948) considered them to be (111) planes. On another face-centred cubic metal, copper, Elam (1936) concluded that the faces were (100) and (110) and Gwathmey and Benton (1942), (110) and (111). It is not known what part is played by the oxide film in the case of uranium, but since the surface of the beads was exceptionally resistant to further oxidation at room temperature, it is probable that the oxide film is UO. This has a sodium chloride type structure and has been reported as having an appreciable vapour pressure at 2000°K (Brewer 1952) so that it might be expected to play a part in the thermal etching process.

Associated with the uranium globules were oxide particles (believed to be OU) several of which may be observed in fig. 3. These particles were generally of a regular cubic outline with no significant surface structure. In some areas, however, oxide particles were observed with fairly regular surface markings of the type shown in figs. 5 and 6. The height of the steps was not measurable by conventional microscopical procedure and appeared to be less than 100 Å; the pitch generally increased progressively as in spiral growths described for other materials (Griffin 1950, Verma 1951, Amelinckx 1952 and Forty 1952). A long search under the microscope however failed to reveal a perfect spiral and the most convincing example observed is shown in fig. 6. Thus although there is no direct evidence that these markings are due to spiral growth from the vapour phase, they may be associated with this phenomenon and be imperfect examples due to the complex conditions operating.

All attempts to produce spiral growths on uranium under conditions similar to those described by Forty (1952) for magnesium, zinc and cadmium have been unsuccessful. Experiments were made in which a thermal gradient was established along the length of a specimen under varying conditions but the only result observed was thermal etching of the type described above. Due to the phase changes on cooling uranium, however, it may be that considerable distortion of the configurations occur and the result is not easily recognized as having originated from a spiral formation.

§ 3. DISCUSSION

The striations or steps developed on the uranium beads are apparently similar in nature to those reported for other metals but (to date) have only formed under specific conditions and not on polished surfaces of multi-grained specimens. Owing to the possible influence of the UO film and the phase changes occurring on cooling to room temperature, it would be difficult to draw any definite conclusions on the mechanism of the process even if profile measurements and an x-ray analysis of the orientation of the step faces were made.

The reason for the addition or omission of a step as in fig. 2 is not clear but it may be associated with the presence of dislocations, in which case the height of the steps might be controlled by dislocations.

ACKNOWLEDGMENT

This note is published by kind permission of Sir John Cockcroft, F.R.S., Director of the Atomic Energy Research Establishment, Harwell.

References

Amelinckx, S., 1952, *Phil. Mag.*, **43,** 562.
Brewer, L., Bromley, L. A., Gilles, P. W., and Lofgren, N. L., 1952, *National Nuclear Energy Series*, Div. VIII, Vol. 6.
Chalmers, B., King, R., and Shuttleworth, R., 1948, *Proc. Roy. Soc.* A, **193,** 465.
Elam, C. F., 1936, *Trans. Faraday Soc.*, **32,** 1604.
Forty, A. J., 1952, *Phil. Mag.*, **43,** 949.
Graf, L., 1945, *Z. Electrochem.*, **48,** 181.
Griffin, L. T., 1950, *Phil. Mag.*, **41,** 196.
Gwathmey, A. T., and Benton, A. F., 1942, *J. Phys. Chem.*, **46,** 969.
Mott, B. W., and Haines, H. R., 1952, *J. Inst. Met.*, **80,** 621.
Shuttleworth, R., 1948, *Metallurgia*, **38,** 125.
Verma, A. R., 1951, *Nature, Lond.*, **167,** 939.

Fig. 1

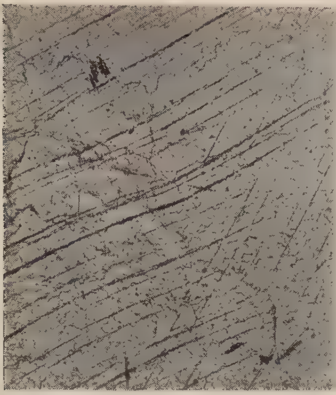

Thermal etching grooves on polished uranium surface. ×150

Fig. 2

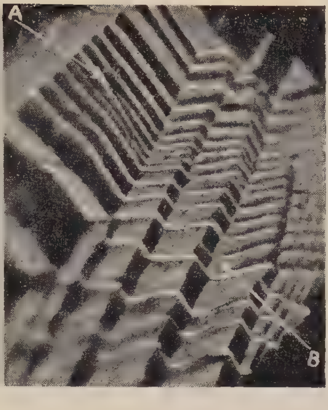

Two series of steps on uranium globule. ×1000

Fig. 3

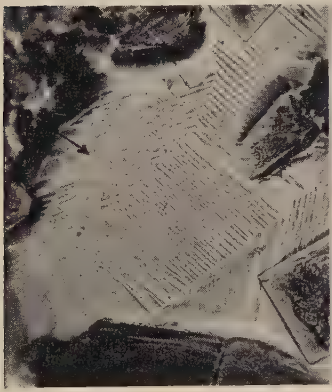

Steps on uranium globule. ×400

Fig. 4

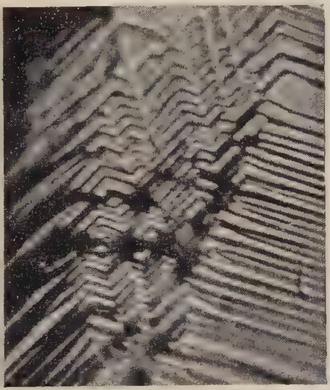

As for fig. 3 after reorientation. ×500

Fig. 5

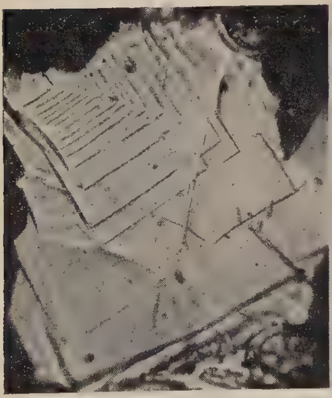

Surface of oxide particle. ×1000

Fig. 6

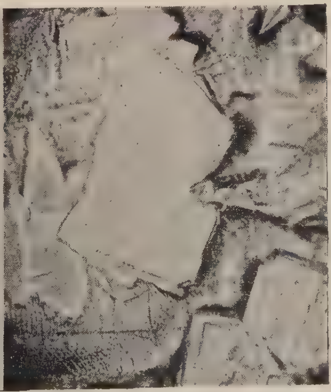

Surface of oxide particle. ×500

Fig. 1

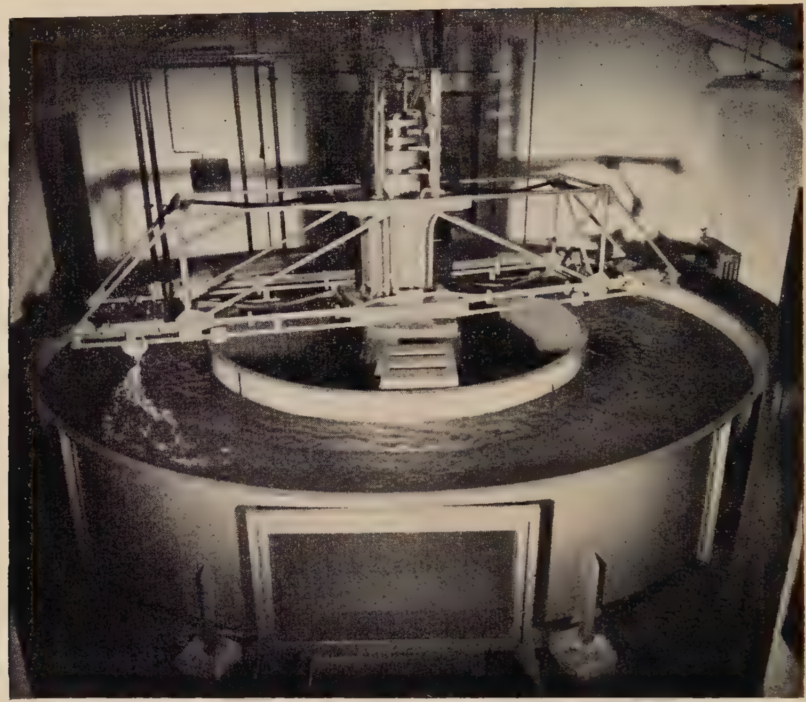

Fig. 2

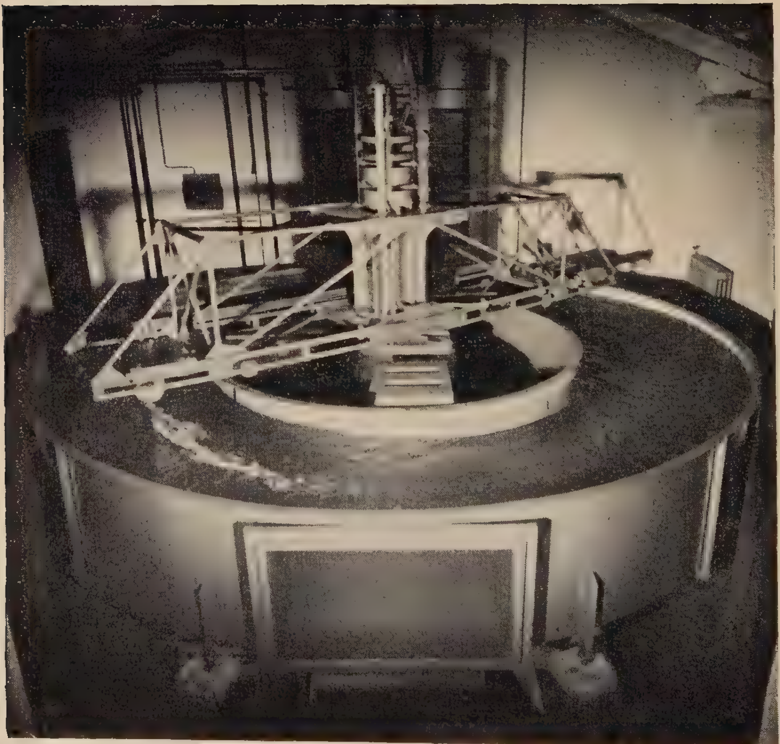

LXXXIX. *Wave Motion in an Annular Tank*

By I. J. CAMPBELL
Admiralty Research Laboratory, Teddington*

[Received April 16, revised June 5, 1953]

ABSTRACT

It has been found that large wave disturbances occur when a water whirling arm is operated at certain speeds. A theoretical treatment of this phenomenon is given. Visual observations of disturbances on the surface of the water in the tank confirm the theoretical expectations.

§ 1. INTRODUCTION

FIGURE 1 (Plate 31) shows a view of a water whirling arm equipment in operation at the Admiralty Research Laboratory: a small model can be suspended on a strut from the end of the arm and towed through the water at speeds of up to 60 f.p.s. in a circular path of radius about 5 feet. The inner radius of the tank is 3·8 feet, the outer radius is 6·8 feet and the depth of water is 22 inches. The appearance of the water surface, as shown in fig. 1, is typical of most operating speeds: disturbances are confined to a thin sheet of spray thrown by the strut and a general but minor ruffling of the surface. At certain critical speeds of operation, however, violent disturbances of the water in the tank occur: this is illustrated in fig. 2 (Plate 31), where the violence of the disturbance may be gauged by noting the large variations in water level round the inner and outer walls of the tank. In this paper the theory of the normal modes of wave motion of the water in an annular tank is invoked to throw light on the phenomenon illustrated in fig. 2. Predictions are made of the nature of possible violent disturbances and of the critical operating speeds at which they may be expected to occur and these predictions are confirmed by observations.

§ 2. THE NORMAL MODES

The theoretical treatment of the normal modes of small amplitude wave motion of the water in (*a*) a rectangular tank and (*b*) a circular tank is given fully in Lamb's Hydrodynamics. The results of the simple extension to the case of an annular tank will be given here.

The notation is defined in fig. 3. The velocity potential φ for any irrotational motion of the water in the tank must satisfy Laplace's equation

$$\frac{\partial^2\phi}{\partial r^2}+\frac{1}{r}\frac{\partial\phi}{\partial r}+\frac{1}{r^2}\frac{\partial^2\phi}{\partial\theta^2}+\frac{\partial^2\phi}{\partial z^2}=0, \quad \ldots \ldots \quad (1)$$

---

* Communicated by the Author.

in order to preserve continuity. Kinematical considerations and the requirement for constant pressure demand that the velocity potential of any small amplitude wave motion shall satisfy the following approximate free surface condition

$$\frac{\partial^2\phi}{\partial t^2}+g\frac{\partial\phi}{\partial z}=0 \qquad \text{when} \qquad z=0. \qquad \ldots\ldots \quad (2)$$

The normal derivatives of ϕ must vanish at the walls and on the bottom of the tank. These conditions suffice to determine the normal modes. Once the velocity potential of such a wave motion has been found, the wave elevation ζ may be evaluated to a sufficient approximation by equating $g\zeta$ to $\partial\phi/\partial t$, evaluated at the undisturbed free surface.

Fig. 3

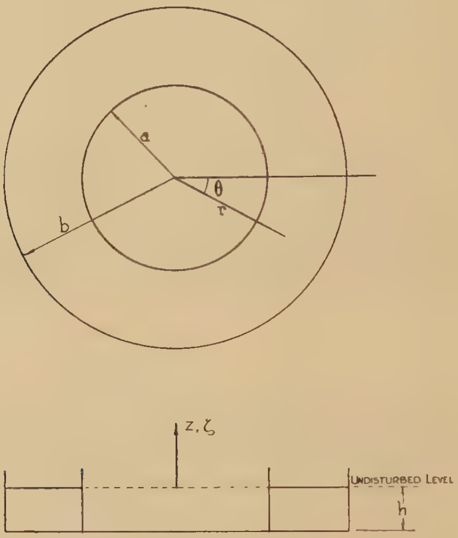

Notation.

It turns out that the wave elevation associated with any normal mode takes one of the following forms :

$$\zeta=(\text{constant})\{Y_s'(ka)J_s(kr)-J_s'(ka)Y_s(kr)\}\begin{Bmatrix}\cos s\theta\\ \sin s\theta\end{Bmatrix}\begin{Bmatrix}\cos \sigma t\\ \sin \sigma t\end{Bmatrix}. \quad . \quad (3)$$

where the functions J_s and Y_s are Bessel functions, s can take the values 0, 1, 2, . . . , k is any root (of which there are an infinite number k_s^0, k_s^1, k_s^2, . . . in ascending order of magnitude) of the following equation :

$$J_s'(ka)Y_s'(kb)=J_s'(kb)Y_s'(ka), \qquad \ldots\ldots \quad (4)$$

and

$$\sigma=kc=\sqrt{(gk\tanh kh)}. \qquad \ldots\ldots \quad (5)$$

When k is the $(n+1)$th root of (4), the corresponding mode will be referred to as the (s, n) mode. Numerical values for most of the roots of (4) can be found conveniently by using an asymptotic series due to McMahon and quoted by Gray, Mathews and MacRobert.* This expression cannot be used for evaluating the lowest root (corresponding to the case when n is zero) for any value of s but such roots may be determined graphically. Any small disturbance of the water in the tank can be represented by a sum of normal modes as defined above but it will appear that for the present purpose, namely examining the possibility of violent disturbances when a model is towed round the channel, each mode has an individual significance.

Surface Appearance

It is clear from (3) that the number of diametrical nodes associated with the (s, n) mode is precisely s. The number of circumferential nodes in any case depends on the properties of $Y_s'(ka)J_s(kr)-J_s'(ka)Y_s(kr)$ considered as a function of r in the range (a, b). For a circular tank, i.e. the case when a is zero, it is known that the number of circumferential nodes associated with the (s, n) mode is precisely n. It is conjectured that this is also true for the case of an annular tank but no rigorous proof has been found. When n is sufficiently large, k_s^n may be replaced by the first term, namely $n\pi/(b-a)$, of McMahon's asymptotic series and each Bessel function may be replaced by the first term of its asymptotic expansion. When this is done, it is found that

$$Y_s'(ka)J_s(kr)-J_s'(ka)Y_s(kr) \sim \{2/\pi k(ra)^{1/2}\} \cos \{n(r-a)\pi/(b-a)\}, \quad (6)$$

which has precisely n zeros in the range (a, b). Also calculations showed that for the A.R.L. tank the conjecture is still true when n is small, at least for the (0, 1), (0, 2), (1, 0), (1, 1), (1, 2), (2, 0), (2, 1) and (2, 2) modes. The conjecture, that in an annular tank the number of circumferential nodes associated with the (s, n) mode is n, is thus at least plausible.

Accepting this conjecture the doubly infinite set of normal modes of wave motion in an annular tank may be pictured in the manner illustrated in fig. 4. Corresponding to the roots of (4) when s is zero, there is a set of axially symmetric normal modes with 1, 2, 3, . . . circumferential nodes respectively: to this, for the sake of uniformity with other sets, may be added the trivial case, in which no motion is possible, represented by the axially symmetric mode with no circumferential nodes. Then there is a set of normal modes, each with one diametrical node and having 0, 1, 2, 3, . . . circumferential nodes respectively. In general there is a set of normal modes, each with s diametrical nodes, s being a positive integer or zero, and having 0, 1, 2, 3, . . . circumferential nodes respectively.

It will be appreciated that the wave elevation in a simple (s, n) mode can take not only the form $f(r) \cos s\theta \cos \sigma t$ but also the form $f(r) \sin s\theta \sin \sigma t$. If both these forms appear simultaneously, the surface elevation is given by $f(r) \cos (s\theta-\sigma t)$. This represents a wave formation displaying at each instant the simple (s, n) nodal pattern but moving unchanged in form round the tank with a period equal to s times the (s, n) modal period, i.e. s times the period of the vertical motion of the water at any point. This observation will turn out to be of great significance in considering the wave formation resulting from the circulation of a strut or strut and model round the tank : a wave pattern rotating unchanged in form round the tank clearly offers the possibility of resonance in response to a disturbance circulating round the tank at the same speed.

---

* See Gray, Mathews and MacRobert, 1931, *Bessel Functions*, 2nd ed. (London: Macmillan and Co. Ltd.), p. 261.

Fig. 4

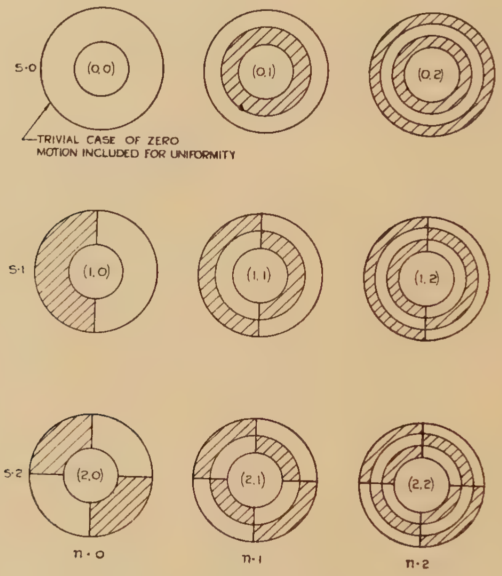

Nodal character of simple modes.

§ 3. WAVE FORMATION DUE TO A CIRCULATING DISTURBANCE

(i) *Scope of Analysis*

This section presents a theoretical analysis of the wave formation round the inner wall of an annular tank, filled with water to only a shallow depth, when a pressure point circulates round the outer wall of the tank. This case is a somewhat restricted one and the treatment is not entirely rigorous but it is possible to draw general conclusions which are subsequently compared with the results of observation.

(ii) *Outline of Method*

The velocity potential ϕ of the wave formation resulting from a pressure distribution $p_0(r, \theta, t)$, which varies with time over the surface, is to be determined. Since the water is shallow, ϕ may be assumed to satisfy the following equation :

$$\frac{\partial^2\phi}{\partial r^2}+\frac{1}{r}\frac{\partial\phi}{\partial\theta}+\frac{1}{r^2}\frac{\partial^2\phi}{\partial\theta^2}-\frac{1}{c^2}\frac{\partial^2\phi}{\partial t^2}=-\frac{1}{\rho c}\frac{\partial p_0}{\partial t}, \quad . \quad . \quad . \quad (7)$$

where c is written for $\sqrt{(gh)}$ and $\partial\phi/\partial r$ must vanish at the walls of the tank. Eventually p_0 will be specialized to the case of a pressure point materializing at zero time and then moving in a circular path round the tank. Since the velocity potential is equal to the impulsive pressure, ϕ will remain unchanged initially everywhere except in the immediate neighbourhood of the newly created pressure point. So the initial values of ϕ and of $\partial\phi/\partial t$ may both be taken as zero.

Multiplying each term of (7) by $e^{-\alpha t}$ and integrating with respect to t over the range $(0, \infty)$, with due regard to the initial values of ϕ and $\partial\phi/\partial t$, yields the following equation:

$$\frac{\partial^2\phi^*}{\partial r^2}+\frac{1}{r}\frac{\partial\phi^*}{\partial r}+\frac{1}{r^2}\frac{\partial^2\phi^*}{\partial\theta^2}-\frac{\alpha^2}{c^2}\phi^*=-\frac{1}{\rho c}\int_0^\infty e^{-\alpha t}\frac{\partial p_0}{\partial t}\,dt, \quad . \quad . \quad (8)$$

where the Laplace transform, ϕ^*, of ϕ is defined as follows:

$$\phi^*(r, \theta, \alpha)=\int_0^\infty e^{-\alpha t}\phi(r, \theta, t)\,dt. \quad . \quad . \quad . \quad . \quad . \quad (9)$$

$\partial\phi^*/\partial r$ is zero at the walls of the tank.

It will be convenient to develop a solution for ϕ^* in a Fourier series, written formally as follows:

$$\phi^*(r, \theta, \alpha)=f_0(r)+f_1(r)\cos\theta+\ldots+f_s(r)\cos s\theta+\ldots$$
$$+g_1(r)\sin\theta+\ldots+g_s(r)\sin s\theta+\ldots \quad . \quad . \quad (10)$$

To this end it is useful to have a formal Fourier series expression for the right-hand side of (8), namely

$$(-1/\rho c)\int_0^\infty e^{-\alpha t}(\partial p_0/\partial t)\,dt=\lambda_0(r)+\lambda_1(r)\cos\theta+\ldots+\lambda_s(r)\cos s\theta+\ldots$$
$$+\mu_1(r)\sin\theta+\ldots+\mu_s(r)\sin s\theta+\ldots, \quad (11)$$

where the $\lambda_s(r)$ and the $\mu_s(r)$ will depend on the particular form of p_0, which is yet to be specified. It follows from (8), (10) and (11), together with the boundary conditions on $\partial\phi^*/\partial r$, that $f_s(r)$ must satisfy the following equation:

$$f_s''(r)+(1/r)f_s'(r)-\{(\alpha/c)^2+(s/r)^2\}f_s(r)=\lambda_s(r), \quad . \quad . \quad . \quad (12)$$

and that $f_s'(a)$ and $f_s'(b)$ are both zero. An expression for f_s in terms of λ_s can now be written down at once, namely

$$f_s(r)=\int_a^b \eta\lambda_s(\eta)F_s(\eta, r)\,d\eta, \quad . \quad . \quad . \quad . \quad . \quad . \quad . \quad (13)$$

where $F_s(\eta, r)$ is the appropriate Green's function. When r lies between a and ξ, the Green's function takes the form

$$F_s(r, \xi)=U_s(b, \xi)U_s(a, r)/V_s(a, b), \quad . \quad . \quad . \quad . \quad . \quad (14)$$

and, when r lies between ξ and b, it takes the form

$$F_s(r, \xi)=U_s(a, \xi)U_s(b, r)/V_s(a, b), \quad . \quad . \quad . \quad . \quad . \quad . \quad . \quad (15)$$

where $$U_s(b, \xi)=K_s'(\alpha b/c)I_s(\alpha\xi/c)-I_s'(\alpha b/c)K_s(\alpha\xi/c), \quad . \quad . \quad . \quad (16)$$

and $$V_s(a, b)=K_s'(\alpha a/c)I_s'(\alpha b/c)-K_s'(\alpha b/c)I_s'(\alpha a/c), \quad . \quad . \quad (17)$$

the functions I_s and K_s being modified Bessel functions. An expression, precisely similar to that relating f_s to λ_s, relates g_s to μ_s. Thus the f_s and g_s can be found when the λ_s and μ_s, corresponding to the surface pressure distribution appropriate to the present problem, are known.

From (10) the solution for ϕ can be determined by inversion of Laplace transforms in the form :

$$\begin{aligned}\phi=\{L^{-1}f_0(r)\}+\{L^{-1}f_1(r)\}\cos\theta+\ldots+\{L^{-1}f_s(r)\}\cos s\theta+\ldots\\ +\{L^{-1}g_1(r)\}\sin\theta+\ldots+\{L^{-1}g_s(r)\}\sin s\theta+\ldots. \qquad (18)\end{aligned}$$

In this solution $L^{-1}f_1(r)$ is given by the following expression :

$$L^{-1}f_1(r)=(1/2\pi i)\int_{\alpha_1-i\infty}^{\alpha_1+i\infty} e^{t\alpha}f_1(r)\,d\alpha, \quad \ldots\ldots \quad (19)$$

α_1 being real and greater than the real parts of all the singularities of the integrand : similar expressions hold good for the other Fourier coefficients. The wave elevation ζ can be deduced by equating $g\zeta$ to $\partial\phi/\partial t$. Examination of $L^{-1}f_s(r)$ and $L^{-1}g_s(r)$ will show how the (s, n) mode responds to the assigned surface pressure distribution, which is to be a circulating pressure point.

(iii) *The Circulating Pressure Point*

The particular surface pressure distribution, $p_0(r, \theta, t)$, of interest here is the circulating pressure point moving round the tank on a fixed radius d with angular velocity ω. By definition $p_0(r, \theta, t)$ will be taken to differ from zero only when certain conditions are all fulfilled together, namely when $t>0$, when $d<r<d+\epsilon$ and when $\omega t<\theta<\omega t+\epsilon$; when these conditions are all fulfilled, $p_0(r, \theta, t)$ is defined to take the value $1/\epsilon^2$. For the case $(d<r<d+\epsilon)$ the function may be expressed as a Fourier series

$$p_0(r,\theta,t)=(1/2\pi\,d\epsilon)+(1/\pi\,d\epsilon)\left\{\sum_{s=1}^{\infty}\cos s\omega t\cos s\theta+\sum_{s=1}^{\infty}\sin s\omega t\sin s\theta\right\}. \quad (20)$$

Proceeding in a purely formal manner with the development of an expression of the type (11), it follows that, for the case $(d<r<d+\epsilon)$,

$$\begin{aligned}(-1/\rho c)\int_0^{\infty} e^{-\alpha t}(\partial p_0/\partial t)\,dt=(1/\pi\rho c\,d\epsilon)\\ \times\left[\sum_{s=1}^{\infty}\{s^2\omega^2/(\alpha^2+s^2\omega^2)\}\cos s\theta-\sum_{s=1}^{\infty}\{\alpha s\omega/(\alpha^2+s^2\omega^2)\}\sin s\theta\right]. \quad . \quad (21)\end{aligned}$$

In the cases $(a\leqslant r\leqslant d)$ and $(d+\epsilon\leqslant r\leqslant b)$ this integral is zero. By comparison with (11), the $\lambda_s(r)$ and the $\mu_s(r)$ are both zero unless the condition $(d<r<d+\epsilon)$ is fulfilled, in which case

$$\lambda_s(r)=s^2\omega^2/\{(\alpha^2+s^2\omega^2)\pi\rho c\,d\epsilon\}, \quad \ldots\ldots \quad (22)$$

and

$$\mu_s(r)=-(\alpha/s\omega)\lambda_s(r). \quad \ldots\ldots\ldots\ldots \quad (23)$$

These expressions can now be used in (13) to evaluate $f_s(r)$ and in the analogous expression to evaluate $g_s(r)$, as follows :

$$f_s(r)=\{s^2\omega^2/\pi\rho c(\alpha^2+s^2\omega^2)\}U_s(a, r)U_s(b, d)/V_s(a, b), \quad . \quad . \quad (24)$$

and

$$g_s(r)=-(\alpha/s\omega)f_s(r). \quad \ldots\ldots\ldots\ldots\ldots \quad (25)$$

In the case where r takes the value a and d takes the value b, appropriate when the wave formation round the inner wall due to a disturbance moving round the outer wall is to be determined, the expression for $f_s(r)$ reduces to the following form :

$$f_s(r)=cs^2\omega^2/\{\pi\rho ab\alpha^2(\alpha^2+s^2\omega^2)V_s(a, b)\}. \quad . \quad . \quad . \quad (26)$$

(iv) *Response of Normal Modes*

A discussion of the terms $L^{-1}f_s(r)$ and $L^{-1}g_s(r)$ in (18) will now lead to a determination through $\partial\phi/\partial t$, which is proportional to the wave elevation, of the response of the normal modes to a circulating pressure point. The response of the normal modes will be examined at the inner wall and it will be supposed that the pressure point circulates round the outer wall : this means that the simplified expression (26) for $f_s(r)$ and the corresponding expression for $g_s(r)$ hold good. This simpler case can be expected to show the main features of what happens in the general case.

Since $f_0(r)$ is zero, so is $L^{-1}f_0(r)$. It follows that modes of the type $(0, n)$, that is, axially symmetric modes, are not aroused by a circulating pressure point.

In the general case, when $s^2\omega^2$ differs in value from k^2c^2,

$$L^{-1}f_s(r)=(1/2\pi i)\int_{\alpha_1-i\infty}^{\alpha_1+i\infty} e^{t\alpha}f_s(r)\,d\alpha, \quad . \quad . \quad . \quad . \quad (27)$$

and the right-hand side is equal to the sum of the residues of $e^{t\alpha}f_s(r)$ at its singularities. $f_s(r)$ has simple poles when α has the value ikc, where k is a root of eqn. (4), and also when α has the value $(-ikc)$. The contribution of these two simple poles to the value of the expression on the right-hand side of (27) is as follows :

$$[L^{-1}f_s(r)]_k=[2s^2\omega^2/\{\pi\rho abk^2(s^2\omega^2-k^2c^2)A_{s,k}\}]\sin kct, \quad . \quad . \quad (28)$$

where $A_{s,k}$ is a numerical constant depending only on s, k, a and b. When this expression is combined with the corresponding one arising from $L^{-1}g_s(r)$, and the result is differentiated with respect to time, it is found that, in the general case, the (s, n) mode is aroused by a circulating pressure point as follows :

$$\zeta=\{(\text{Factor})/(s^2\omega^2-\sigma^2)\}\{\cos(\sigma t-s\theta)+(1-s\omega/\sigma)\sin\sigma t\sin s\theta\}. \quad . \quad (29)$$

In the case when $s^2\omega^2$ has the value k^2c^2, the significant term, for the (s, n) mode, in $L^{-1}f_s(r)$ is as follows :

$$[L^{-1}f_s(r)]_{s\omega}=-(c/\pi\rho abs\omega A_{s,s\omega/c})t\cos s\omega t. \quad . \quad . \quad . \quad (30)$$

There is a similar significant term in $L^{-1}g_s(r)$. Combining these terms and deriving the wave elevation, it follows that, in the particular case when $s^2\omega^2$ has the value k^2c^2, the (s, n) mode is aroused by a circulating pressure point as follows :

$$\zeta=(\text{Factor})t\sin s(\omega t-\theta). \quad . \quad . \quad . \quad . \quad . \quad . \quad . \quad (31)$$

In point of fact, ζ contains some other terms appropriate to the (s, n) mode but these have been neglected since their amplitude does not increase with t.

(v) *Conclusions*

The preceding analysis enables useful conclusions to be drawn about how the normal modes of wave motion of the water in an annular tank will respond when a strut or strut and model move round the tank with angular velocity ω. Although the analysis was confined to a special case, the following conclusions may be expected to be valid in the general case :

(*a*) Modes of the type $(0, n)$, that is, axially symmetric modes, are never aroused by a circulating strut.

(*b*) The (s, n) mode is aroused in the following way in the general case $(s\omega \neq \sigma,\ s \neq 0)$, $\sigma/2\pi$ being the normal frequency of the (s, n) mode :

$$\zeta = \{(\text{Factor})/(1-\sigma^2/s^2\omega^2)\}\{\cos(\sigma t - s\theta) + (1 - s\omega/\sigma)\sin\sigma t \sin s\theta\}.$$

When $s\omega$ is nearly equal to σ, this represents a wave travelling unchanged in form round the tank with a small variation superposed.

(*c*) The (s, n) mode is aroused in the following way in the case $(s\omega = \sigma,\ s \neq 0)$:

$$\zeta = (\text{Factor})t \sin(\sigma t - s\theta) + \text{terms whose amplitude does not grow with time.}$$

Thus a large amplitude wave, travelling unchanged in form round the tank, can be expected to grow up when ω has one of the values σ/s.

Thus, according to theoretical expectations, the strut has certain critical speeds, namely when ω has one of the values σ/s, where $\sigma/2\pi$ is the frequency of any (s, n) mode. Near these speeds the corresponding (s, n) mode of wave motion in the tank may be expected to build up a large amplitude: the surface appearance will be that of a simple (s, n) nodal pattern rotating round the tank at about the same speed as the strut.

§ 4. EXPERIMENTAL OBSERVATIONS

The theoretical expectations have been confirmed by visual observations of the wave patterns arising in the A.R.L. tank when a strut and model were towed round at speeds near the critical speeds for the simplest modes as tabulated below. It is difficult to observe visually the nodal character of more complicated modes. In general, at arbitrarily selected speeds of strut and model, no wave disturbance builds up. In the table below, $\omega/2\pi$ is the frequency with which the strut completes circuits of the tank.

Mode	Critical values of $\omega/2\pi$	
(s, n)	Calculated	Observed
(1, 0)	0·229	0·235
(1, 1)	0·922	0·982
(1, 2)	1·31	1·38
(2, 0)	0·216	0·221
(2, 1)	0·475	0·500
(2, 2)	0·660	0·703
(2, 3)	0·805	0·850
(3, 0)	0·200	0·205
(3, 1)	0·330	0·345
(3, 2)	0·443	0·461
(3, 3)	0·537	0·562

Mode	Critical values of $\omega/2\pi$	
(s, n)	Calculated	Observed
(4, 0)	0·183	0·189
(4, 1)	0·260	0·266
(4, 2)	0·338	0·350
(4, 3)	0·405	0·425
(5, 0)	0·167	0·172
(5, 1)	0·220	0·226
(5, 2)	0·276	0·282
(5, 3)	0·328	0·340

The differences between the calculated and observed critical values of $\omega/2\pi$ can be ascribed to the swirl set up round the tank by the circulating strut and model. The observed value is effectively measured relative to a fixed radius of the tank : relative to the water the strut and model are moving more slowly. This explains why the observed values are always greater than the calculated values. The actual magnitude of the swirl depends on the speed of the strut and, up to a point, on how long the arm has been running at the time of observation.

In all the cases listed except one the wave patterns built up could be clearly seen to have the expected numbers of diametrical and circumferential nodes. The exception was the (1, 2) mode : at the high speed required to arouse this mode a large swirl builds up and wavelets arising as the water streams past cracks and projections on the tank wall give the surface a rough appearance : the condition of the surface prevented certain observation of the number of circumferential nodes in this particular case. In all cases the wave pattern rotated round the tank, as expected, at the same speed as the strut.

The amplitude of the waves set up will depend on the wave energy put into the water by the strut and model, on how close to the critical value the arm is run and on the damping at the sides and bottom of the tank. The damping has not been considered in the theory but will certainly vary from mode to mode. The wave amplitudes at the outer wall were about 1 inch in a depth of 22 inches for most of the modes listed. The (1, 1) mode is an exceptional example of a mode which can easily be persuaded to build up an amplitude greater than 6 inches.

Modes, other than those in the systematic series set out above to provide experimental evidence in support of the theoretical predictions, have also been observed but it seems likely that the very complicated modes with large numbers of diametrical and circumferential nodes are too heavily damped to be aroused by a circulating strut and model to any great extent.

§ 5. SUMMARY

It has been demonstrated that the normal modes of wave motion of the water in an annular tank form a doubly infinite set whose nodal character appears to be as illustrated in fig. 4, each mode being characterized by the number, s, of diametrical nodes and the number, n, of circumferential nodes. When a strut and model are towed round the tank at an arbitrarily selected speed, the water in the tank is relatively undisturbed by wave motion. But when the strut and model are towed round with a frequency approximately equal to the frequency of the (s, n) mode divided by s, then a wave disturbance of fairly large amplitude is liable to appear. The wave disturbance takes the form of the (s, n) nodal pattern rotating round the tank at about the same speed as the strut.

ACKNOWLEDGMENT

This paper is published by permission of the Admiralty.

XC. *On Tin Whiskers*

By F. C. Frank
H. H. Wills Physical Laboratory, University of Bristol*

[Received May 18, 1953]

Summary

The growth of tin whiskers is explained as a process in which oxidation of the whisker surface develops a stress which draws out a continuing thread of metal from the main mass. A mechanism is provided by a dislocation in the main mass which travels continuously around the root of the whisker. It then follows that the whisker axis should be parallel to the Burgers vector of the dislocation, i.e. a slip direction in the crystal. All that is needed to start the process is an oxidizing or other reactive atmosphere, a small knob on the surface, and a dislocation. The order of magnitude of the growth rate can be satisfactorily accounted for. The substantially uniform thickness of whiskers is explained because the growth rate increases rapidly with diminution of radius, but below a certain radius the process fails because the tensile stress at the root fractures the whisker. The angular bends produced in whiskers subjected to a very high bending stress is attributed to an unusual kind of deformation twinning.

Some metals, e.g. tin and cadmium, spontaneously grow fine whiskers on their surfaces by mere preservation in air (Compton *et al.* 1951). The probability of whisker growth is dependent on the way in which the surface was prepared, in ways not wholly elucidated. The whiskers are remarkably strong (Herring and Galt 1952). The present writer was first instructed about these whiskers in a private discussion with Herring and Galt some two years ago. Various possible mechanisms of whisker growth were discussed, including, in principle, the one which forms the subject of this note. As he recollects, it was the present writer who suggested the mechanism, while the driving force to operate it was suggested by Herring, who proposed that it came from surface oxidation, effectively reducing the surface free energy to a negative value and so encouraging a process by which the surface area of the body spontaneously increases. There were obviously alternative conceivable (even if improbable) mechanisms, which could be classified as those involving growth at the root and those involving growth at the tip, and we agreed that an experimental decision on this matter was desirable. A screw dislocation along the axis of the whisker is apparently needed for mechanisms of tip-growth, and the rather surprising demonstration by

---

* Communicated by the Author.

Eshelby (1953) that the dislocation would be in stable elastic equilibrium removed an obvious difficulty in the way of such mechanisms. One such has been published by Peach (1952), in which the driving force for whisker growth comes from the reduction of dislocation energy in the interior of the specimen : it requires remarkably easy diffusion of atoms along dislocation cores. All mechanisms of this type are now eliminated in the case of tin by the experimental demonstration by Koonce and Arnold (1953) that tin whiskers grow at the root. The mechanism discussed below appears to be in agreement with all the presently known facts.

If a dislocation terminates on a crystal surface, there is always some motion of the dislocation which will expose new atoms at the surface. For a screw dislocation, this motion is a glide, raising a new step in the crystal surface. For an edge dislocation the motion is a climb, exposing a new row of atoms in the surface which still remains flat. (The terminology is that of Frank 1951.) In consequence, the dislocation line in equilibrium, supposing it to be anchored at an interior point (e.g. at a dislocation node) will terminate at right angles to the free surface only if the net surface free energy, after allowing for chemical reaction with the environment (hereafter oxidation, for short) is zero. In general, it will have an equilibrium angle of incidence which we shall count as positive when the dislocation is displaced from the normal so as to expose fewer atoms and negative when it is displaced from the normal so as to expose more atoms. Positive and negative angles of incidence are thus associated with positive and negative values of the net surface free energy. Let us suppose the net surface free energy is negative : a nearly equivalent statement is that the metal oxide, even when very finely divided, is thermodynamically stable with respect to bulk metal and air. Then a dislocation end will travel over the metal surface unless and until it finds a position of equilibrium, determined by its anchor point, the net surface free energy, and elastic interactions with other dislocations, with the free surface, and any other sources of stress or elastic inhomogeneities. If in its travel, it meets a groove in the surface, since it has effectively a line tension, it will usually attach itself to the groove, and continue along the groove in its further travel. The rate of travel, supposing the surface oxidation rate imposes no delay, will be governed by the rate of diffusion of vacancies from or to the dislocation line in the interior. This is necessary, except when the dislocation is a pure screw, and it can be this only instantaneously, if in its motion it passes through a fixed point. Suppose now it attaches itself to a groove which forms a closed path : unless in this closed path it reaches a position of equilibrium, it will go round and round the same path indefinitely. The periphery of any small projection from a smooth surface can provide such a groove. For each circuit made by the dislocation end, the knob will be displaced by a distance and direction corresponding to the Burgers vector of the dislocation. The result of many circuits will be the growth of a cylinder, based on the original peripheral groove, its generators being parallel to the Burgers vector of the dislocation. A prediction from this theory for the mechanism of growth is that the axis of a whisker will always be parallel to a possible Burgers vector of a dislocation in the crystal: that is, in general, a close-packed direction.

For each circuit, a number of vacancies must leave the dislocation line, equal in volume to the right sectional area of the cylinder multiplied by the length of the Burgers vector. Since, then, there is always a source of vacancies near the root of a growing whisker, one might suppose these would sometimes settle on the surface of the whisker, progressively reducing its cross-section. Since, however, its side surfaces all belong to the zone of a close-packed direction, they are more nearly close-packed than a randomly chosen surface of the crystal, as we may suppose the surrounding flat surface to be. Hence all the vacancies may diffuse to the latter surface: or the reduction of the whisker may proceed a certain way on some faces of the cylinder until it forms a prism bounded by particularly close-packed surfaces.

To discuss the rate of the process, let us idealize the model by considering the whisker to be a circular cylinder, normal to the surrounding surface, and the dislocation line anchored at a point on the axis of the cylinder, coplanar with the free surface. Then the sweeping arm of the dislocation is a pure edge, sweeping in a plane, and the remaining portion may be a pure screw parallel to the fibre axis, but stretching into the interior of the main mass, not along the fibre. We shall assume that the surface oxidation process is rapid, and draws the dislocation end around, curving the dislocation into some spiral form, and that the rate-controlling process is the diffusion of vacancies away from this curved dislocation.

The observed growth rates, of the order of some millimetres per year. say 10^{-8} cm/sec, require an emission of about 10^7 vacancies per second from the root of a whisker of radius 1 micron. This is an emission rate of 3×10^{14} per cm^2 per sec. It may be compared with the equilibrium number of wandering vacancies which cross unit area in unit time according to a vacancy theory of diffusion. This is $a^{-4}D_s$, where D_s is the coefficient of self-diffusion and a the interatomic distance. According to the measurements of Fensham (1950, 1951), made over the temperature range 180°–223°C, the self-diffusion coefficients of tin are

$$D_c=3{\cdot}6\times 10^{-6}\exp(-9400/RT)\ \mathrm{cm^2/sec},$$

$$D_a=9{\cdot}2\times 10^{-8}\exp(-6700/RT)\ \mathrm{cm^2/sec}.$$

According to a vacancy theory of diffusion, since a tin atom has neighbours on the c-axis, but none precisely on the basal plane, there is a mechanism for transfer in the c-direction without transfer in the a-direction, but no mechanism for transfer in the a-direction without transfer in the c-direction. Hence D_c cannot be validly extrapolated by Fensham's formula below the temperature (88°C) at which D_c and D_a are equal.

For lower temperatures D_c should be proportional to D_a, and of the same order of magnitude, the process responsible for a higher value of D_c at higher temperature ceasing to be of importance. The extrapolated values at room temperature (290°K) are $D_c=3{\cdot}6\times10^{-13}$ cm²/sec and $D_a=9{\cdot}2\times10^{-13}$ cm²/sec. To our required accuracy we can therefore take the self-diffusion coefficient of tin at room temperature to be isotropic and equal to 10^{-12} cm²/sec : $a^{-4}D_s$ is then about 10^{18} per cm² per second, so that the required unidirectional excess is only a small fraction of this.

The energy of a dislocation ring of radius ρ is approximately

$$E=\tfrac{1}{2}\mu a^2\rho \ln (\rho/a), \qquad (1)$$

where μ is the rigidity modulus. The number of vacancies liberated in its complete collapse is

$$n=\pi\rho^2/a^2. \qquad (2)$$

The differential energy per vacancy is consequently

$$E'=dE/dn=(\mu a^4/4\pi\rho) \ln (e\rho/a)\sim\mu a^4/\rho, \qquad (3)$$

e being the base of natural logarithms. Since μa^3 is about 3 ev, E' is about 10^{-3} ev when ρ is 1 micron. The vacancy concentration in equilibrium with such a ring exceeds that in equilibrium with straight dislocations (or flat free surfaces) by a factor

$$\alpha=\exp (E'/kT)\sim1+E'/kT. \qquad (4)$$

The same may be taken for any arc of dislocation line of the same curvature provided it is not subject to large stresses from neighbouring dislocations. The number of vacancies diffusing in unit time from a length l of curved dislocation to a surface maintaining the ordinary equilibrium vacancy concentration N_{vac} a mean distance R away is given by the concentration excess, $N_{\text{vac}}[\exp (E'/kT)-1]$, divided by the diffusion impedance $(1/2\pi lD_{\text{vac}}) \ln (R/r_0)$, where D_{vac} is the diffusivity of vacancies and r_0 is the distance from the dislocation line at which it is assumed to maintain its own equilibrium vacancy concentration. Thus the net number of vacancies emitted per unit time is

$$n'=2\pi lN_{\text{vac}}D_{\text{vac}}[\exp (E'/kT)-1]/\ln (R/r_0). \qquad (5)$$

Since according to a vacancy theory of diffusion

$$D_s=(1/6)a^3N_{\text{vac}}D_{\text{vac}}, \qquad (6)$$

(5) gives

$$n'=12\pi la^{-3}D_s[\exp (E'/kT)-1]/\ln (R/r_0). \qquad (7)$$

Taking $E'/kT=4\times10^{-2}$, and $R/r_0=10^4$, we have

$$n'\sim0{\cdot}15la^{-3}D_s. \qquad (8)$$

Since $a^{-2}D_s$ is about 10^3 sec⁻¹, it follows that a spiral of one turn would give $n'\sim10^6$ sec^{-1}, about ten times too small. For a greater length of spiral we must revise the calculation so as to take account of the interactions between the parallel arcs of dislocation.

The state of strain around a dislocation spiral of s turns, with an overall radius r, the Burgers vector being normal to the plane and the sense of the spiral being such that the stress is tensile at the centre and compressive at the periphery, will be taken as equivalent to that produced when the faces of a lens-shaped cavity of thickness sa and radius r in an elastic medium are forced into contact and welded together, the external forces then being removed. The energy is

$$E=\beta\mu s^2a^2r, \quad \ldots \ldots \ldots \quad (9)$$

where β is a factor of order unity : its exact calculation, bearing in mind that the cavity is situated at the junction of cylindrical and plane boundaries of the solid, would not be simple. The equivalent number of vacancies is

$$n=\pi r^2 s/2a^2. \quad \ldots \ldots \ldots \quad (10)$$

Hence the differential energy per vacancy, with constant r, is now

$$E'=dE/dn=4\beta\mu sa^4/\pi r. \quad \ldots \ldots \ldots \quad (11)$$

This exceeds the value of E' for the former case (eqn. (3)) approximately by the factor s, the number of turns in the spiral. The steady state value of s may be estimated by equating dE/ds to $2\pi rQ/a$ where Q is the free energy released by oxidation per surface lattice site of the metal. This gives

$$s=\pi Q/\beta\mu a^3. \quad \ldots \ldots \ldots \quad (12)$$

In this formula both Q and β are uncertain, the former being proportional to the thickness of oxide layer formed in a time of the order of magnitude 1 second. Each molecule of SnO_2 formed liberates approximately 6 ev (Kubaschewski and Evans 1951). We shall say only that values of s of the order of magnitude 10 or 100 are reasonably likely. Combination of eqns. (11) and (12) gives

$$E'=4Qa/r. \quad \ldots \ldots \ldots \quad (13)$$

We must also consider the mutual interference of neighbouring turns of the spiral in the diffusion process. There has to be, in time average, a uniform flux of vacancies from the area covered by the spiral. The diffusion impedance, represented above as $\ln(R/r_0)/2\pi lD_{\text{vac}}$, cannot for any increase in l fall below the value corresponding to uniform steady emission from this surface which we can estimate roughly as $1/2rD_{\text{vac}}$. This introduces a factor approximately equal to s which is unfavourable to whisker growth.

Thus the two effects of mutual interference between turns of the spiral tend to compensate each other, and do so fairly completely so long as $E'<kT$. Only when $E'>kT$ is there a substantial gain in rate, by the factor

$$(kT/E')[\exp(E'/kT)-1].$$

The rate of growth of a whisker is now given by

$$dL/dt=n'a^3/\pi r^2=(12D_s/\pi r)[\exp(4Qa/rkT)-1], \quad \ldots \quad (14)$$

which for large radii is inversely proportional to r^2, increasing more rapidly with decrease of radius below $4Qa/kT$. This radius is about

1 micron if Q is about 20 ev, corresponding to the formation of a triple layer of oxide: and the growth rate is then of the right order of magnitude.

This suffices to explain why whiskers are thin. Now we need to explain why they are not thinner. The probability that a wandering dislocation will meet a knob and start it growing into a whisker is presumably proportional to its radius, but if this were the only reason we ought to see a few very thin whiskers growing very fast. However, by the same considerations that led to eqn. (9), we may estimate that there is a tensile stress at the root of the whisker of the order of magnitude $\mu sa/r$, again with a rather uncertain numerical factor. For very small radii this must reach the ultimate fracture stress of the perfect crystal, and snap the incipient whisker off at the root instead of continuing to draw out an indefinite length of coherent metal.

The theory leads us to expect an induction period before the growth of whiskers, firstly because dislocations must first find their knobs, and secondly because the driving force on a single turn of spiral is relatively small, as we have seen above, increasing as further spiral turns are wound around it. The growth should accelerate and settle down to a steady rate when the dislocation has wound itself up into a rotating spiral of stationary form.

Our simplifying assumption that the dislocation line had an anchor point in the plane of the free surface is inessential. Parallel edge dislocations exert forces on each other tending to hold them in a plane perpendicular to the Burgers vector. On account of these forces, the spiral should remain substantially planar, except near the centre, without any central anchor point.

The same mechanism can in principle operate to produce porosity, drilling holes in the surface instead of growing whiskers. To initiate a hole, we need a circular groove with banks steeper on the outside than the inside, like the inside bottom of a wine-bottle. This is not likely to go on for so long, partly because the growing tip of a hole recedes from the free surface, which is the likely source of vacancies, and partly because the hole grows into the dislocation network, and will lose its dislocation if it passes a node on which the dislocation is anchored. It is also likely to be slower because if $E' > kT$, the exponential factor is unfavourable to growth in this case.

One further characteristic of tin whiskers requiring explanation is the sharp angular bends they acquire if bent round a cylinder to a strain exceeding 2 or 3%, as described by Herring and Galt (1952). The present writer would interpret this phenomenon as a twinning process of an unusual kind. It will be recollected that there are two different planes passing through a given point in a body which remain undeformed after a homogeneous shear. As a result of the shear, the angle 2ϕ between these two planes changes to its supplement, and conversely. The shear may reduce to a simple shear on either of these planes, and an ordinary twin forms as a plate or lens parallel to one or the other. The magnitude of the shear is 2 cot 2ϕ. We may conceive of a process in which a wedge of material bounded by the two different undeformed planes undergoes the twinning shear. There are two such possibilities : one in which an initially obtuse wedge becomes acute and the other in which an initially acute wedge becomes obtuse. In either, the portions of the matrix on either side of the wedge are rotated relatively to each other by an angle of $\pi-4\phi$. The resulting bend in a rod can be as large as this, or less, according as the edge of the wedge is perpendicular to the axis of the rod or inclined to it. It is difficult to predict intermediate configurations in the formation of such a twin. One which would have relatively low energy would contain parallel laminae of ordinary twins within the volume of the wedge, but it is not clear how or whether these could nucleate in the substantially perfect crystal : but with elastic strains of 2 or 3% in a metal ‘ almost anything ’ may happen. In the example shown by Herring and Galt the whisker is bent through about 70°. Hence ϕ is about $27\frac{1}{2}°$, or less, and the corresponding twinning shear 1·4 or more. It is doubtless unwise to try and identify a twinning process on such meagre information : nevertheless the crystallography of tin suggests a hypothetical mode. The lattice of tin is equivalent to that of diamond, shrunk by a factor 0·38 along a cube axis. Expansion along this axis and contraction along one of the other cube axes of diamond will regenerate the tin lattice. The corresponding value of ϕ is arc tan 0·38=21° and the corresponding shear 2·2.

REFERENCES

COMPTON, K. G., MENDIZZA A., and ARNOLD, S. M., 1951, *Corrosion*, **7,** 327.

ESHELBY, J. D., 1953, *J. Appl. Phys.*, **24,** 176.

FENSHAM, P. J., 1950, *Australian J. Sci. Res.* A, **3,** 91 ; 1951, *Ibid.* A. **4,** 229.

FRANK, F. C., 1951, *Phil. Mag.* [7], **42,** 809.

HERRING, C., and GALT, J. K., 1952, *Phys. Rev.*, **85,** 1060.

KOONCE, S. E., and ARNOLD, S. M., 1953, *J. Appl. Phys.*, **24,** 365.

KUBASCHEWSKI, O., and EVANS, E. Ll., 1951, *Metallurgical Thermochemistry* (London : Butterworth-Springer Ltd.), p. 254.

XCI. *The Mass of the V_1^0-Particle*

By R. Armenteros, K. H. Barker, C. C. Butler, M. S. Coates and M. G. Sowerby
The Physical Laboratories, The University, Manchester*

[Received April 16, 1953]

Abstract

Accurate measurements have been made on the decay products of 22 low-energy V_1^0-particles. It is shown that the experimental data are consistent with the decay process

$$V_1^0 \rightarrow p^+ + \pi^- + (42^{+3}_{-2}) \text{ mev},$$

the secondary particles being emitted isotropically in the rest system of the V_1^0-particle. The corresponding mass of the V_1^0-particle is $(2195 \pm 6) m_e$. The results are compared with those obtained by other groups of workers.

§ 1. Introduction

Armenteros *et al.* (1951) were the first workers to show that one type of neutral V-particle decays into a proton or a heavy positive meson and a light negative meson. Somewhat later the Manchester workers (Armenteros, Barker, Butler and Cachon 1951) analysed a number of decays of this type and concluded that the positive particle is probably a proton and the negative particle a π-meson. The small number of decays then available was analysed according to the following scheme :—

$$V_1^0 \rightarrow p^+ + \pi^- + Q. \quad . \quad . \quad . \quad . \quad . \quad . \quad . \quad . \quad (1)$$

The Q-value, or kinetic energy released in the rest system of the unstable particle when it decays, was found to be about 45 mev. Many other workers have found similar results. A detailed discussion of the data available in 1951 was given by Butler (1951). More recently, extensive experiments have been carried out by Leighton *et al.* (1953), Fretter *et al.* (1953) and Bridge *et al.* (1953).

The data discussed in this paper were obtained on the Pic-du-Midi (2867 m) using the magnet and cloud chamber described by Armenteros, Barker, Butler and Cachon (1951). Decays with heavily ionizing positive secondary particles, with masses greater than 800 m_e, are selected for the analysis, thus avoiding confusion with V_2^0-particles, which decay into two light mesons (cf. Armenteros, Barker, Butler and Cachon 1951, Barker 1953).

§ 2. A Summary of the Properties of the Decay Products of V_1^0-Particles

The main properties of the decay products of V_1^0-particles have been discussed by several groups. No new evidence on the nature of the secondary particles is given in this paper but it seems desirable to summarize briefly the most important results of the various experiments.

---

* Communicated by the Authors.

(i) *The Positive Secondary Particle*

Several groups (e.g. Armenteros, Barker, Butler and Cachon 1951, Leighton *et al.* 1953) have reported a considerable number of mass determinations for positive secondary particles, using momentum measurements and ionization estimates. The mass values are distributed round the proton mass. These mass measurements, however, are not very accurate and do not exclude the possibility that the positive secondary has a mass of $1500 m_e$ and may be a χ-meson, while in a few cases the mass may be as low as $1000 m_e$. No group, however, has reported observing a decay of a slow positive secondary particle. We estimate that these particles have been observed for a proper time of at least 5×10^{-8} sec. Therefore very few of the positive secondary particles are likely to be heavy mesons, unless their lifetime is longer than 5×10^{-8} sec.

Only one example of a heavy negative meson associated with a light positive meson has been reported (Leighton *et al.* 1953), although at least 200 decays with slow positive secondaries about as massive as the proton have been observed. Therefore, assuming that both positively and negatively charged heavy mesons would be produced in equal numbers, we conclude that the majority of the heavy positive secondary particles are probably protons. This conclusion is confirmed by the results of Bridge *et al.* (1953), who observed 12 heavy secondary particles coming to rest in thin lead plates inside their cloud chamber. The sign of these particles is unknown but they are about as massive as the proton. No visible decay products were produced and, therefore, it is most unlikely that the heavy particles were unstable mesons, such as the χ-mesons or S-particles.

(ii) *The Negative Secondary Particle*

Mass determinations by several groups show that the mass of the negative secondary particle is approximately (200–300) m_e. The results of Leighton *et al.* (1953), however, suggest that it is usually a π-meson. Support for this conclusion has been obtained by Armenteros, Barker, Butler and Cachon (1951), Leighton *et al.* (1951) and the authors who have observed the decays in flight of three negative secondary particles. These decays were characteristic of the π-meson. The corresponding positive particle of one π-meson was a proton or heavy positive meson (Leighton *et al.* 1951). Two secondary particles observed by Bridge *et al.* (1953), which were light mesons, made nuclear interactions in thin lead plates. In both cases the other secondary was heavily ionizing, so that the two decays were probably produced by V_1^0-particles decaying into protons and negative π-mesons.

(iii) *The Existence of Neutral Secondary Particles*

No direct evidence for the existence of interacting neutral secondary particles has been found, although Fretter *et al.* (1953) and Bridge *et al.*

(1953) have searched for electron cascades produced by γ-rays or by the decay of π^0-mesons. Indirect tests for the presence of a neutral particle have been made using the spatial orientation of the decay products with respect to the origins of the unstable particles. If only the two charged secondary particles are produced, then the forks should be coplanar with the nuclear interactions producing the V_1^0-particles. The most important results are those of Bridge *et al.* (1953). These workers have examined the ‘ coplanarity ’ of 15 forks produced by low-energy V_1^0-particles. They were all found to be coplanar, within the accuracy of the measurements. An approximate theoretical calculation by Brueckner and Thompson (1952) shows that, if a light neutral particle is produced, there should be a marked departure from coplanarity for such low-energy events. We conclude, therefore, that the V_1^0-particle decays into only two secondary particles.

The evidence available at present on the nature of the secondary particles suggests that the scheme (1) originally used by Armenteros *et al.* is probably correct for the majority of the V_1^0-particles.

§ 3. The Momentum Errors

Details of the camera used to photograph the chamber and of the methods used to measure track curvatures have been given previously (Armenteros, Barker, Butler and Cachon 1951). However, in the earlier work no correction was applied for the fact that the track image on the film is not an orthogonal projection. This correction, which can be very large for tracks steeply inclined to the plane of the chamber, is easily calculated from the stereoscopic reprojection measurements ; for the present results the correction is rarely greater than ten per cent (cf. Leighton *et al.* 1953). Leighton *et al.* have also pointed out an associated curvature correction which should be made if the magnetic field has an appreciable non-axial component. The correction, which would be tedious to apply, has not been made since it is never likely to be greater than 2 or 3% for the Pic-du-Midi magnet.

The track lengths available for measurement, given in columns (2) and (3) of table 1, are small, the average length being 7–8 mm on the film. The most important errors in the curvature measurements are due to multiple coulomb scattering in the cloud chamber gas and to the inherent track noise. The noise, which is due mainly to the random diffusion of the ions formed along the path of a particle prior to the onset of condensation, is approximately inversely proportional to the square of the track length. For a minimum ionization track of good quality 1 cm long on the film, the R.M.S. noise is equivalent to a curvature of about $0{\cdot}25\ \mathrm{m}^{-1}$; for a heavily-ionizing track of the same length the noise curvature is somewhat smaller. The average momentum corresponding to a curvature of $0{\cdot}25\ \mathrm{m}^{-1}$, for the Pic-du-Midi chamber with a mean magnetic field of 7500 gauss and an average magnification of 0·1, is about 10 Bev/c. The mean gaseous distortion level, determined

Table I. Measurements on the Secondary Tracks of 22 V_1^0-particles

(1)	(2)	(3)	(4)	(5)	(6)	(7)	(8)	(9)	(10)	(11)	(12)
1	6	4	8–15	194± 30	181^{+36}_{-24}	29±2	52^{+18}_{-13}	65^{+22}_{-15}	47^{+17}_{-12}	47^{+7}_{-6}	+0·04
2	6	10	3–4	565± 80	171± 8	49±1	43± 4	54± 4	43± 4	106± 5	+0·61
3	6	7	2–3	436± 54	200±20	42±3	52±10	65±11	47± 9	98±10	+0·42
4	8	2·5	2–4	504± 46	34^{+22}_{-9}	114±4	27^{+10}_{-5}	26^{+11}_{-5}	35^{+11}_{-6}	32^{+21}_{-9}	+1·05
5	6	20	4–6	293± 32	108± 4	86±1·5	37± 3	44± 3	39± 3	99± 4	+0·73
6	12	10	3–4	420± 30	160± 8	40±1	33± 3	43± 4	30± 3	79± 4	+0·49
7	8	6	4–7	205± 31	149±12	38±1	37± 6	48± 7	32± 6	56± 5	+0·18
8	7	12	2–5	405± 40	179± 9	45±1	45± 4	57± 5	41± 4	93± 5	+0·44
9	8	10	2–4	582± 68	172±10	51·5±2	47± 5	56± 6	47± 5	111± 7	+0·63
10	3·5	8	4–10	346± 52	165±13	57±4	48± 8	60± 9	47± 7	104±10	+0·44
11	10	5	2–4	497± 49	110± 9	73±3	39± 6	44± 6	43± 6	97± 8	+0·81
12	7	6	2–5	605^{+125}_{-90}	33± 5	123±3	37^{+11}_{-8}	34^{+9}_{-7}	46^{+14}_{-11}	28± 4	+1·06
13	4·5	4·5	>10	124^{+54}_{-29}	176^{+29}_{-21}	61±2	64^{+18}_{-13}	78^{+20}_{-14}	61^{+17}_{-12}	73^{+20}_{-11}	−0·23
14	4	5·5	3–6	430±100*	166^{+25}_{-19}	32±2	31^{+11}_{-9}	41^{+13}_{-11}	29^{+10}_{-8}	66^{+8}_{-7}	+0·47
15	6	6	4–7	360± 70*	155^{+25}_{-18}	66±4	51^{+14}_{-10}	61^{+16}_{-11}	50^{+13}_{-10}	114^{+16}_{-13}	+0·53
16	6	6·5	4–7	360± 70*	169±12	38±2	38± 7	49± 7	36± 6	74± 7	+0·40
17	8·5	10	4–8	250± 32	164± 8	44±2	44± 4	56± 5	40± 4	74± 5	+0·24
18	12	12	2–3	690± 63	320±16	17±0·5	59± 8	75± 9	45± 7	65± 3	+0·37
19	4	5	2–5	560±150*	79± 6	95±3	44±12	46±10	42±14	79± 6	+0·98
20	2·5	8	3–6	430±100*	82± 6	92±6	34± 7	37± 7	32± 9	81± 6	+0·94
21	3·5	3	3–5	180^{+52}_{-33}	86^{+15}_{-11}	110±6	29^{+8}_{-6}	34^{+9}_{-7}	30^{+8}_{-6}	85^{+14}_{-10}	+0·86
22	7	6	2–4	514^{+98}_{-73}	236^{+37}_{-27}	45±4	69^{+19}_{-15}	83^{+21}_{-16}	64^{+18}_{-14}	122^{+18}_{-15}	+0·43

* Positive momentum calculated from ionization assuming proton.

Column (1). Event number. Columns (2) and (3). Useful track length in mm on the film for the positive and negative secondary particles respectively. Column (4). Ionization range for positive secondary (I/I_{min}). Columns (5) and (6). Momentum measurements in units of Mev/c on positive and negative secondaries, respectively (i.e. p_+ and p_-). Column (7). Angle of fork in degrees. Columns (8), (9) and (10). Q-values (Mev) for schemes (1), (2) and (3) respectively. (Proton mass=1836 m_e, π-meson 276 m_e.) Column (11). The transverse momenta p_T (Mev/c). Column (12). The number α.

by measurements on long meson tracks in zero magnetic field, is equivalent to an R.M.S. curvature of 0·2 m^{-1} and never makes a major contribution to the error. The total curvature error, taken as the root mean square of the sum of the squares of the effects of track noise, gas scattering and measurement error, is assumed to be symmetrically distributed. Hence some of the quoted momentum errors are asymmetric.

In the conversion of track curvature to particle momentum the average magnetic field along the track has been used, and this may introduce a systematic error as large as 1 or 2%. It is likely that any residual systematic errors in the momentum estimates are mainly random and simply broaden the calculated Q-distributions.

§ 4. The Experimental Data

Measurements on twenty-two forks produced by V_1^0-particles are given in table 1. The errors in the momenta, given in columns (5) and (6), are standard errors and have been assessed in the manner described in § 3, while the errors in the angles, which are never important, have been estimated.

The twenty-two events were chosen because they have heavily ionizing positive secondary particles, which were probably protons, and have tracks long enough for accurate measurements to be made. Approximate ionization estimates for the positive particles are given in column (4) of table 1. The momenta of five of the positive secondary particles cannot be measured with sufficient accuracy; useful values can be obtained, however, using the ionization estimates and assuming the masses.

Six of the decays listed in table 1 were published by Armenteros, Barker, Butler and Cachon (1951). They have now been re-measured and the necessary systematic corrections applied.

§ 5. The Q-Values

The twenty-two decays are analysed first of all on the basis of the two-body decay scheme (1). The Q-values, given in column (8) of table 1, have a mean value of 43·6 Mev. The main uncertainty in an individual Q-value for a V_1^0-decay, when the positive secondary is heavily ionizing, is usually due to the error in the momentum of the negative meson (cf. Leighton *et al.* 1953). The frequency histogram for the Q-values, shown in fig. 1 (*a*), is obtained by distributing the observations between the 10 Mev cells. The observed distribution is asymmetrical; Leighton *et al.* (1953) have pointed out that this is to be expected since, for a given percentage accuracy in the momentum and angle measurements, the error in Q increases approximately proportionally to Q. An approximately normal histogram can be obtained by plotting a histogram of the values of log Q, as is shown in fig. 1 (*b*). The Gaussian distribution on the log scale transformed to the linear scale of Q (fig. 1 (*a*)) has a spread of $(^{+13}_{-10})$ Mev, which is somewhat greater than the average error in the individual Q-values. The best Q-value is (42^{+3}_{-2}) Mev. In § 3 it was pointed out that residual systematic errors in the momenta probably do not exceed 2%. An error of this magnitude would change individual Q-values by about 2 Mev.

Fig. 1

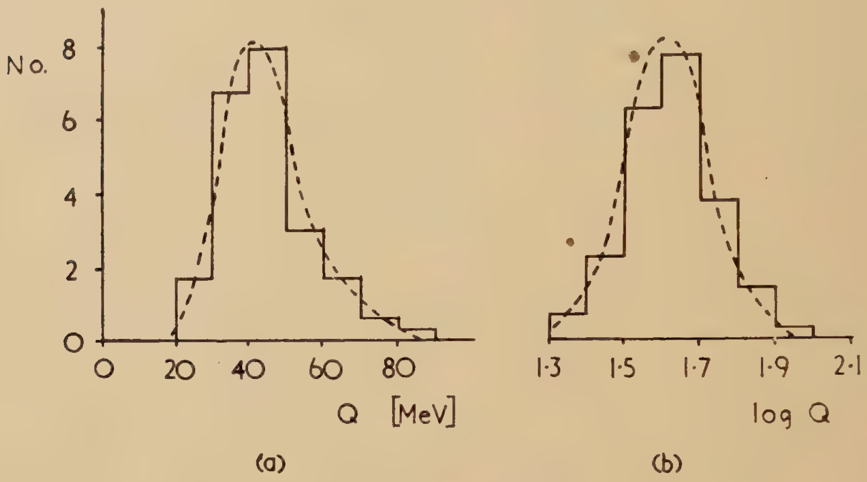

Frequency histograms of Q-values

(*a*) The Q-value histogram assuming scheme (1).
(*b*) The histogram of the values of log Q, assuming scheme (1).

Both histograms have been constructed in the following manner. Suppose an event with a Q-value of (37^{+11}_{-9}) Mev is to be plotted; it is distributed uniformly between (28–48) Mev so that in the intervals (20–30), (30–40) and (40–50) Mev there are contributions of 0·1, 0·5 and 0·4 respectively. Therefore each event contributes the same area to the histogram. The various contributions in the 10 Mev cells are added to obtain the final histogram.

It should be pointed out that the unique Q-value obtained for scheme (1) does not prove that this decay process has been chosen correctly. Q-values are given in columns (9) and (10) of table 1 for the following two possible decay schemes :—

$$V_1^0 \rightarrow \mathrm{p}^+ + \mu^-, \qquad (2)$$

$$V_1^0 \rightarrow \chi^+ + \pi^-, \qquad (3)$$

where the mass of the χ-particle is assumed to be 1500 m_e. The best Q-values are (51^{+4}_{-3}) Mev and (41^{+3}_{-2}) Mev for schemes (2) and (3) respectively.

The deviation of the individual Q-values from the best Q-value ranges are shown in table 2. The best Q-value ranges are given in row (1) of table 2 and the number of decays with Q-values which differ from the ranges by various amounts are given in rows (2), (3) and (4). There is no indication of an abnormal number of accurate Q-values at the edges of the Q-value distributions. Thus the examination of the Q-value histograms shows that each one is approximately consistent with a unique Q-value.

The Q-value distribution for scheme (1) is somewhat broader than the individual errors indicate. This may be due to systematic errors (cf. § 3) or possibly to the presence of a neutral secondary particle. Brueckner and Thompson (1952) have made a theoretical investigation of the shape of the apparent Q-value distribution assuming that the neutral particle is either a π^0-meson or a neutrino. They describe the Q-value calculated assuming only the two charged secondary particles as an apparent Q-value. A χ^2-test shows that the two theoretical distributions are incompatible with the present data and it can be concluded that the majority of the V_1^0-particles decay without the production of neutral secondary particles (cf. § 2 (iii)).

Table 2. Numbers of Decays Deviating by Various Amounts from the Best Q-values

Best Q-value	Scheme (1) (40–45) Mev	Scheme (2) (48–55) Mev	Scheme (3) (39–44) Mev
No. <1.S.D.	16	13	18
No. >1.S.D. <2.S.D.	5	8	3
No. >2.S.D. <3.S.D.	1	1	1

§ 6. The Angular Distribution of the Secondary Particles in the Rest System

For a two-body decay process, the secondary particles are expected to be distributed isotropically in the rest system of the unstable particle. The fraction of the events in which the proton is emitted backwards in the rest system can be found from the values of $\alpha=(p_+^2-p_-^2)/P^2$, where p_+, p_- and P are the momenta of the secondary particles and the V_1^0-particle respectively. This parameter α was first defined by Armenteros and Podolanski (1951, unpublished). Armenteros, Barker, Butler and Cachon (1951) showed that α is greater or less than the value $\alpha^*=(m_+^2-m_-^2)/M^2$, depending on whether the proton is emitted forwards or backwards in the rest system. M, m_+ and m_- are the masses of the V_1^0-particle and its secondaries respectively. The value of α^* for a decay into a proton and a π-meson with a Q-value of 42 Mev is 0·69, and from the values of α tabulated in column (12) of table 1 it can be seen that in 15 out of the 22 decays the proton was emitted backwards in the rest system. However, only decays with heavily ionizing positive secondary particles have been considered in this analysis. This procedure probably introduces a selection bias. For example, there are 11 decays with positive secondary particles having $I/I_{\min} \geqslant 3$ and with primary momenta greater than 400 Mev/c; eight of these have $\alpha<\alpha^*$, so that for 73% of the observed decays the proton is emitted backwards in the rest system. On the assumption that the differential momentum spectrum of the V_1^0-particles is flat in this region, it can be shown that the expected fraction is 60%. It is probable that there are other sources of bias, introduced by the selection procedure. It may be noted that the results of other groups (Fretter *et al.* 1953, Bridge *et al.* 1953, Leighton *et al.* 1953) also show bias effects.

The isotropy of emission can be investigated in a more detailed manner by examining the distribution of the transverse momentum component, p_T. This theoretical distribution, given by Armenteros, Barker, Butler and Cachon (1951), is modified by experimental errors in a manner which can readily be calculated (cf. Barker 1953). From the individual values of p_T, given in column (11) of table 1, the frequency histogram in fig. 2 has been constructed in a manner identical to that used earlier for the Q-values. The contribution of events with forward emitted protons ($\alpha > 0{\cdot}69$) is shaded. The dotted curve in fig. 2, which is the theoretical distribution for a Q-value of 42 MeV modified by an average error of 10%, is consistent with the experimental histogram. Hence, taking into account the selection bias, it is concluded that the available data are in agreement with the assumption of isotropic emission of the secondaries in the rest system of the decaying V_1^0-particle.

Fig. 2

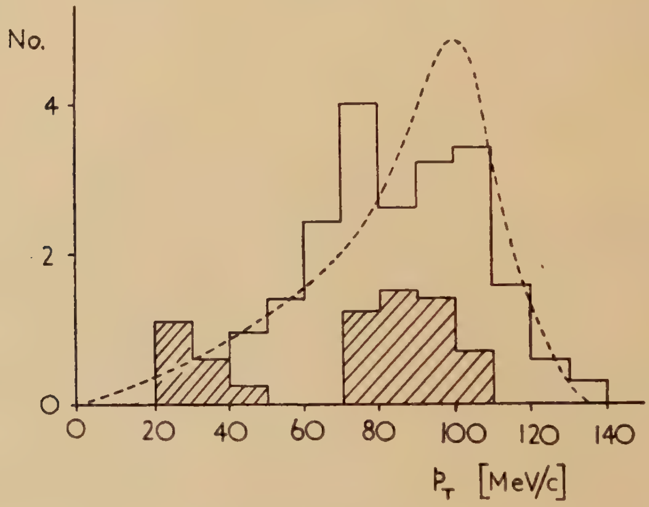

The p_T-distribution.

§ 7. Discussion

It is possible that a small fraction of the decays listed in table 1 were not produced according to scheme (1). An example of a particle decaying into a heavy negative particle of mass (450–1000) m_e and a positive meson (Leighton *et al.* 1953) is mentioned in § 2, where it was pointed out that not more than one or two of the decays with heavy positive secondaries, usually attributed to V_1^0-particles, are likely to be due to these particles.

Decay number 13 in table 1, however, is a possible example. When interpreted by scheme (2), the Q-value is considerably greater than 42 MeV, but it is consistent with this value. If we now interpret the event by the following scheme discussed by Barker (1953)

$$V_3^0 \rightarrow \tau^+ + \pi^- + Q, \quad . \quad . \quad . \quad . \quad . \quad . \quad . \quad (4)$$

the Q-value is 53 MeV, close to other values reported by Barker. Therefore, this decay can be explained by either of schemes (1) or (4).

The Q-values discussed in § 5 can be compared with those obtained recently by other groups. Leighton *et al.* (1953) have published a histogram of 62 Q-values for V_1^0-particles, assuming scheme (1). The average error of a single Q-value in this distribution is 30%. The distribution has a peak at about 35 MeV and stretches up to 100 MeV, with some indication of a subsidiary peak at 75 MeV. The present data are consistent with the general form of this distribution but they do not confirm the existence of the second peak at 75 MeV.

Bridge *et al.* (1953), using a multiplate chamber, have obtained 22 Q-values for V_1^0-particles, assuming scheme (1). Each fork is coplanar with the origin of the V_1^0-particle and the range of one (or sometimes both) of the secondaries can be measured. These measurements enable Q-value ranges to be calculated for each decay ; they are consistent with a unique Q-value within the range (35–40) MeV. This value and the peak at (35 ± 3) MeV found by Leighton *et al.* are appreciably lower than the best Q-value of (42^{+3}_{-2}) MeV found from the present data. The discrepancy may be either purely statistical or due to residual systematic errors.

§ 8. CONCLUSIONS

The analysis of the decays of 22 low-energy V_1^0-particles shows that they can be interpreted by any of the two-body schemes (1), (2) or (3). The evidence described in § 1, however, is overwhelmingly in favour of scheme (1) and thus we conclude that the majority of the V_1^0-particles decay into a proton and a negative π-meson with a Q-value of (42^{+3}_{-2}) MeV. The corresponding mass of the V_1^0-particles is $(2195 \pm 6)m_e$.

ACKNOWLEDGMENTS

We wish to thank Professor P. M. S. Blackett, F.R.S., for his continued interest and support for our work, and Dr. G. D. Rochester for reading the manuscript. We remain indebted to Dr. J. Rösch, the Director of the Observatoire du Pic-du-Midi, for permission to work at the Observatory. The physicists of the École Polytechnique working at the Pic-du-Midi have given us considerable assistance with the experimental work. We have received a financial grant from the Department of Scientific and Industrial Research, who have given M. S. Coates and M. G. Sowerby maintenance allowances.

REFERENCES

ARMENTEROS, R., BARKER, K. H., BUTLER, C. C., CACHON, A., and CHAPMAN, A. H., 1951, *Nature, Lond.*, **176,** 501.

ARMENTEROS, R., BARKER, K. H., BUTLER, C. C., and CACHON, A., 1951. *Phil. Mag.*, **42,** 1113.

BARKER, K. H., 1953, *Proc. Roy. Soc.* A, in the press.

BRIDGE, H. S., PEYROU, C., ROSSI, B., and SAFFORD, R., 1953, *Phys. Rev.*, in the press.

BRUECKNER, K. A., and THOMPSON, R. W., 1952, *Phys. Rev.*, **87,** 390.

BUTLER, C. C., 1951, *Progress in Cosmic Ray Physics* (Amsterdam : North Holland Publishing Company), p. 105.

FRETTER, W. B., MAY, M. M., and NAKADA, M. P., 1953, *Phys. Rev.*, **89,** 168.

LEIGHTON, R. B., WANLASS, S. D., and ALFORD, W. L., 1951, *Phys. Rev.*, **83,** 843.

LEIGHTON, R. B., WANLASS, S. D., and ANDERSON, C. D., 1953, *Phys. Rev.*, **89,** 148.

XCII. *The Intensity of the Photon Component at* 70 000 *feet Altitude*

By John E. Hooper
H. H. Wills Physical Laboratory, University of Bristol*

[Received April 27, 1953]

Abstract

The intensity of high energy γ-rays traversing photographic emulsions can be determined by measurements on the electron-pairs resulting from the materialization of the quanta. A difficulty in the practical application of the method arises from the failure to observe short or steeply dipping tracks. A method of correcting for unobserved tracks of electron-pairs is discussed, and is used to obtain an estimate of the vertical intensity of the photon component of the cosmic radiation at 54° N. and at an altitude of 70 000 feet. It is convenient to express the intensity in terms of the ratio of the number of quanta to the number of high energy nucleons at the same altitude. A value of $2{\cdot}88 \pm 0{\cdot}26$ for this ratio has been found. The result is in satisfactory agreement with that calculated on the basis of reasonable assumptions about the energy and frequency of production of π^0-mesons in nuclear collisions in the atmosphere.

§ 1. Introduction

Previous attempts to obtain information about the intensity of the photon component of the cosmic radiation have been made with counters (e.g. Jánossy and Rossi 1940). There are, however, serious difficulties in obtaining reliable information by this method, particularly through the difficulty of distinguishing effects due to neutrons and γ-rays (Clay 1949) and no attempt appears to have been made to measure directly the intensity of the photon component at high altitudes. Of the various instruments at present available for the detection of extremely high energy photons, the nuclear emulsion is one of the most satisfactory. Not only does it allow individual photons to be detected with considerable efficiency ; it also permits the energy of favourable examples to be determined by observations of the energy of the pairs of electrons produced by the materialization of the photons. The most important difficulty met in applying the method is associated with the fact that in searching for electron tracks, many of the shorter or more steeply dipping tracks are inevitably missed. It is therefore necessary to develop a reliable method of allowing for this ‘ loss ’ of tracks.

---

* Communicated by Professor C. F. Powell, F.R.S.

The density of the electron-pairs in Ilford G5 nuclear emulsions. exposed at 70 000 feet altitude for 100 minutes at 54° N. (Camerini, Coor, Davies, Fowler, Lock, Muirhead and Tobin 1949) has been measured in this laboratory in the course of an experiment on the lifetime of the neutral meson (Carlson, Hooper and King 1950, later referred to as 'C'). In this experiment the plates were extremely carefully examined on account of the great importance attached to observing every electron-pair. The emulsions used were 400 microns thick, and a value of 24±2 pairs per cm^2 emulsion was obtained. This result has been confirmed by O'Ceallaigh (1950) who searched the same series of emulsions for electron-pairs related to π–μ decay events. The observed density of electron-pairs in the emulsion is thus found to be

$$N_O=600\pm50 \text{ pairs/cm}^3 \text{ emulsion.}$$

§ 2. CORRECTION FOR UNOBSERVED EVENTS

Although consistent, the above values are too low because of a failure to observe all the pairs. It will be assumed that the 'loss' occurs only for tracks which are particularly short, or which dip very steeply. A correction for this effect can be made in the following manner. At 70 000 feet the zenith angle distribution of the electron-pairs is known to be isotropic in the lower hemisphere (C). It follows that if the origins of the pairs are distributed at random, the number in a given volume of emulsion with tracks of length greater than l, $N(l)$, is given by the relation

$$N(l)=K[\sqrt{(X^2+l^2)}-l], \qquad \ldots\ldots \quad (1)$$

where K is a constant whose value depends on the total density of events, and X is the thickness of the slab of emulsion, whose lateral dimensions are assumed to be very large compared with X. For simplicity, it has been assumed that the two tracks of an electron-pair are of the same length, an assumption that is approximately true for all but the longest tracks, or for those of electrons of very low energy.

The figure shows the distribution in length of the electron tracks as defined by eqn. (1), together with the distribution observed experimentally. In determining the latter distribution the length of the shorter track of a pair has been plotted in every instance. The theoretical distribution has been normalized to the experimental one by adjusting K so that the predicted number of pairs with lengths between 2000 microns and 4000 microns is equal to that observed experimentally. It is immediately apparent that very large numbers of shorter events have not been observed. The calculated ratio, N_T/N_O, of the actual number of pairs to that observed is

$$N_T/N_O=2{\cdot}74.$$

The corresponding value of the total density of pairs is

$$N_p=1640\pm137 \text{ pairs/cm}^3 \text{ emulsion.}$$

§ 3. Ratio of the Photon Intensity to the Nucleon Intensity

The mean free path in the emulsion of a γ-ray for the production of an electron pair is known to be 4·6 cm. This figure has been calculated for the known energy spectrum of the photons and takes into account the variation of the cross-section for pair-production with energy (C). Thus the total length of photon path in the emulsion is

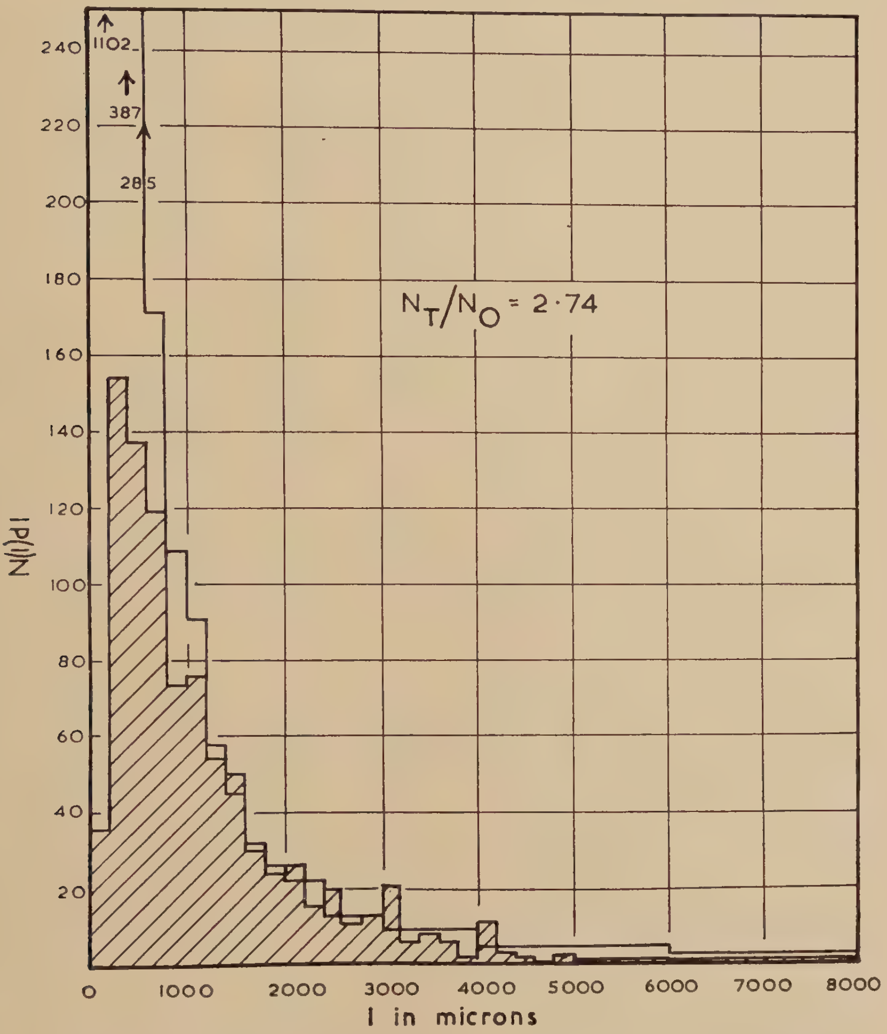

The calculated (unshaded) and observed (shaded) distributions in length of electron-pairs.

$$L_p = 4{\cdot}6 \times N_p = 7600 \pm 630 \text{ cm per cm}^3 \text{ emulsion.}$$

The corresponding length of nucleon track in the emulsion may be found in a similar manner. Nuclear disintegrations in the same series of emulsions have been studied by Camerini *et al.* (1951). These workers observed 15 300 such disintegrations in 87 cm^3 emulsion. Of these, 11 100 were produced by primary particles of low energy and have no 'shower' particles associated with them. The remainder, 4200 events, were produced by primary particles of higher energy, and have one or more 'shower' particles associated with them. Most of these events were produced by particles with an energy >1000 MEV (Camerini, Davies. Fowler, Franzinetti, Muirhead, Lock, Perkins, Yekutieli 1951) and they alone will be considered, because it is then possible to use the nucleon cascade without ionization loss (Messel 1951) when comparing the final experimental result with that obtained from simple assumptions. The density of such events is

$$N_s = 48{\cdot}5 \pm 0{\cdot}7 \text{ stars/cm}^3 \text{ emulsion.}$$

We assume that the interaction length of the high energy nucleons is 25 cm, corresponding to a geometrical cross-section of the nuclei for collisions with protons (e.g. Froelich, Harth and Sitte 1952). It is further assumed that very few charged π-mesons enter the emulsions from the surrounding atmosphere, an assumption justified by the short lifetime of the particles and the absence of all but small quantities of local matter in which the π-mesons might be generated (Lock and Yekutieli 1952).

Thus we find for the total length of nucleon track in the emulsion

$$L_n = 1200 \pm 20 \text{ cm nucleon track/cm}^3 \text{ emulsion.}$$

On account of the geometry of the sensitive volume of the emulsions. a direct comparison of L_p and L_n will only lead to a true value of the relative intensity of the photon component if the zenith-angle distributions of the particles which enter the plates are closely similar. This is not so. While the zenith-angle distribution of the photons is isotropic in the lower hemisphere, (C), that of the nucleons decreases with increasing zenith angle. The actual angular distribution of the nucleons may be computed from a knowledge of their absorption in the atmosphere and the use of the Gross transform. From this treatment it follows that the angular distributions of the protons and neutrons are the same, provided that their interaction lengths are equal. At 70 000 feet the angular distributions both of the photons and of the nucleons are similar in the cone of half angle 20° about the vertical. It is therefore convenient to confine the observations to the relative lengths of tracks with directions within this cone, and thus to obtain the ratio of the vertical intensities of the two components. With this procedure it is found that the length of nucleon track which satisfies this condition is

$$L_{nv} = 160 \pm 3 \text{ cm nucleon track/cm}^3 \text{ emulsion}$$

and the corresponding length of photon track is

$$L_{pv} = 460 \pm 40 \text{ cm photon track/cm}^3 \text{ emulsion.}$$

The ratio of the vertical intensity of the photons to that of the high energy nucleons is now given by a direct comparison of the two lengths :

$$R=N_{pv}/N_{nv}=L_{pv}/L_{nv}=(460\pm40)/(160\pm3)=2{\cdot}88\pm0{\cdot}26.$$

§ 4. DISCUSSION

Most of the photons which enter the plates are produced by the decay of π^0-mesons emitted from nuclear disintegrations in the atmosphere above the plates. The number of stars produced, as a function of atmospheric depth, may be found from the theory of the nucleon cascade as developed by Messel (1951), together with the corresponding vertical nucleon intensity. We have assumed that the ratio of neutral to charged π-mesons created in energetic nuclear collisions is 0·5 (C), and that the average number of mesons produced per star is 2·2 (Camerini *et al.* 1951). This value has been calculated for those disintegrations in which one or more ' shower ' particles are produced. The neutral mesons are further assumed to be produced with the same distribution in energy as the charged mesons, a distribution which has been determined by Camerini, Fowler, Lock and Muirhead (1950). At very high energies the differential energy spectrum of the mesons is assumed to be of the form

$$N(E)dE=a\,.\,E^{-2{\cdot}7}dE.$$

This leads to the correct form of the spectrum of the μ-mesons at sea-level in this energy range ($E>10\,000$ MEV ; see Wilson 1946). It is to be remarked that the altitude-intensity curve of the photons is dependent on the form of the spectrum of the neutral mesons from which they originate.

In order to test the reliability of the above assumptions they have been employed to calculate the intensity of the various components of the cosmic radiation as a function of atmospheric depth. The results obtained were found to be in satisfactory agreement with the experimental results obtained by Schein (quoted by Montgomery 1949, p. 163), and with the curves and experimental points given by Rossi (1948, fig. 2).

Using these results it is found that the ratio of the vertical intensities of photons to high energy nucleons ($E>1000$ MEV) at an atmospheric depth of 50 g/cm² air is

$$R=2{\cdot}62\ ;$$

a result in satisfactory agreement with that obtained experimentally.

In obtaining the above value of R we have neglected those photons which arise in cascade showers initiated by electrons from the decay of μ-mesons. Rossi (1949) has shown that the proportion of electrons at this altitude which arises from the decay of μ-mesons is of the order of 20%. As the plates were exposed at an atmospheric depth which corresponds to just over one radiation length, the proportion of the total number of photons to which these electrons give rise must be small. The true value of R should therefore be a few per cent higher than that quoted above.

ACKNOWLEDGMENTS

The author wishes to take this opportunity of thanking Prof. C. F. Powell, F.R.S., for his interest and encouragement in the course of this work. He further wishes to express his thanks to Dr. W. O. Lock and Dr. G. G. Harris for helpful discussions and criticism. The work has been carried out as part of a research programme supported by the Department of Industrial and Scientific Research, to which body the author is also indebted for a maintenance grant.

REFERENCES

CAMERINI, U., COOR, T., DAVIES, J. H., FOWLER, P. H., LOCK, W. O., MUIRHEAD, H., and TOBIN, N., 1949, *Phil. Mag.*, **40,** 1073.

CAMERINI, U., FOWLER, P. H., LOCK, W. O., and MUIRHEAD, H., 1950, *Phil. Mag.*, **41,** 413.

CAMERINI, U., DAVIES, J. H., FOWLER, P. H., FRANZINETTI, C., MUIRHEAD, H., LOCK, W. O., PERKINS, D. H., and YEKUTIELI, G., 1951, *Phil. Mag.*, **42,** 1241.

CARLSON, A. G., HOOPER, J. E., and KING, D. T., 1950, *Phil. Mag.*, **41,** 701.

CLAY, J., 1949, *Rev. Mod. Phys.*, **21,** 82.

FROELICH, F. E., HARTH, E. M., and SITTE, K., 1952, *Phys. Rev.*, **87,** 504.

JÁNOSSY, L., and ROSSI, B., 1940, *Proc. Roy. Soc.* A, **175,** 88.

LOCK, W. O., and YEKUTIELI, G., 1952, *Phil. Mag.*, **43,** 231.

MESSEL, H., 1951, *Comm. Dublin Inst. Advanced Studies*, Series A, No. 7.

MONTGOMERY, D. J. X., 1949, *Cosmic Ray Physics* (Princeton : University Press).

ROSSI, B., 1948, *Rev. Mod. Phys.*, **20,** 537 ; 1949, *Ibid.*, **21,** 104.

WILSON, J. G., 1946, *Nature, Lond.*, **158,** 414.

XCIII. *Experiments on the Reduction of Crystals of Silver Bromide*

By H. D. KEITH and J. W. MITCHELL
H. H. Wills Physical Laboratory, University of Bristol*

[Received April 23, 1953]

ABSTRACT

Crystals of silver bromide in the form of thin sheets with plane parallel surfaces have been reduced to metallic silver by a variety of methods. Before reduction, they were treated with bromine to destroy all traces of chemical fog on the surfaces and they were not again exposed to actinic light to form either a surface or an internal latent image. Reduction by photographic developers was initiated at a limited number of centres on the surface and resulted in the production of masses of silver with one of the following characteristic forms: (1) compact masses of coherent micro-crystals of silver occupying cavities bounded by (111) surfaces of the silver bromide crystal; (2) rigid projections based upon such masses and consisting of agglomerates of micro-crystals of somewhat smaller dimensions; and (3) loosely tangled bundles of micro-crystals linked by ribbon-like filaments of silver. The conditions under which silver is produced in these different forms are outlined. A series of model experiments is described which provides evidence on the mechanisms of reduction. The complexity of the problem is emphasized.

§1. INTRODUCTION

SOME of the most difficult unsolved problems of photographic research are associated with development, which is not surprising considering the complicated character of the system which has to be investigated. The reduction to metallic silver of the exposed micro-crystals of a photographic emulsion is dependent upon processes of diffusion, adsorption and dissolution. The gelatine swells in the developer and the reducing agent diffuses to the surface of the crystal. For one mechanism of development, usually referred to as chemical development, the two reactants—silver ions derived directly from the silver bromide crystal and molecules of the reducing agent—are adsorbed, in competition with other substances, at or near the interface between a silver nucleus of the latent image and the silver bromide. If they are negatively charged, as is often the case, the molecules of the developing agent must surmount a potential energy barrier to reach the adsorption sites; this is because under normal conditions of photographic development the surface of the crystal carries a negative charge. Reaction results in the formation of silver atoms and oxidation products of the developer. Bromide ions and the oxidation

---

* Communicated by the Authors.

products then diffuse away from the zone of reaction. In a second mechanism of development, referred to as pre-fixation physical development and operative when solvents for silver bromide are present, dissolution processes depending upon the formation of complex silver ions play an important role. These ions diffuse through the medium to the silver nuclei where they are adsorbed together with molecules of the reducing agent and react to give silver atoms and oxidation products. From observations which have been made during the present experimental work, it is clear that the processes of adsorption and dissolution can be profoundly influenced by the addition to the developer of traces of many organic and inorganic substances. During the course of development, reaction products accumulate in the layer of gelatine in which the microcrystals of silver bromide are suspended. These include the oxidation products of the reducing agent, which may be adsorbed either by silver or by silver bromide, and alkali bromide which is a solvent for silver bromide. Such products may modify the mechanism of reduction and must diffuse through the swelled gelatine to escape into the solution.

The number of successive processes involved in development, and the sensitivity of some of these processes to slight changes in the composition of the developing solution gives rise to great complexity. As in many other systems in which reaction occurs at interfaces, a number of alternative and competing mechanisms are possible. Which of these is predominant and decides the form in which the developed silver is produced and the kinetics of reduction is determined by many factors. It is difficult to establish these factors in experiments with photographic emulsions. The purpose of the present work is to establish them for a simpler system, large crystals of silver bromide in contact with reducing solutions.

Experimental research on photographic development has proceeded along three main lines. The object of the first group of essentially thermodynamic investigations has been to answer the question: under what physico-chemical conditions can a reducing solution cause the reduction of silver bromide to metallic silver? This field has been extensively studied by Reinders (1934, 1935, 1938) and Abribat (1952) and their co-workers. They have shown that a definite relationship, which is independent of the nature of the developing agent, exists between the potential of a silver electrode and the potential of an oxidation reduction electrode in a solution which is just capable of reducing silver bromide. Such researches permit a reasonably precise definition of the conditions under which reduction is possible. These workers have, moreover, shown that the presence or absence of a latent image does not determine whether or not reduction can occur under certain specified conditions: the function of the latent image is to catalyse rather than to make possible the reduction of the silver bromide.

The second group of investigations has been concerned with the mechanism of the reduction of silver bromide to metallic silver. This group can be further sub-divided into studies of the processes involved in the reduction of silver bromide and studies of the form in which the silver is produced. It is well known that two quite distinct processes may be operative (Mees 1942). In chemical development, it is usually assumed that silver ions from the silver bromide are reduced at the interface between a silver nucleus and the silver bromide crystal. In physical development, on the other hand, silver ions first pass into solution and then react directly or indirectly with molecules of the reducing agent on the surfaces of the silver nuclei. As regards the form in which the silver is produced by development the simplest methods of investigation utilize the optical microscope in conjunction with high speed cinematography and the electron microscope.

When the precise mechanisms of reduction have been established and when the form in which the developed silver is produced has become known through microscopic investigations, it becomes profitable to inquire into the kinetics of the different alternative mechanisms. This provides the third field of research activity and here many contributions have been made by James and his co-workers at Rochester. These researches can, in principle, account for the differentiation between exposed and unexposed crystals of silver bromide which is effected by any satisfactory photographic developer.

The results established by all these investigations have been summarized in a series of recent review articles (James and Kornfeld 1942, Mees 1942, James 1943, 1946, 1950, Berg 1948, and Abribat 1952). In these articles, also, critical accounts are given of the different mechanisms which have been proposed, mainly on theoretical grounds, for the interpretation of the experimental results. Three theories of photographic development have been advanced by different authors and all have been extensively criticized; there is at present no general agreement on the subject. First, there is the supersaturation theory of Ostwald, Abegg and Schaum which postulates that the silver bromide passes into solution where silver ions react with molecules of the developing agent to form silver atoms which remain in solution in the absence of nuclei upon which they can condense. Then there are the different theories which regard development as a catalyzed heterogeneous reaction occurring at the interface between a silver nucleus and the solution (physical development) or between a silver nucleus and the silver bromide (chemical development) due mainly to Sheppard and James. Finally, theories which ascribe photographic development to the operation of an electrode mechanism have been advanced by Gurney and Mott (1938) (see also Mott 1948), Dankov (1939), and Bagdasar'yan (1943, 1944).

Whatever may be the details of the mechanism of development, it is clear that silver ions must combine with electrons provided by molecules of the developing agent to form silver atoms and that bromide ions must pass into the solution. The theories which regard development as a catalyzed heterogeneous reaction implicitly suppose that the silver nucleus does not act as an electrical conductor during the development process. It is assumed that silver ions and molecules of the reducing agent are adsorbed together at the site of reaction. Reaction results in the formation of silver atoms on the surface of the silver nucleus and oxidation products of the reducing agent are desorbed into the solution. The charging of the silver nucleus positively or negatively through the adsorption of silver ions or molecules of the reducing agent is not usually considered in discussions of this type of heterogeneous mechanism. The charging of the silver nucleus in contact with the silver bromide or the solution is, on the other hand, postulated in all the electrode mechanisms of photographic development. A silver nucleus, large enough to behave in the same way as a silver electrode, would normally acquire a positive charge in a solution containing silver ions in the absence of an oxidation reduction system. In a solution capable of reducing silver bromide to metallic silver, it would acquire a negative charge. The adsorption of a silver ion should therefore give a silver nucleus a positive charge able to diffuse to any site on the surface of the nucleus. A negative charge, also mobile, should arise from the adsorption of a molecule of the reducing agent and the formation of its oxidation product. The successive transfer of positive and negative charges in this way should result in the formation of silver atoms ; oxidation products of the reducing agent and bromide ions from the surface of the crystal passing into the solution. It does not thus appear necessary to postulate the adsorption of silver ions and molecules of the developing agent at adjacent sites, as is usually done in the theories which regard development as a catalyzed heterogeneous reaction, and there appears to be no good reason for excluding the participation of electrode mechanisms in the reduction of silver halides.

The main object of the present experimental work was to study the reduction of large single crystals of silver chloride and silver bromide by a number of methods ; it was hoped that the experimental results would allow a decision to be made in favour of one or more of the suggested mechanisms of reduction. A number of workers have treated relatively large micro-crystals of silver halides grown from supersaturated solutions in ammonia or hydrobromic acid with photographic developers and many of their observations have been confirmed in similar experiments during the course of the present investigation. Crystals produced by solidifying sheets of molten silver bromide between glass plates were first used for experiments on development by Dankov and Kochetkov (1942). The discs which they employed consisted of a few large crystals and we have followed the method which they introduced in the bulk of our own experimental work. Later, for similar experiments, Boissonnas (1949 a, b, 1950, 1951) used discs obtained by sawing up large crystalline masses of silver bromide produced by the Kyropoulos method. To remove all traces of mechanical disturbance, he polished the discs on soft cloths moistened with a dilute solution of potassium cyanide. When the surfaces of crystals made by either of these methods are treated with photographic developers, specks of silver with well-defined geometrical contours are produced. Dankov and Kochetkov (1942) assumed that they consisted of single crystals of silver and that their formation provided evidence to support the theory of photographic development previously advanced by Dankov (1939). We shall see later that this assumption was not justified. Boissonnas recognized that the contours of the specks were determined by the intersections of (111) planes of the silver bromide structure with the surface of the crystal. Both Dankov and Kochetkov (1942) and Boissonnas (1950) noted the growth of projections on the specks under certain conditions of development.

The results which have been obtained in the present work support an electrode mechanism for the reduction of silver bromide, some features of which are similar to those of the mechanism proposed by Bagdasar'yan (1943), as will be seen in § 4.

The striking effects observed when traces of antifoggants, blue black toners, potassium iodide, potassium cyanide, sodium thiosulphate and other inorganic and organic sulphur compounds are added to the reducing solutions will be described and interpreted in another paper.

§ 2. EXPERIMENTAL TECHNIQUES

Material for Experimental Work

The method which was used for preparing thin sheets of silver bromide has already been described by Hedges and Mitchell (1953). The thin sheets of silver bromide were cut into square pieces with a side of approximately 7 mm and mounted on 3 in. × 1 in. glass slides using a small quantity of Canada Balsam. Before use, they were treated with a 10% solution of potassium bromide saturated with bromine for thirty minutes and thoroughly washed.

Electrolytic Reduction of the Surfaces of Crystals of Silver Bromide

For these experiments, the 3 in. × 1 in. slide carrying a section of silver bromide was placed on a glass frame which rested on the stage of the microscope. The square piece of silver bromide was surrounded by a glass ring and covered with a thin film of water. A pointed silver cathode mounted on a flat spring of molybdenum was brought just into contact with the surface of the specimen by suitably loading the spring. Surrounding the cathode, which was insulated almost to the point with a coating of black wax, was a ring-shaped anode of silver wire, the lower surface of which was approximately 3 mm above the upper surface of the specimen. When a potential difference, which was measured with a standard potentiometer, was applied between the two electrodes, the surface of the crystal in the neighbourhood of the cathode was reduced.

For other related experiments, two glass rings, one of which surrounded the specimen, were cemented on to the 3 in. × 1 in. slide. The specimen was covered with distilled water, a dilute solution of ammonium nitrate, or a solution with the composition of a photographic developer from which the reducing agent had been omitted. The adjacent cell formed by the other glass ring was filled to a lower level with a photographic developer. The wide end of a tapering section of silver foil 0·001 in. thick dipped into this cell, while the very fine point of the section made contact with the surface of the crystal of silver bromide in the other cell. A piece of wet filter paper or a bridge filled with a solution of ammonium nitrate connected the two cells.

Experiments with Crystals covered with Graphite Films

For one series of experiments, uniform thin films of graphite were deposited on the surfaces of mounted crystals of silver bromide by plunging them beneath the surface of a diluted solution of ‘ Aquadag ’ colloidal graphite and then slowly withdrawing them. The graphite film deposited in this way was thoroughly dried. In some experiments, it was made the cathode of an electrolytic cell ; in others, the crystals covered with graphite films were treated with a reducing solution. For still other experiments, two strips of colloidal graphite were painted on the ends of the specimen to act as the cathode and the anode for an electrolysis experiment.

Reduction of Crystals of Silver Bromide with Photographic Developers

In all the experimental work which will be reported in this paper, development was initiated at fog centres on the surfaces of the crystals. The mounted specimen was simply surrounded with a glass ring and covered with a thin film of the reducing solution which was allowed to act for a definite time. The surface of the specimen was then rinsed with distilled water or with 2% acetic acid followed by distilled water and dried. For microscopic examination it was mounted in Canada Balsam and protected with a cover glass.

Observations of the Early Stages of Development

With the method of reduction described in the previous section. it was not convenient to make observations during the progress of development, particularly at the earliest stages. A modified technique was introduced for this part of the work. The specimen was prepared for an experiment by covering it with a $1\frac{1}{4}$ in. × 1 in. cover glass, strips of the same cover glass being cemented along the edges of the 3 in. × 3 in. slide to act as spacers. The underside of the cover glass was separated from the upper surface of the specimen by 0·010 in. The slide was mounted on the stage of the microscope and illuminated with orange red light using a 1·3 N.A. achromatic condenser. A ×100 oil immersion objective was then focused on the upper surface of the specimen. When all the optical adjustments were completed and the illumination was satisfactory, a drop of developer was placed at the edge of the air gap between the cover glass and the slide. It was drawn rapidly into the gap by capillary attraction and the microscope was immediately re-focused. With this arrangement, development could be followed from its earliest stages ; it was possible to observe the absence of any significant induction period in most of the experiments. Although comparative experiments indicated that the use of a thin film of developer did not modify the mechanisms operative during the earliest stages of development, it was perfectly clear that serious modification was introduced in the later stages, due to the exhaustion of the developer and the accumulation of oxidation products of the developer and of alkali bromide. Because of this, the results obtained with the thin film technique will be reported only in so far as they relate to the early stages of development.

Observations of the Form of the Developed Silver with the Electron Microscope

Two methods have been used for preparing specimens for examination in the electron microscope. When specks of silver and specks with projections were to be examined, unmounted crystals of silver bromide were taken and developed. They were rinsed and transferred to a beaker of 2 cm^3 capacity containing a dilute solution of sodium thiosulphate which loosened the particles of developed silver so that they fell to the bottom. The beaker was then inclined on a lump of Plasticene at an angle of 45° and the particles were collected with a fine capillary tube. They were thoroughly washed and transferred to a thin Formvar film. This method did not give satisfactory results with filamentary silver. It was found that the filamentary silver was always only loosely attached and that satisfactory preparations could be made simply by gently pressing a thin Formvar film into contact with the surface of a crystal which had been developed and carefully washed and then slowly peeling it off. Specimens were often prepared by both methods for examination with the optical microscope after being mounted in Canada Balsam.

Electrolytic Reduction of Solutions containing Silver Ions

In these experiments, solutions were electrolyzed in a thin film cell with a gap of 0·010 in. prepared by separating a 1 in. × 1$\frac{1}{4}$ in. cover glass from a 3 in. × 1 in. glass slide with narrow strips of cover glass. The anode was a square ended piece of silver foil 0·001 in. in thickness and the cathode a tapering section from the same foil. The electrodes were pushed into the air gap, the separation of the tip of the cathode from the anode being 0·1 in. The gap was then filled with the solution and the slide was placed on the stage of the microscope. The condenser and objective were adjusted and the microscope was focused on the tip of the cathode. The phenomena accompanying the electrolysis of the solutions could be studied from the earliest stages with this apparatus.

§ 3. EXPERIMENTAL RESULTS

Electrolytic Reduction of a Silver Bromide Crystal

The application of a potential difference between the point cathode and the ring anode of the electrolytic cell caused the reduction of the surface of the silver bromide crystal in the immediate neighbourhood of the silver point. Masses of silver with well-defined geometrical contours were formed in cavities bounded by surfaces parallel to (111) planes of the silver bromide crystal. Experiments which were made with the intention of determining the minimum potential which has to be applied to cause electrolysis did not give reproducible results. Localized reduction occurred until the applied potential exceeded approximately 2 volts, when projections began to grow out over the surface of the crystal along ⟨100⟩ or ⟨110⟩ directions (fig. 1, Pl. 32). This recalls the behaviour previously observed in experiments on the surface conduction of dry crystals of silver bromide (Mitchell 1952). The rate of growth of these projections and also the rate of development of branching growths along the same directions depended upon the magnitude of the applied potential. When the potential difference was removed or, alternatively, when the polarity was reversed, the apparently solid masses of silver which had been formed dispersed into clouds of particles of colloidal silver in Brownian motion. This striking phenomenon provides a very convenient method for producing colloidal silver for experimental work. The particles could be observed with the microscope for considerable periods and it was found that they coagulated slowly to form aggregates consisting initially of 3, 4 or 6 particles. The shape of the aggregates was established by examining the diffraction patterns which were formed along their axes under suitable conditions of illumination. The deductions made in this way were confirmed by transferring samples, after periods of storage, to very thin Formvar films and examining the shape and dimensions of the silver crystals with the electron microscope (fig. 2, Pl. 32). It was always found that the crystals were of definite forms, squares, triangles and hexagons predominating. The dispersion of the masses of colloidal silver could be effected only immediately after their formation ; an interlocking mass of crystallites was soon formed which could not be dispersed. These experiments are of importance in demonstrating that colloidal silver is the primary product of the electrolytic reduction of silver bromide under these conditions. They also demonstrate that the masses of colloidal silver are able to conduct electrons, because the cathode makes contact with the mass in its central part while reduction takes place at the interface with the silver bromide. There will be an electrical double layer at the interface, the silver being positively charged with respect to the silver bromide, and the most direct interpretation of the experimental results is that electrons from the cathode are conducted through the mass of colloidal silver to the interface, where they combine with silver ions to form silver atoms. Bromide ions pass into the solution and drift to the anode where silver bromide is formed. The irreproducibility of the attempted measurements of a critical decomposition potential is probably connected with concentration polarization phenomena.

With the twin cell apparatus described in the section on experimental techniques, it was established that, if a conducting path for ions was provided by a bridge, silver bromide could be locally reduced in the neighbourhood of a silver electrode, the other end of which was dipping into a photographic developer. With pure distilled water in the cell in which the specimen was mounted, the form and characteristics of the silver produced round the silver electrode were identical with those of the silver which appeared at the cathode of an electrolytic cell as described at the beginning of this section. When a solution with the composition of a metol hydroquinous photographic developer from which the reducing agents had been omitted was used, the specks of silver formed by reduction at the silver electrode could not be dispersed to particles of colloidal silver. If the concentration of potassium bromide was increased and the solutions were saturated with silver bromide, fine acicular microcrystals of silver were formed on the surface of the silver electrode in contact with the solution, in addition to the direct reduction of the silver bromide which occurred round the tip of the electrode. All these effects were independent of the nature of the reducing agent in the developer contained in the other cell. The formation of filamentary silver was observed in some experiments in which sulphur compounds were present in the cell containing the silver bromide.

Reduction of a Silver Bromide Crystal with an Aluminium Point

The same apparatus as in the previous section was used for the next series of experiments. A finely pointed aluminium wire was fixed on to the flat spring with wax and its tip was brought into contact with the surface of the crystal by loading the spring. Contact between the point and the crystal was immediately followed by rapid local reduction of the silver bromide to a mass of silver occupying a cavity in the surface. Although the silver mass was soft and initially could be deformed with a glass probe, it could not be dispersed under any conditions. This is not surprising considering that aluminium bromide is formed along with silver in these experiments. The trivalent aluminium ions exert a powerful coagulating influence on colloidal silver, as was confirmed experimentally by adding a dilute solution of aluminium bromide to a suspension of colloidal silver formed, as described in the previous section, by the reduction of a crystal of silver bromide at a silver cathode. The aluminium bromide caused immediate coagulation of the colloidal silver and all Brownian movement ceased dramatically. These experiments on the reduction of silver bromide with aluminium extend the electrode mechanism by introducing the effect of ions capable of causing the coagulation of colloidal silver. Such ions are present in most photographic developers.

Further Experiments on the Electrolytic Reduction of a Silver Bromide Crystal

For these experiments, the surface of the crystal was covered with a thin conducting film of graphite. The same apparatus was used as for the experiments of the first part of this section. The silver point was brought into contact with the graphite film in the centre of the crystal and made the cathode while the ring acted as the anode. When the electrodes were covered with a thin film of water and a potential difference was applied, the crystal was reduced at a number of points on the surface. That this had occurred was revealed by gently wiping the wetted ball of a finger over the surface of the crystal to remove the graphite film. Masses of silver of remarkably regular geometrical form were produced at localized reduction centres (fig. 3, Pl. 33). It was demonstrated that they consisted of colloidal silver occupying cavities, the surfaces of which were parallel to (111) planes of the silver bromide crystal. The colloidal silver could be readily dispersed soon after its formation by covering the surface of the crystal with distilled water and disturbing the masses with a finely pointed glass probe. Immediately after the removal of the thin film of graphite, the silver could also be washed out of the cavities with a fine jet of water. The cavities after such treatment are shown in fig. 4 (Pl. 33).

This series of experiments demonstrates that when the surfaces of crystals of silver bromide are reduced by physical methods, the resulting masses of silver which have regular geometrical contours are not single crystals but aggregates of colloidal particles or micro-crystals of silver. It appears that, in these experiments, electrons are transferred through the conducting graphite film from the cathode to the reduction centres where they combine with silver ions to form silver atoms ; bromide ions pass into solution and drift to the anode.

For further experiments, crystals were prepared by painting two strips of colloidal graphite each 2 mm wide on the ends. This left a gap, 3 mm wide in the centre. The crystal was then surrounded by a ring, covered with a thin film of water and the two strips were made the anode and the cathode of the electrolytic cell. When a potential difference of about 1 volt was applied, the silver bromide was locally reduced under the cathode in the same manner as in the previous series of experiments.

Reduction of Crystals covered with Films of Graphite by Photographic Developers

Crystals of silver bromide covered with thin conducting films of graphite were now treated with different photographic developers. After the removal of the graphite film, it was found that the character and the distribution of the resulting masses of silver was superficially indistinguishable from that in the previous series of experiments. The masses of silver produced by developers made from ferrous citrate and ferrous malonate dissolved in corresponding buffer solutions could sometimes be dispersed to colloidal silver immediately after their formation, but never after the system had been left undisturbed for a short period. If ordinary commercial developers containing divalent ions such as carbonate ions and sulphite ions were used, it was found that the surface of the crystal was reduced at a number of localized points in precisely the same way, but the resulting masses of silver could never be dispersed. When the surface of a crystal was covered with a thin film of graphite, the observed rate of development was very much greater than when a bare surface of the same crystal was reduced with the same developer. These experiments suggest that electrons are transferred to the graphite film by molecules of the developer which pass into the oxidized form, and that the electrons are conducted to the development centres where they combine with silver ions at the interface between the silver and the silver bromide, bromide ions escaping into the solution. The fact that silver masses of exactly the same characteristics are formed at a slower rate in the absence of the graphite film suggests that the same mechanism is operative but that the electrons have now to be transferred directly to the silver masses from adsorbed molecules of the reducing agent. The smaller active surface area would account for the slower rate.

The Reduction of Crystals of Silver Bromide with Ferrous Developers

The direct reduction of the surface of an unexposed single crystal of silver bromide with a ferrous developer results in the formation of masses of silver with the same characteristics as those illustrated in figs. 3 and 4. The masses occupy cavities the surfaces of which are parallel to (111) planes of the silver bromide crystal. When developers produced by dissolving well washed ferrous hydroxide in a slight excess of citric, malonic or oxalic acid and then adding the sodium salt of the corresponding acid to produce a buffer solution were used, the masses of silver were sometimes plastic and readily deformable with a finely pointed glass probe immediately after their formation. On several occasions, part of the freshly formed mass of silver at the corner of a speck was dispersed during the washing and probing of the surface, giving rise to colloidal silver in Brownian motion. Dispersion could not, however, always be induced and it was not found possible to establish the precise conditions which hindered the recrystallization of the mass of silver or which resulted in the formation of crystalline silver from the outset of reduction.

The interest of these experiments lies in the observation of the dispersion and crystallization of the colloidal silver formed on some occasions as the primary product of reduction and in the absence, during the early stages of reduction, of the secondary phenomena which will be described in the following sections. The results were clearly related to those obtained in the electrolytic reduction experiments. The surfaces of the masses of silver appeared to remain level with the surface of the silver bromide crystal and when examined under vertical illumination showed a characteristic surface structure, revealed by differences in reflectivity of various parts, which did not change during the progress of development. This provides evidence that silver is not being produced on the upper surface of the mass by the reduction of silver ions from the solution because, when this occurs, the appearance of the surface changes continuously with time. The observation is not surprising on account of the dispersion of the silver masses which was sometimes observed and the initial absence of solvents for silver bromide in the developers. The only possible solvent in the system is sodium bromide produced during development.

If this accumulates near the surface of the crystal, as happens, for example, when the thin film technique is used, a mechanism (see below) involving the reduction of silver ions in contact with the upper surface of the speck of silver is brought into play.

The Reduction of Crystals of Silver Bromide with Glycin and Hydroquinone Developers

The developers used for these experiments were prepared by dissolving glycin and hydroquinone in solutions of sodium carbonate or sodium hydroxide through which a stream of nitrogen was being bubbled to exclude oxygen. The rapid darkening of solutions of hydroquinone which occurs in the presence of oxygen was thus avoided. The appearance of the masses of silver produced by these developers was very similar to that of the masses obtained with ferrous developers. The reduction of the surface of the crystal occurred at a number of well separated centres and examination under vertical illumination showed that the mechanism during the early stages was dependent almost entirely upon the discharge of silver ions from the solid silver bromide. After reduction had been in progress for a considerable time, it was evident that another mechanism was coming into operation and that silver was being produced on the upper surfaces of the silver specks ; this led to the growth of protuberances from many centres on those surfaces. When the silver was dissolved away with warm concentrated nitric acid, it was observed that the masses had, as in the previous cases, been formed in cavities which on (100) surfaces had the form of inverted square based pyramids. Electron micrographs taken of a number of masses, too small to be clearly resolvable with the optical microscope, showed that they consisted of aggregates of micro-crystals of silver. This, together with many other observations, provides definite evidence that they are not single crystals of silver as was assumed by Dankov and Kochetkov (1942) and also by Boissonnas ; it accounts for the fact that no x-ray diffraction pattern which could be attributed to single crystals of silver was observed in our previous work (Keith and Mitchell 1952). When these reagents are used for reducing crystals of silver bromide, the silver is produced in poly-crystalline form from the earliest stages of reduction.

The observations so far described were made on crystals with surfaces near a (100) orientation. When (111) surfaces were reduced with these developers, and also with ferrous developers under same conditions, strikingly different behaviour was apparent. This is illustrated in fig. 5 (Pl. 34), which shows the boundary between an approximately (100) and an approximately (111) surface of a polycrystalline specimen of silver bromide after reduction with a solution containing hydroquinone and sodium carbonate. At the beginning of reduction, specks of silver of roughly triangular form were produced on the (111) surfaces and these specks almost immediately grew filaments of silver on their upper surfaces. The filaments curled over and made contact with the surface ; further triangular specks were then produced at the points of contact and the process was repeated. The silver specks were formed in flat based triangular cavities in the surface of the crystal which were revealed when the silver was dissolved away with warm nitric acid. Examination of the surface of the crystal with the phase contrast microscope showed that extensive local dissolution had occurred under the masses of filamentary silver. This suggests that they are formed by a process involving silver ions in solution, an interesting observation considering that no solvents for silver bromide were present in the developers used for the experiments. It is clear that the reducing solution surrounding a mass of silver will be impoverished in silver ions compared with that elsewhere on the surface and this fact alone must promote the local dissolution of the crystal. Processes of dissolution occurring even in the absence of solvents for silver bromide whereby silver ions pass into solution to be reduced after adsorption by masses of silver appear to play an important role during reduction particularly in the absence of organic substances which are strongly adsorbed by silver bromide. Figure 6 (Pl. 34), is another example of the production of a mass of filamentary silver of roughly triangular external form on a (111) surface of a crystal of silver bromide reduced with a metol hydroquinone developer containing sodium sulphite. It has been noted that the reduction of (111) surfaces with most developers is likely to result in the formation of filamentary silver. Little difference was observed in the form in which this silver was produced by different developers and it seemed that more information about mechanisms of development could be obtained from experiments on (100) surfaces. For this reason, (111) surfaces have not been extensively used for the present experimental work. The crystals with a (111) orientation were prepared by Hedges and Mitchell (1953).

Reduction of Crystals of Silver Bromide with Commercial Metol Hydroquinone Developers

The growth of projections on specks of silver during the later stages of reduction was mentioned in the previous section ; it may be attributed to the effect of the accumulation of alkali bromide and possibly also of oxidation products of the developer in the reducing solution. Most commercial metol hydroquinone developers contain sodium sulphite as a preservative and this salt also exerts a considerable general solvent action on the surfaces of the crystals, silver ions passing into solution in the form of complex sulphite ions. It is, therefore, not surprising that reduction proceeds in two distinct stages when these solutions are used. In the first stage, a mass of silver is formed with apparently the same characteristic properties as those described in the previous section. Silver produced by treating the surface of a crystal of approximately (100) orientation with D163 (see Kodak Formulary) is illustrated in fig. 7 (Pl. 35). One of the specks, at a much earlier stage of reduction, is shown in the electron micrograph of fig. 8 (Pl. 35). At this stage, projections had not begun to form. This behaviour appears to be characteristic of all developers compounded with reducing agents of medium activity and containing moderate concentrations of solvents for silver bromide. The concentration of silver ions in the solution rises steadily from the time when the developer is brought into contact with the silver bromide due to the solvent action of the sodium sulphite. This brings a second mechanism into play and the expansion of the base of the speck then occurs at a much slower rate. A projection grows steadily, as illustrated in fig. 9 (Pl. 36), for reduction with ID2 (see Ilford Formulary), and under vertical illumination it is observed that small crystals are being continuously formed on the surface of the projecting mass of silver which is thus extended laterally and upwards. The observation of the formation of these crystals during actual development with the thin film technique is naturally based on the examination of diffraction patterns. The deductions thus made have, however, been confirmed, as will be evident from fig. 10 (Pl. 36), by examining the masses with the electron microscope. The one illustrated here was produced with D163 but similar masses are obtained with ID2. It is to be noted that the crystals of silver near the base are large and well formed while those near the tip are very fine and closely interlocking.

Taken as a whole, the observations of this section provide clear evidence for the participation of two mechanisms in the reduction of (100) surfaces of large single crystals of silver bromide. The first mechanism depends upon the transference of electrons from molecules of the developing agent to silver ions at the interface between the silver speck and the silver bromide. Silver atoms are formed which build up the rigid coherent masses of silver which are observed. The second mechanism depends on the discharge of silver ions which have first passed into solution, usually in complex form, due to the general dissolution of the surface of the silver bromide crystal under the influence of solvents for silver bromide in the reducing solution. When this mechanism is operative, silver atoms are formed at the interface between the silver and the solution through the combination of silver ions with electrons provided by molecules of the reducing agent. This results in the growth of the protuberances which has been described. Which of these mechanisms plays the more important role is determined by the concentration of solvents for silver bromide in the developer. The second mechanism is also favoured by the addition of antifoggants which form stable complexes with silver ions.

On (111) surfaces, both D163 and ID2 produce tangled masses of microcrystals of silver linked by ribbon-like sections, which are usually of roughly triangular external form similar to that of the mass shown in fig. 6.

Experiments with Developers of Medium Activity containing Considerable Concentrations of Sodium Sulphite

This class includes the majority of fine grain developers which contain relatively high concentrations of sodium sulphite. With these developers, the growth of the base of a mass of silver at a development centre is largely suppressed at an early stage of reduction although the formation of a definite base on a (100) surface has usually been observed. There is often a long induction period during which the concentration of silver ions in complex form in the solution rises due to the solvent effect of the sodium sulphite ; the second mechanism of reduction then takes over and, thereafter, rigid projections which consist of smooth surfaced nodular rod-like masses or of elongated clusters of very fine micro-crystals are formed. By examining the silver bromide crystals with the phase contrast microscope, it was established that extensive general dissolution of the surface occurred during development. The silver produced by reducing a (100) surface with DK20 (see Kodak Formulary) is illustrated in fig. 11 (Pl. 37). A similar surface after reduction with D25 (see Kodak Formulary) is shown in fig. 12 (Pl. 37). Although crystals of silver at the surfaces may be attached to these masses of silver by short ribbon-shaped filaments, there is no clear evidence for the formation of the type of filamentary silver which is produced by developers of higher activity on (100) surfaces even when they do not contain solvents for silver bromide. The evidence suggests that the silver is mainly produced by the mechanism in which silver ions are reduced at the interface between the mass of silver and the solution.

Experiments with Reducing Solutions containing Amidol and Sodium Sulphite

The activity of these developers is considerably less than that of solutions containing amidol and sodium carbonate which will be mentioned in the next section. When the surfaces of crystals of (100) orientation are reduced with D170 (see Kodak Formulary), initially square based specks are usually formed followed by the development of projections. Loosely attached masses of filamentary silver are produced when (111) surfaces are reduced with this developer. These are illustrated in fig. 13 (Pl. 38), an electron micrograph which should be compared with the illustrations in Mees (1942, pages 312 and 313).

Experiments with Reducing Solutions of High Activity

For the next series of experiments, reducing solutions were prepared by dissolving *p*-aminophenol, amidol and metol in sodium carbonate or sodium hydroxide solutions through which nitrogen was being bubbled to exclude oxygen. The reduction of surfaces of crystals of silver bromide of any orientation with these solutions never produced rigid coherent masses of silver. Projecting bundles of tangled filaments which drifted in the solution were always formed and reduction occurred at a much higher rate than with any of the other developers used. Typical bundles of filaments are illustrated in fig. 14 (Pl. 39) which shows the result of reducing a (100) surface with a solution containing amidol and sodium carbonate. Figure 15 (Pl. 39) is an electron micrograph of the central part of one of the filamentary bundles. It will be observed that crystals of silver are attached to the surfaces of the bundle by scarcely resolved filaments. These crystals appear as brilliantly illuminated diffraction discs in the optical microscope.

They are observed to be carried upwards with the growth of the mass of silver without change in form or configuration. This suggests that they are formed in the immediate neighbourhood of the interface between the silver and the silver bromide.

The mechanism of reduction operative under these conditions is apparently quite different from any previously encountered. Cavities of well-defined geometrical form are not formed on the surface of the crystal. Even on surfaces of (100) orientation, highly irregular depressions are produced and there is always extensive dissolution of the surrounding surface. The growth of the filamentary mass occurs with extreme rapidity and it is difficult to make visual observations during the early stages. The impression is gained that the bundles of filaments are projected upwards from the base through the formation there of further filaments. At the same time, the base expands outwards due to the spreading and growth of filaments near the edges of the bundle. It appeared that the bundles of filaments were not rigidly attached at the base to the crystals of silver bromide, and that many individual filaments could sweep across a limited extent of the surface.

All the observations are consistent with the working hypothesis that the filaments are charged negatively through the transference of electrons from molecules of the reducing agent. The electrons are concentrated at the extremities and the neutralization of the negative charge by silver ions continues the growth of the filaments. These silver ions are derived directly from the surface of the crystal of silver bromide at its interface with the filamentary bundle and bromide ions escape into the solution. There was no evidence for the operation of a mechanism involving the reduction of silver ions at the interface between the bundle of filaments and the solution. In fact, considering the high rate of formation of the bundles and the initial absence of solvents for silver bromide in the reducing solution, it is difficult to see how such a mechanism could be brought into play.

The formation of filamentary silver when surfaces of (111) orientation are reduced with developers of lower activity has already been noted. Many careful microscopic observations of the production of filamentary silver under different conditions have been made with inconclusive results. It is most desirable that methods of high speed photomicrography should be employed for this investigation. When high power objectives are used, the events occur too rapidly for accurate visual perception. It seems that on (111) surfaces filaments grow at both extremities and this is attributed to the high rate of dissolution of the surfaces in the neighbourhood of development centres. If the filaments are negatively charged by the developer the charge will be concentrated at the extremities where silver ions can attach themselves to form silver atoms and preserve the filamentary structure.

On (100) surfaces, with all developers, the formation of masses of filamentary silver was promoted by the addition of traces of inorganic and

Fig. 1

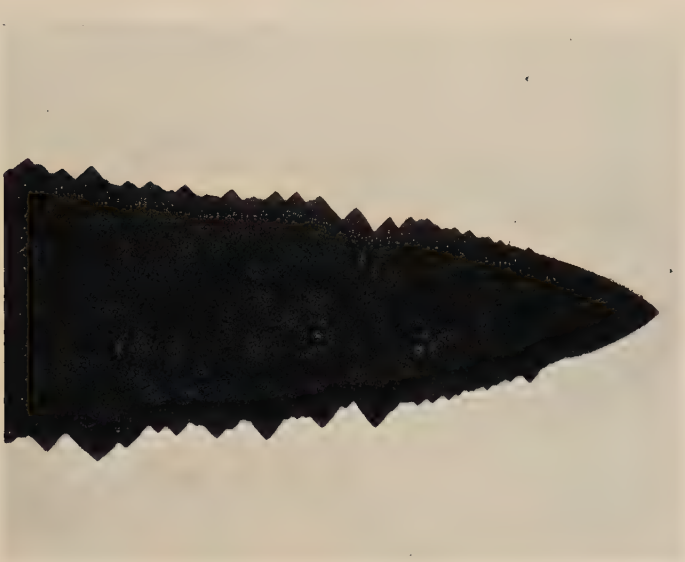

The tip of a projecting mass of colloidal silver produced by electrolytic reduction of a (100) surface of a silver bromide crystal. The axis of the mass lies approximately along a [100] direction and the lateral facets along [110] directions. ×400

Fig. 2

Crystals of silver produced by the coagulation and recrystallization of particles of colloidal silver. ×11 000

Fig. 3

Masses of colloidal silver produced by the cathodic reduction of the surface of a crystal of silver bromide which was covered with a thin conducting film of graphite. ×800

Fig. 4

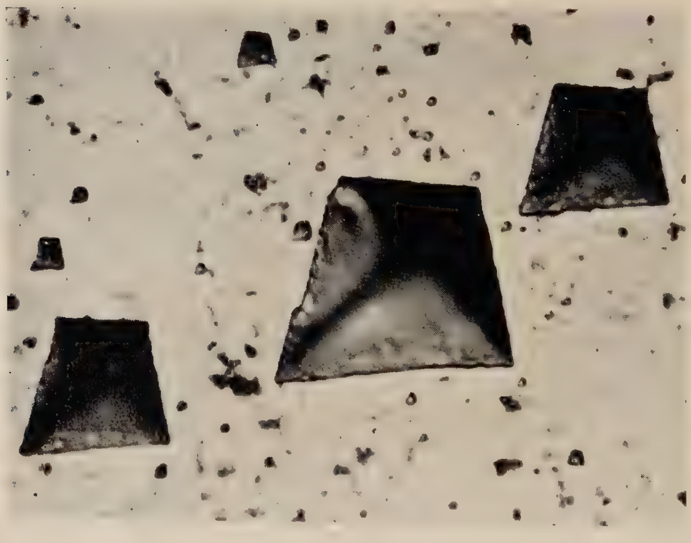

Cavities in the surface of a crystal of silver bromide revealed by washing away the colloidal silver which had been produced by cathodic reduction with a fine jet of water. ×1 600

Fig. 5

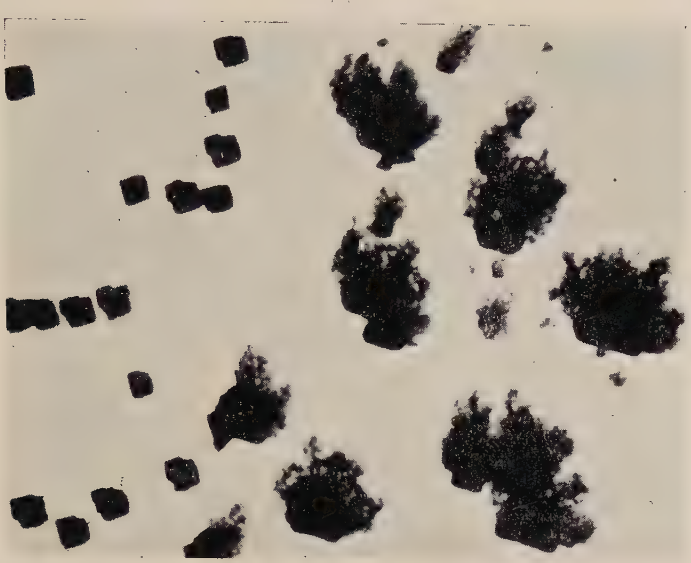

Silver produced by reducing two adjacent crystals of silver bromide with different orientations with a solution containing hydroquinone and sodium carbonate under precisely the same conditions. The left hand crystal has an orientation near that of a (100) surface and the right hand crystal near that of a (111) surface. The boundary between the two crystals is not visible. ×640

Fig. 6

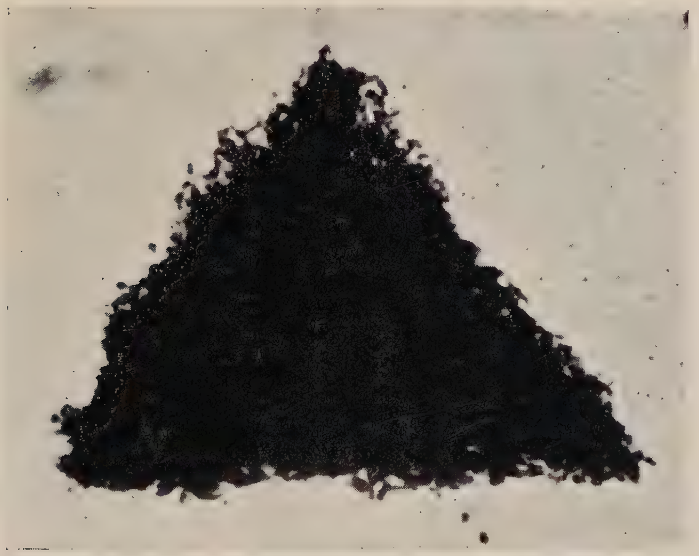

Mass of filamentary silver produced by the reduction of a (111) surface of a crystal of silver bromide with a metol hydroquinone developer (see Hedges and Mitchell 1953). ×3 200

Fig. 7

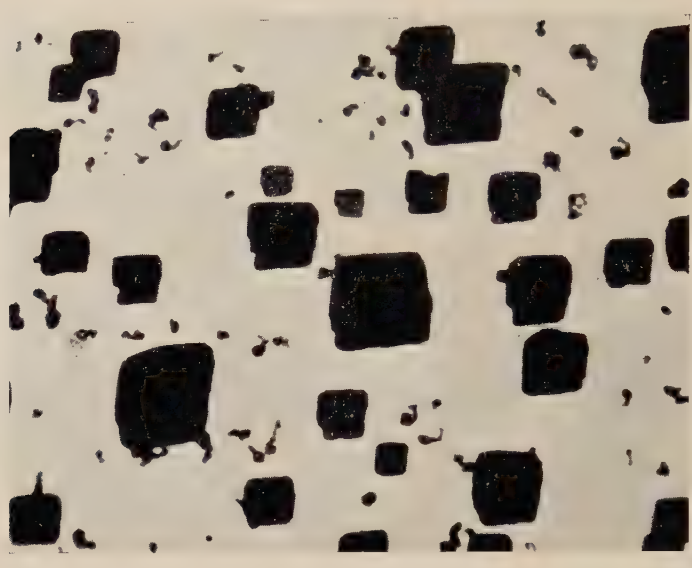

Polycrystalline masses of silver produced during the early stages of the reduction of a crystal of silver bromide with a (100) surface by D163, a metol hydroquinone developer. ×1 600

Fig. 8

An electron micrograph of a small speck of silver detached from the surface of a specimen similar to that of fig. 7 at an earlier stage of reduction. ×12 000

Fig. 9

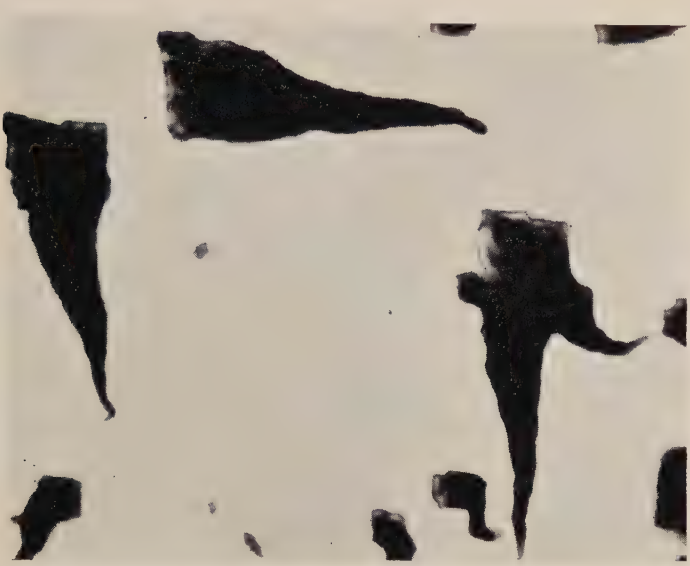

Masses of silver produced by the reduction of a (100) surface of a crystal of silver bromide with ID2, a metol hydroquinone developer. ×1 500

Fig. 10

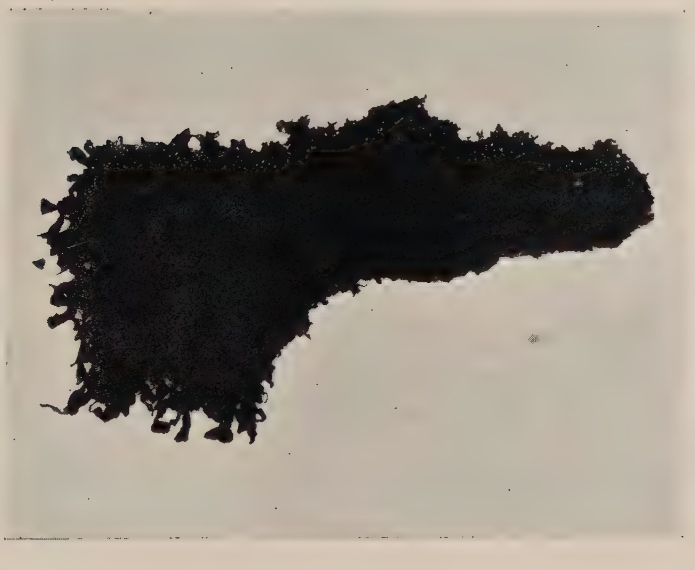

Electron micrograph of the base and projection of a mass of silver produced by the reduction of a (100) surface of a silver bromide crystal with D163, a metol hydroquinone developer. ×2 500

Fig. 11

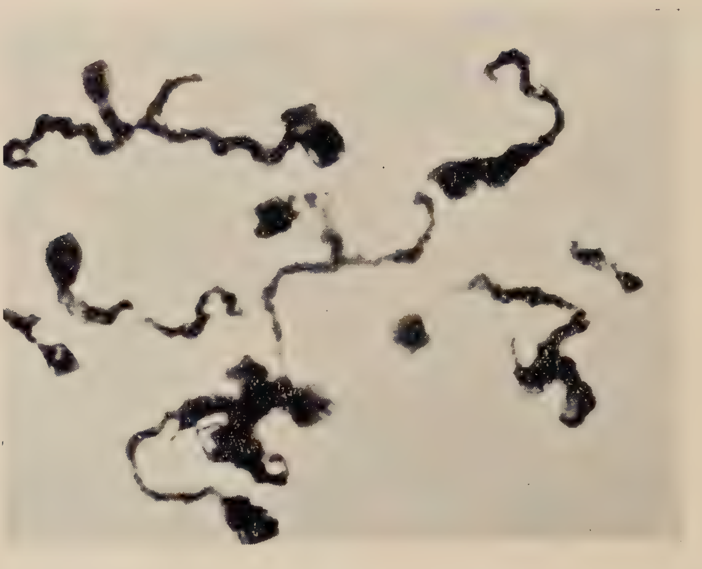

Elongated masses of micro-crystals of silver produced by reducing a (100) surface of a silver bromide crystal with DK20, a fine grain developer containing sodium sulphite and potassium thiocyanate. ×1 600

Fig. 12

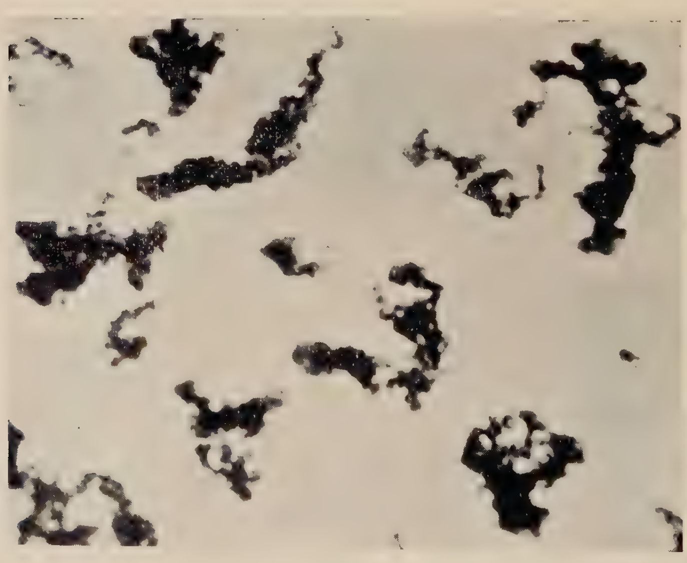

Aggregates of micro-crystals of silver produced by reducing a silver bromide crystal with an orientation near (100) with D.25, an ultra fine grain developer containing metol and sodium sulphite. ×1 600

Fig. 13

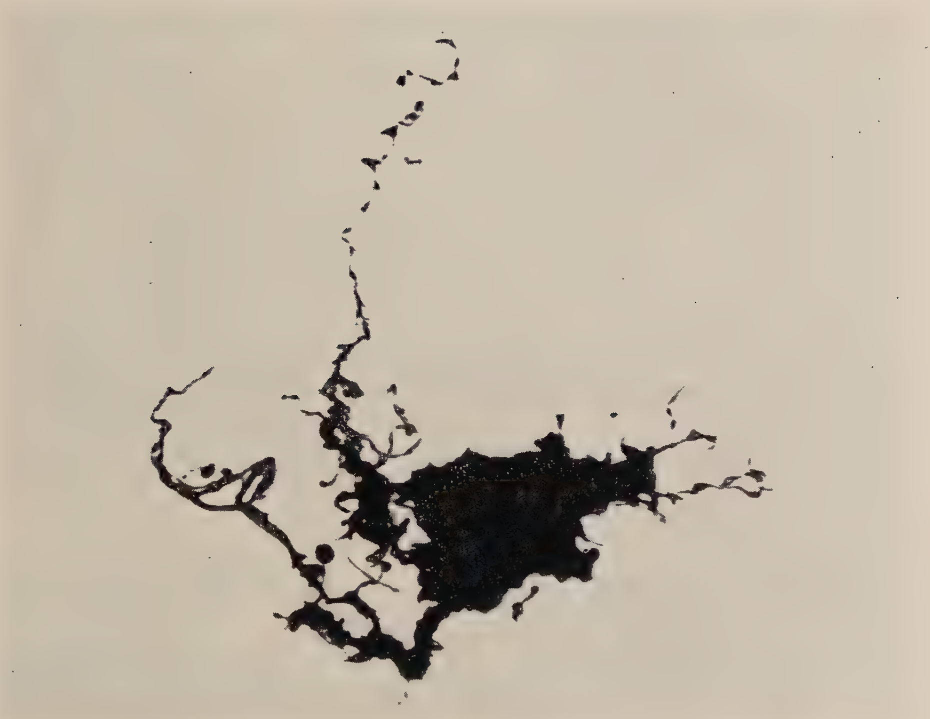

An irregular mass of filamentary silver resulting from the reduction of a (111) surface of a silver bromide crystal with D170, a developer containing amidol and sodium sulphite. ×10 000

Fig. 14

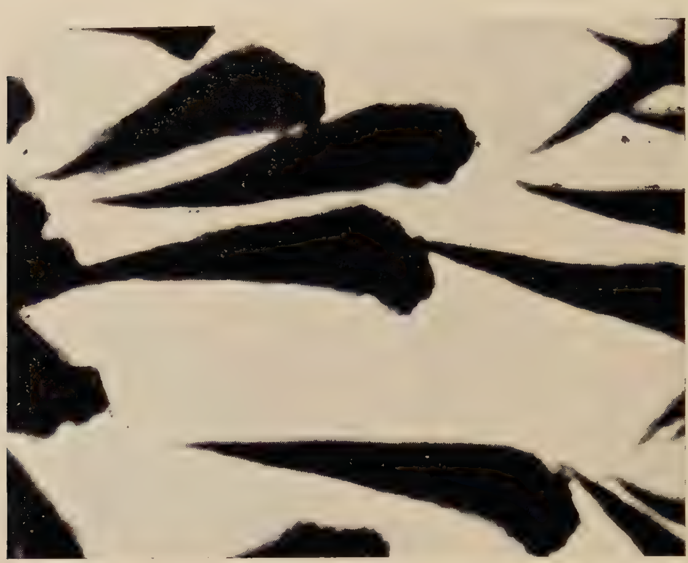

Projecting bundles of micro-crystals of silver linked by filamentary sections produced by reducing a (100) surface of a silver bromide crystal with a developer containing amidol and sodium carbonate. ×1 600

Fig. 15

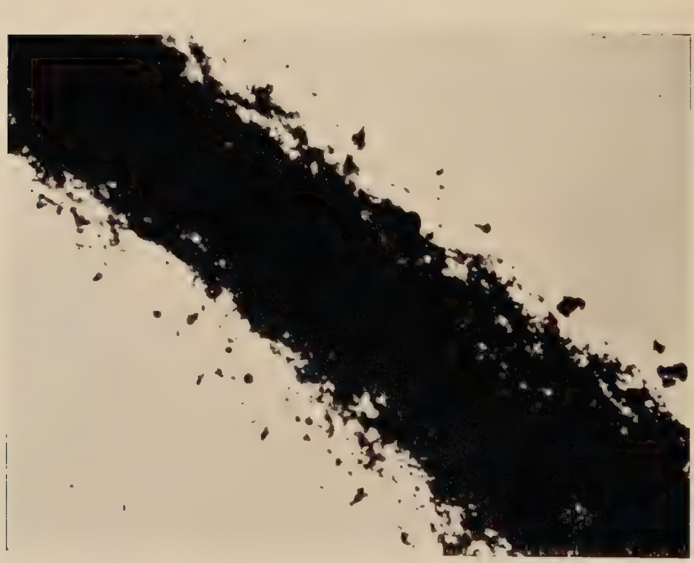

An electron micrograph of the central section of a bundle similar to those illustrated in fig. 14. The crystals at the surfaces are linked to the mass by scarcely resolved filaments of silver. ×11 000 organic sulphur compounds such as sodium thiosulphate and allyl thioures, and of other compounds which might be adsorbed by or react with the surfaces of the silver crystals. It was apparent that the formation of filamentary silver was not entirely an electrical phenomenon and that it was influenced by adsorption processes which might modify the condition of the silver surface.

Experiments on the Electrolysis of Solutions containing Silver in Complex Ionic Form

The object of these experiments was to study the form in which metallic silver was produced at the cathode when solutions containing sodium sulphite, sodium carbonate and potassium bromide, with the compositions found in normal photographic developers were saturated with silver bromide and then electrolysed in a thin film cell of the type described in the section on experimental techniques. When the potential difference between the anode and the cathode was below a certain critical value, the electrolysis of the solutions resulted in the formation of fine needles of silver, the form of which was quite different from that observed when dilute solutions of silver nitrate were electrolysed. Masses of needles grew rapidly in the general direction of the anode and, at the same time, lateral needles appeared which themselves developed further needles. The effect was thus to produce a tangled mass of interlocking needles like a gorse bush. These masses of silver closely resembled those produced during the later stages of development with solutions containing solvents for silver bromide. With low differences of potential, the form in which the silver was produced was largely independent of the precise composition of the solution although minor variations were observed. This series of experiments thus provides some evidence supporting the working hypothesis that the projections, consisting of masses of silver needles which are formed during the later stages of reduction with many developers, arise from the operation of an electrode mechanism involving the discharge of silver ions from the solution.

When sodium sulphite or other active sulphur compounds were present and the potential difference between the anode and the cathode was increased beyond the critical value mentioned above, an entirely different electrolytic mechanism was brought into play. Under these circumstances, instead of silver needles, tangled billowing masses of filamentary silver were formed. With the passage of time, these filamentary masses became consolidated and formed rigid aggregates of matted silver filaments which thickened and ultimately, in many cases, formed needles of silver in the low field region behind the rapidly advancing billowing front. When the current was interrupted, the loose masses of silver filaments drifted away from the cathode in the general direction of the anode in the circulating fluid of the thin film and their characteristics could then be clearly deduced from their diffraction patterns. The deduction that they consisted of silver crystals linked by filamentary sections was confirmed by examining the filaments in the electron microscope. It was then found that they were apparently of the same form as those produced by treating the (111) surfaces of crystals of silver bromide with most standard photographic developers. Filaments have not yet been produced at the cathode in model experiments in which solutions which did not contain a sulphur compound were electrolysed. There is thus not a complete parallelism between these experiments and those with chemical reducing solutions. As a working hypothesis, we assume that silver ions are not readily incorporated on silver surfaces which are covered with thin films of silver sulphide or of certain other substances. If films with this property are produced by reaction or adsorption soon after the formation of the silver surfaces, the thickening of a filament will be largely prevented ; because the reaction of silver ions and molecules of the developer, whether by a catalytic or an electrolytic mechanism, will occur mainly at the freshly formed extremities. This hypothesis is consistent with many observations which have been made.

The relationship between the electrolytic experiments and those with photographic developers appears to be as follows. When the applied potential lies below a certain critical value, rigid acicular masses of micro-crystals of silver are formed by the reduction at the cathode of silver ions from the solution. This corresponds to the formation of projections consisting of similar micro-crystals during the reduction of the surfaces of crystals of silver bromide with solutions containing considerable concentrations of solvents for silver bromide. When the applied potential exceeds the critical potential, billowing masses of filamentary silver are formed provided that the solution contains at least traces of a sulphur compound. If this experiment is relevant to the action of reducing agents on crystals of silver bromide, the mass of filamentary silver attached to the cathode and receiving electrons from it will represent the bundle of filaments of silver which is charged negatively by the transfer of electrons from molecules of the reducing agent. In both cases, the negative charge will be concentrated at the extremities of the filaments and neutralized there by silver ions with the result that the filaments are extended. In the experiments with reducing solutions of high activity not containing solvents for silver bromide the silver ions are derived from the surface layers of the silver bromide crystal. In other cases where filaments are formed they may be derived either from the crystal or from the solution.

§ 4. CONCLUSIONS

The experimental work on the reduction of crystals of silver bromide which has been described in this paper, together with a great number of other observations which have not been included for lack of space, reveals a pattern of behaviour of considerable complexity. Taken as a whole, the experimental results suggest that at least three mechanisms are involved, depending on the rate of reduction and the precise physico-chemical conditions of the experiments. It cannot be too strongly emphasized that the operation of these different competing mechanisms can be profoundly influenced by the addition of chemical compounds which are strongly adsorbed by the active surfaces— of silver bromide and of silver— or which form stable complexes with silver ions in the solution.

Gelatine has not been present during the reduction of the crystals of silver bromide in any of the experiments actually described in this paper; gelatine has, however, been introduced by us on many occasions in the form of a dried layer of hardened gelatine on the surfaces of the crystals and as an addition to the developers. In general, the presence of an inert gelatine does not influence the form in which the silver is produced by any particular reducing solution, but it may greatly reduce the number of active development centres. The presence of gelatine may, of course, modify the kinetics of the reduction process, but kinetic studies have not been part of the present investigation.

Neither a surface nor an internal latent image consisting of particles of silver was formed prior to any of these experiments. The centres at which reduction is initiated are of three types: (1) localized imperfections in the otherwise regular sub-structure of the crystals, (2) particles of foreign material, most probably of silver oxide and (3) particles of silver produced by random processes at the beginning of reduction. These three sources of fog can be eliminated (1) by annealing the specimens at a temperature within 50°C of the melting point after their separation from the plates, (2) by annealing in an atmosphere of hydrogen bromide and bromine and (3) by depositing layers of effective hydrophilic colloids on the surfaces which protect them from rapid spontaneous reduction in the reducing solutions.

Once visible nuclei of silver have appeared either spontaneously or at chemical or physical fog centres, development proceeds by one or more of three mechanisms which lead to the formation of silver in the following forms: (1) compact masses of coherent micro-crystals of silver with regular geometrical contours occupying cavities with surfaces parallel to (111) planes of the silver bromide crystal; (2) rigid projections based on masses of silver of the type described under (1) and also consisting of coherent masses of micro-crystals of silver; and (3) tangled masses consisting of micro-crystals of silver linked together by very thin ribbon-shaped filaments.

On (100) surfaces, reducing solutions of low activity not containing solvents for silver bromide produce square specks of silver consisting of masses of interlocking micro-crystals. The mechanism operative under these conditions appears to be a very simple one. Silver ions are adsorbed by the silver speck at its interface with the silver bromide. Electrons are transferred to the silver speck at its interface with the solution from adsorbed molecules of the reducing agent which then pass into the oxidized form. There are thus two influences at work, one charging the speck positively and the other negatively corresponding with the behaviour of a silver electrode when immersed in a solution containing silver ions or in a reducing solution. The neutralization of the charges on the speck results in its growth through the addition of silver atoms. This leaves a negative space charge in the interfacial region with the silver bromide, and a positive space charge in the solution near the upper surface. These space charges are neutralized by the drift of bromide ions from the interfacial region into the solution.

When silver ions are present in considerable concentration in complex form in the solution, which will always be the case when solvents for silver bromide such as sodium sulphite, potassium thiocyanate, sodium thiosulphate and alkali bromides are present, another possibility exists for the formation of silver atoms at development centres. Both silver ions and molecules of the developing agent may now be adsorbed at the interface between the silver speck and the solution, reaction leading to the addition of silver atoms to the speck and the formation of the oxidation product of the developing agent. When this mechanism is active, a tapering projection, consisting of a rigid mass of micro-crystals of silver is formed upon the square specks on (100) surfaces.

During the later stages of development, there are thus two competing mechanisms: one in which silver ions and electrons combine to form silver atoms at the interface between the silver speck and the silver bromide, and the other in which silver ions from the solution combine with electrons to form silver atoms at the interface between the speck and the solution. The first mechanism leads to the lateral development of the base of the silver mass and the second to the growth of a conical projection away from the base.

When reducing agents of steadily increasing activity are used for preparing developers for reducing (100) surfaces of silver bromide crystals, an abrupt change in mechanism is noted when the activity exceeds a certain value. From this point onwards, projecting conical masses consisting of micro-crystals of silver linked by ribbon-shaped filaments of silver are formed instead of compact specks. The masses rest in irregularly shaped cavities in the surface of the crystal.

We shall now outline what we believe to be the reasons for the formation of filamentary silver during the reduction of silver bromide. According to the electrode mechanism, reduction depends upon two processes, the adsorption of silver ions which charges nuclei or masses of silver positively, and the adsorption of molecules of the reducing agent with the formation of the oxidation product which charges them negatively. The system is never in equilibrium and the rates at which these two processes occur are important. They will be the same only under exceptional circumstances, the slower one usually determining the kinetics of the whole reaction. When the two electrode mechanisms of reduction which have so far been considered are operative, it is suggested that the silver is either uncharged or positively charged with respect to both the silver bromide and the solution. This will happen when, as was postulated by Bagdasar'yan (1943), the adsorption and incorporation of silver ions occurs at an equal or greater rate than the transference of electrons.

We suggest that silver is produced in filamentary form when the rate of transference of electrons to silver nuclei or silver masses exceeds the rate of incorporation of silver ions, so that the silver becomes negatively charged. This condition can be realized when the total concentration of silver ions available for charging silver nuclei is reduced, or when the rate of incorporation of silver ions is reduced by the formation of complex ions, or by the formation of thin films on the surfaces of the silver nuclei by reaction or adsorption. The negative charge will be concentrated at the extremities of elongated nuclei and at points ; its neutralization there by silver ions whether derived from the solid silver bromide or from the solution will produce silver in filamentary form. It might be argued that filamentary silver should be produced whenever the nuclei are charged, whether positively or negatively, but a little consideration shows that this will not be the case. If an elongated nucleus incorporates silver ions anywhere on its surface, the positive charges may be concentrated at the extremities and neutralized there by electrons but the resulting silver atoms will be located where the silver ions were adsorbed.

It appears that there are four ways in which the above condition can be satisfied. First, filaments are produced instead of specks on (100) surfaces when the concentration of silver ions in the solution or on exchange sites on the surface of the silver bromide is lowered in accordance with the law of mass action by the addition of a soluble bromide to the developer. The formation of filamentary silver on (111) surfaces with most reducing agents can also be discussed on the same basis. Under comparable conditions, the surface density of reduction centres is usually greater on (111) than on (100) surfaces and the rate of reduction at individual centres appears to be higher. Both these factors increase the local concentration of bromide ions around reduction centres on (111) surfaces compared with (100) surfaces, and favour the formation of filamentary silver. Secondly, alkaline solutions containing reducing agents of high activity such as *p*-aminophenol, metol and amidol always produce filamentary silver, even on (100) surfaces. The transference of electrons from molecules of the reducing agent to silver nuclei probably occurs at a higher rate than with reagents of lower activity such as hydroquinone or glycin ; this thereby causes reduction at a higher rate and producing a higher local concentration of bromide ions around the development centres. Two factors are thus operative in determining the difference of behaviour of developers of increased activity ; the increase in the rate at which negative charges are transferred to the nuclei and the decrease in the local concentration of silver ions and therefore in the rate at which positive charges are transferred. Thirdly, filamentary silver is produced when compounds which form complexes with silver ions, or are strongly adsorbed by silver bromide, are added to the reducing solutions. Antifoggants such as benztriazole and its derivatives provide typical examples. The silver complexes usually have a low solubility and high stability. The addition of the compounds reduces the total concentration of silver ions in the solution, the concentration of free silver ions, and the rate at which silver ions can leave the surface of a silver bromide crystal. Their presence in the system reduces the rate at which silver ions can be incorporated into the surface layers of silver nuclei and probably leaves the electron transference process practically unaffected. Fourthly, the addition to the reducing solution of chemical compounds which can react with silver surfaces, or be adsorbed by them to form stable films, promotes the formation of filamentary silver under conditions where masses of micro-crystals would otherwise be formed. Examples of these compounds are sodium thiosulphate and thioureas (which probably form surface films of silver sulphide) and organic compounds including many containing sulphur and nitrogen, which may either react with a freshly formed silver surface in alkaline solutions to form silver sulphide or form stable adsorbed layers. Although the presence of the compounds which give rise to them may reduce the concentration of silver ions in the solution, it appears that the primary function of these thin films of silver sulphide, or adsorbed layers of other substances, is to hinder the building of silver ions on to the surface of silver nuclei. The transference of electrons to silver ions to form silver atoms occurs most readily after the incorporation of the silver ions in the surface layers of silver masses, because the distances between the atomic nuclei are then the same as in metallic silver and the trapping of the electron does not necessitate nuclear displacements. In the presence of reactive sulphur compounds, of the type which we have been discussing, incorporation of silver ions will only occur on freshly formed silver surfaces because, soon after the formation of the surfaces, thin films of silver sulphide and other substances will be formed upon them by reaction or adsorption. The presence of the films should interfere less with the transference of electrons to the silver from molecules of the reducing agent. Thus whether an electrode mechanism or a catalysed heterogeneous mechanism is operative, these conditions will favour the formation of filamentary silver. It is considered that the observations of the present experimental work, taken as a whole, favour an electrode mechanism for the formation of filamentary silver.

ACKNOWLEDGMENT

This work has been supported by a grant from the Kodak Research Laboratories, Harrow, which is gratefully acknowledged.

REFERENCES

ABRIBAT, M., 1952, *Photo. J.*, **92 B**, 25.

BERG, W. F., 1948, *Reports on Progress in Physics*, **11**, 248.

BAGDASAR'YAN, KH. S., 1943, *J. Phys. Chem. U.S.S.R.*, **17**, 336 ; 1944, *Acta Physicochim., U.S.S.R.*, **19**, 421.

BOISSONNAS, C. G., 1949 a, *Sciences et Industries photographiques* [2], **20**, 361 ; 1949 b, *Experientia*, 5, 282 ; 1950, *C.R. Acad. Sci., Paris*, **230**, 1278 ; 1951, *Fundamentals of Photographic Sensitivity* (London : Butterworth), p. 36.

Dankov, P. D., 1939, *C.R. Acad. Sci., U.S.S.R.*, **24,** 773.

Dankov, P. D., and Kochetkov, A. A., 1940, *C.R. Acad. Sci., U.S.S.R.*, **26,** 785.

Gurney, R. W., and Mott, N. F., 1938, *Proc. Roy. Soc.* A, **164,** 151.

Hedges, J. M., and Mitchell, J. W., 1935, *Phil. Mag.* [7], **44,** 357.

James, T. H., 1943, *J. Chem. Phys.*, **11,** 338 ; 1946, *J. Chem. Education*, **23,** 595 ; 1950, *Advances in Catalysis* (New York : Academic Press), p. 105.

James, T. H., and Kornfeld, G., 1942, *Chem. Rev.*, **30,** 1.

Keith, H. D., and Mitchell, J. W., 1952, *Sciences et Industries Photographiques* [2], **23,** 260.

Mees, C. E. K., 1942, *The Theory of the Photographic Process* (New York : Macmillan), p. 305.

Mitchell, J. W., 1952, *Sciences et Industries Photographiques* [2], **23,** 218.

Mott, N. F., 1948, *Photo. J.*, **88 B,** 119.

Reinders, W., 1934, *J. Phys. Chem.*, **38,** 783 ; 1935, 9^{me} *Int. Congress photogr. Paris*, p. 345.

Reinders, W., and Boukers, M. C. F., 1938, *Trans. Faraday Soc.*, **34,** 912.

XCIV. *The Chain* ^{79}As–$^{79\mathrm{m}}$Se *in Slow Neutron Fission of* ^{235}U

By J. G. Cuninghame
Atomic Energy Research Establishment, Harwell, Didcot, Berks*

[Received April 15, 1953, revised MS. May 22, 1953]

Abstract

^{79}As and $^{79\mathrm{m}}$Se have been found as slow neutron fission products of ^{235}U. The half life of ^{79}As has been measured as $9{\cdot}01 \pm 0{\cdot}15$ min, its maximum β-energy as $2{\cdot}3 \pm 0{\cdot}1$ Mev and its fission yield as $(5{\cdot}3 \pm 0{\cdot}5) \times 10^{-2}$ %. The half life of $^{79\mathrm{m}}$Se has been measured as $3{\cdot}88 \pm 0{\cdot}06$ min and its maximum conversion electron energy as $0{\cdot}098 \pm 0{\cdot}014$ Mev. The assignment of mass 79 to the 9 min arsenic activity is confirmed. Details of the rapid arsenic purification procedure developed and aluminium absorption curves for ^{79}As–$^{79\mathrm{m}}$Se and for $^{79\mathrm{m}}$Se are given.

§ 1. Introduction

Nine minute ^{79}As was first reported by Butement (1950) who discovered a 9 min activity as a result of a (γ, p) reaction on selenium and gave it the probable mass assignment of 79. A 10 min activity was later found in the arsenic fraction resulting from the irradiation of selenium with fast neutrons or deuterons and the nuclide was reported to have a maximum β-energy of approximately $2{\cdot}1$ Mev with negligible γ-rays of appreciable energy (Van der Haack *et al.* 1952).

$^{79\mathrm{m}}$Se was first reported by Flammersfeld *et al.* (1950) as a metastable state of ^{79}Se with a half-life of $3{\cdot}9$ min emitting a γ-ray of energy 90 ± 10 kev. The mass assignment was later confirmed by Rutledge *et al.* (1952) who reported the half-life as $3{\cdot}5 \pm 0{\cdot}2$ min and the γ-ray energy as $95{\cdot}9 \pm 0{\cdot}3$ kev.

The object of this work was to see whether the 9 min arsenic isotope was present in the slow neutron fission of ^{235}U and if so, to measure its fission yield and confirm its mass assignment. Arsenic isotopes previously reported in ^{235}U slow neutron fission are 38 hr ^{77}As and 91 min ^{78}As.

§ 2. Experimental

Methods previously used (Winsberg 1944, Meinke 1949) for the separation of arsenic from irradiated uranium took too long for the present investigation and so the following procedure was evolved :—

---

* Communicated by the Author.

1. The irradiated uranium solution was added to the standardized arsenite carrier in dilute sulphuric acid, oxidized to arsenate with potassium bromate and reduced again with potassium metabisulphite. (This oxidation-reduction procedure is considered in the discussion section.)

2. The reduced solution was then placed in an arsine generator with a mercury cathode as described by Rogers and Heron (1946). Arsine was generated for 15 min with the cell at about 80°c, at a cathode current density of about 2·5 amp/cm^2 and passed through lead acetate solution before collection in silver nitrate.

3. Antimony carrier was added to the silver nitrate solution, followed by sodium chloride, the solution filtered and a ferric hydroxide scavenge carried out.

4. Arsenic metal was then precipitated by ammonium hypophosphite in the presence of antimony hold-back carrier from 1 : 1 hydrochloric acid solution.

5. The arsenic was dissolved in brominated hydrochloric acid and then distilled from concentrated hydrobromic acid in the presence of antimony, tellurium and tin hold-back carriers, into concentrated hydrochloric acid.*

6. Arsenic was reprecipitated, slurried with water, filtered on to a tared filter paper, dried and counted. The chemical yield was obtained by weighing after the decay curves were completed.

This procedure took approximately 45 minutes and gave a chemical yield of roughly 35%. Arsenic metal is a very suitable precipitate for counting, being fine and even.

The ^{79m}Se which was grown from ^{79}As was separated by direct precipitation from hydrochloric acid solution with solid hydroxylamine hydrochloride.

The irradiations were performed in a pneumatic tube of the Harwell Pile at a flux of approximately 10^{12} neutrons/cm^2/sec.

All counts except those on ^{79m}Se were carried out in the same position on the same counter. This counter was an end-window Geiger counter with a mica window 1·7 mg/cm^2 thick. The distance between window and source was 2·5 cm. The counter used for the ^{79m}Se was similar. All count-rates were corrected for air and counter-window absorption by means of the absorption curves ; for back-scattering from 12 mg/cm^2 of filter paper on an aluminium tray thick enough to give ‘ saturation-backscattering ’ by use of the factor $1{\cdot}20 \pm 0{\cdot}09$ taken from the work of Burtt (1949) ; for self-scattering and self-absorption for ^{79}As by plotting fission-yield against precipitate weight (fig. 1)—this shows no effect due to increasing precipitate weight with the fairly thin sources used, as expected for a hard β-emitter ; and for the soft electrons from ^{79m}Se by interposing a total thickness of 16 mg/cm^2 of aluminium between source and counter and correcting back along the extrapolated absorption curve for ^{79}As. The ^{140}Ba standard was counted in the same position in the same counter and was also fully corrected.

---

* In some experiments steps 4 and 5 were repeated.

§ 3. Results

Fission Yield Determinations

Five satisfactory experiments yielded the results given in table 1. A sample decay curve is given as fig. 2.

The half-life found for ^{78}As was 87·5±2 min (all figures for error are standard deviations) compared with 91·0±0·6 min found by Surgarman.

Fig. 1

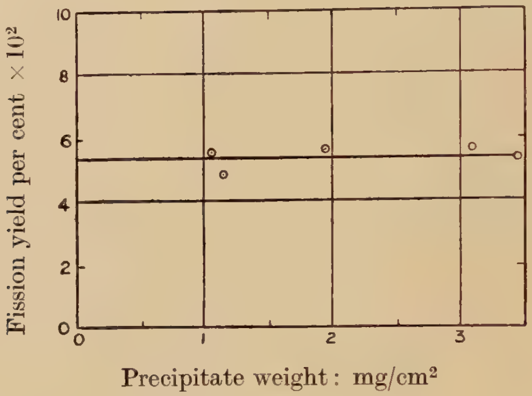

Self-absorption curve: ^{79}As

The fission yield found for ^{78}As was (1·6±0·2)×10^{-2} % compared with Sugarman's value of 2·0×10^{-2} %. Our value has been calculated assuming there is no independent fission yield of ^{78}As and by the rather unsatisfactory method of calculating the yield from the observed arsenic counts and from assumed decay constants for ^{78}Ge and ^{78}As. This method is not to be compared in accuracy with Sugarman's and the error quoted is merely an expression of the self-consistency of the results and does not allow for possible systematic errors in the method. It is included only to show that it results in a figure of the right order when compared with the results for ^{79}As. As with the ^{79}As, full counting corrections have been

Table 1. Results of Fission Yield Determinations

Run No.	Pile irradiation (min)	Measured half life in min		Measured fission yield in % × 10²		Wt. of arsenic precipitate in mg/cm²	No. of arsenic distillations
		^{78}As	^{79}As	^{78}As	^{79}As		
1	10	85	9·25	—	5·5	1·05	2
2	10	89·5	9·05	—	5·3	3·45	1
3	10	86	8·94	—	4·8	1·15	1
4	40	89	9·00	1·5	5·6	3·10	2
5	40	88	8·80	1·6	5·6	1·95	2

applied. Similar corrections have been applied to the ^{140}Ba which was used as a standard. Its fission yield was assumed to be 6·1%.

The half-life found for ^{79}As was 9·01 ± 0·15 min and the fission yield $(5{\cdot}3 \pm 0{\cdot}5) \times 10^{-2}$ %. The fission yield was calculated assuming that the parent ^{79}Ge (if any) had a negligibly short half-life compared to the irradiation period. That this is so is proved by the fact that fission yields found are constant, although the irradiation time is varied by a factor of four. An attempt was made to grow ^{79}As from separated germanium fission product but this was a failure since a sufficiently rapid germanium purification method was not available.

Fig. 2

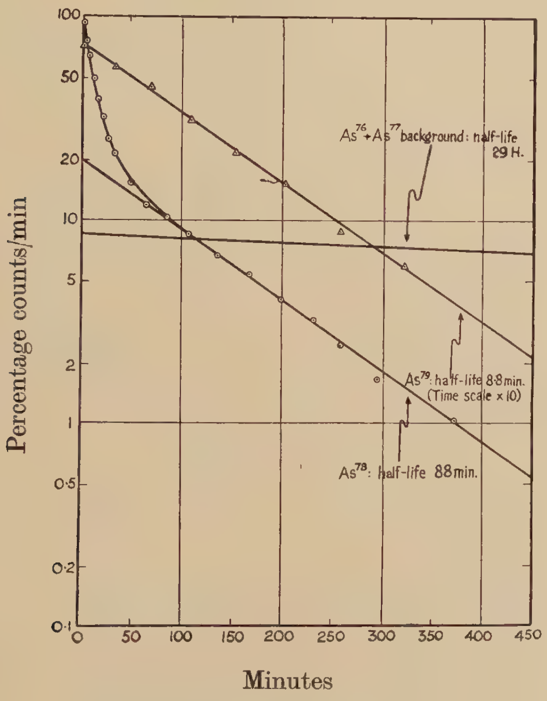

Decay curves : ^{78}As and ^{79}As

The corrections involved in the determination of the count-rate are considered in the experimental section above.

^{79m}Se was separated from purified arsenic and its half-life measured. The result from three experiments was 3·88 ± 0·06 min. There was no sign of 17 min ^{81}Se in these samples.

Absorption Measurements

Aluminium absorption curves were taken of the β-particles of ^{77}As, ^{78}As, ^{79}As and for the electrons of ^{79m}Se grown from the ^{79}As. The results of the energy determinations are given in table 2.

The curve for ^{77}As was obtained by irradiation of pure GeO_2 for 12 hours and separating the arsenic which had grown in after a cooling period of 12 hours. The curve for ^{78}As was obtained from fission product arsenic by subtraction of the ^{77}As curve and also of a proportion of ^{76}As which was always found in the fission product mixtures due to arsenic impurity in the uranium nitrate used. The curve for ^{79}As+^{79m}Se in equilibrium (fig. 3) was obtained as a result of nine runs with subtraction of ^{76}As, ^{77}As and ^{78}As. No γ background was observed. The curve for ^{79m}Se (fig. 4) which is a typical conversion electron curve, was obtained as a result of three runs on the separated selenium.

Table 2. Results of Absorption Measurements

Nuclide	Observed range mg/cm^2	Estimated max. energy of β MeV
^{77}As	250	0·7
^{78}As	2090	4·1
^{79}As	1128±50	2·3±0·1
^{79m}Se	14±2	0·098±0·014 (of conversion electron)

Fig. 3

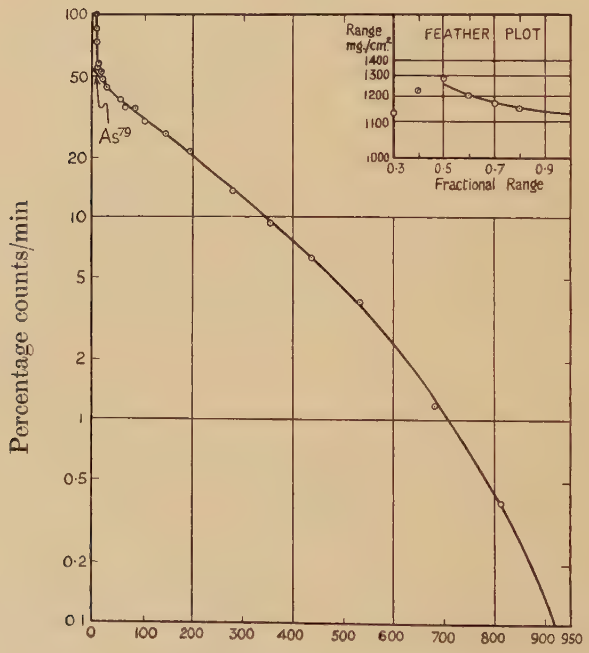

Absorber thickness: mg/cm^2
Aluminium absorption curve: ^{79}As–^{79m}Se

§ 4. DISCUSSION

The growth of ^{79m}Se from the 9 min arsenic confirms the mass assignment for the short lived arsenic and further confirmation is given by the fact that the measured fission yield falls on the smooth mass-yield curve for ^{235}U slow neutron fission. A mass assignment of 81 is precluded by the fact that no ^{81}Se was found.

In agreement with Sugarman (1953) no trace was found of the ~40 min arsenic activity reported by Brightsen *et al.* (1951) although in the earlier stages of the work an impurity (believed to be antimony) of half-life ~30 min was observed.

Fig. 4

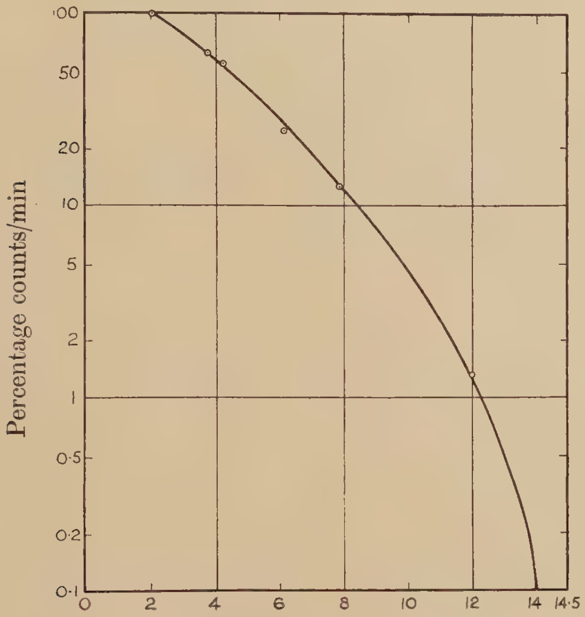

Absorber thickness: mg/cm^2
Aluminium absorption curve: ^{79m}Se

In earlier experiments it was noticed that the fission yield obtained was roughly inversely proportional to the concentration of arsenic carrier after addition to the irradiated uranium solution, and it was assumed that this was caused by some of the active arsenic being in the pentavalent state and not exchanging with the trivalent carrier, a fact which had been previously observed (Wilson and Dickinson 1937). This assumption was confirmed by the fact that once the oxidation-reduction process given in the purification procedure was adopted the yields obtained rose above the highest value previously reached and were then constant in spite of large variations in the carrier concentration.

ACKNOWLEDGEMENTS

The author wishes to thank the Director of the Atomic Energy Research Establishment for permission to publish this work ; Dr. G. B. Cook of the Establishment for suggesting the problem and for many discussions on it ; and Mr. B. D. Pate of the Establishment for discussions on the chemistry of arsenic.

REFERENCES

BRIGHTSEN, R. A., SHURE, K., FISHER, C., and CORYELL, C. D., 1951, *Phys. Rev.*, **81,** 298.
BURTT, B. P., 1949, *Nucleonics*, **5,** No. 2, 28.
BUTEMENT, F. D. S., 1950, *Nature, Lond.*, **165,** 149.
FLAMMERSFELD, A., and HERR, W., 1950, *Z. Naturforsch.*, **5a,** 569.
VAN DER HAACK, P. J., DE VRIES, A. E., and ATEN, A. H. W., 1952, *Physica*, **18,** 20.
MEINKE, W. W., 1949, *U.S. Report* No. A.E.C.D. 2738.
ROGERS, D., and HERON, A. E., 1946, *Analyst.*, **71,** 414.
RUTLEDGE, W. C., CORK, J. M., and BURSON, S. B., 1952, *Phys. Rev.*, **86,** 775.
SUGARMAN, N., 1953, *Phys. Rev.*, **89,** 570.
WILSON, J. N., and DICKINSON, R. G., 1937, *J. Amer. Chem. Soc.*, **59,** 1358.
WINSBERG, L., 1944, *Radiochemical Studies : The Fission Products*, 1st ed., Vol. 9, Div. IV National Nuclear Energy Series (New York : McGraw-Hill), p. 1440.

XCV. *The Valency of the Transition Metals in Some Binary and Ternary Alloys*

By H. Jones, F.R.S.
Department of Mathematics, Imperial College, London*

[Received April 29, 1953]

Summary

The changes of valency of transition metal atoms in different alloy systems is considered. Reasons are given for expecting the valency to decrease as the electron concentration in the conduction band increases. Rough agreement with the experimental results of Haworth and Hume-Rothery is obtained in the cases of Mn, Fe and Co. Suggestions are made to account for the apparent fractional valency of Ni.

§ 1. Introduction

It is known that in binary alloys which crystallize in the γ-brass structure, and in which one component is a transition element, of either the first or the second long period, the transition metal atoms must act with zero valency if the characteristic electron–atom ratio 21/13 is to be maintained. On the other hand it has been shown by Haworth and Hume-Rothery (1952) that when the metals Mn, Fe, Co, and Ni are taken into solid solution, in β-phase alloys of the type Cu–Zn or Cu–Al, they appear to have a valency of approximately 1 or 2, except for Ni which in some cases, but not all, has apparently a fractional valency of about 0·6. Again, in the series of alloys $CrAl_7$, $MnAl_6$, $FeAl_3$, $CoAl_4$, $NiAl_3$, and in some ternary alloys rich in aluminium of the kind studied by Raynor (1949), the transition metals appear to possess negative valencies. It appears that, with the possible exception of $FeAl_3$, these negative valencies increase in unit steps from Ni to Cr; the actual values put forward by Raynor, $-0{\cdot}6$ for Ni, $-1{\cdot}7$ for Co and so on, are the result of applying certain theoretical considerations.

The purpose of this note is to suggest an explanation of these changes of valency with the changes of environment of the transition metal atoms. When the percentage of the transition metal in the alloy is small, say less than 20 atomic per cent, as in the cases we are considering, we shall assume that the d-electrons lie in localized states about their respective atoms. It is just possible that in certain cases this assumption is invalid, for instance when Ni is dissolved in Cu so that the d-states of the solute and the solvent nearly match. However, in alloys like $MnAl_6$, or when there is 1 or 2% Fe in systems like Cu–Zn–Fe there can be no doubt that the assumption is correct. When this is the case it implies that the number of d-electrons per atom is integral, and that their energy levels are discrete.

---

* Communicated by the Author.

In a many-electron problem, treated by the Hartree–Fock method, there appears to be no reason why there should not be a localized and an extended partial wave function, within the total wave function, both having the same eigenvalue. The Hartree–Fock equations for the two wave functions are, of course, quite different due to the difference in both the ordinary and the exchange potentials. This situation arises in practice, presumably, when, for example, a Cu atom is dissolved in aluminium, and also in aluminium rich Ni–Al alloys. In the following discussion we assume that every transition metal atom, in the alloys considered, has an integral number of d-electrons ; that there is a single eigenvalue for all these electrons (we neglect the splitting due to the crystalline field), and that there is no general restriction on the position of this eigenvalue relative to those of the conduction band.

§ 2. THE EQUILIBRIUM DISTRIBUTION OF THE ELECTRONS

Let x be the fraction of the transition metal atoms to the total number of atoms, and let ν be the number of d-electrons per transition metal atom. Let n be the number of conduction electrons per atom of the crystal, and N the total number of electrons per atom under consideration. Thus

$$N=n+x\nu, \quad . \quad . \quad . \quad . \quad . \quad . \quad . \quad . \quad . \quad . \quad (1)$$

where n can take a continuous range of values, but ν only integral values up to 10. The total energy of this electronic system per atom, measured relative to all the electrons at rest at infinity, we denote by $E(n, \nu)$. If we keep N fixed, and the state of lowest energy is that for which $\nu=\nu_0$, we have

$$E(N-x\nu_0-x, \nu_0+1)>E(N-x\nu_0, \nu_0), \quad . \quad . \quad . \quad . \quad (2)$$

and

$$E(N-x\nu_0+x, \nu_0-1)>E(N-x\nu_0, \nu_0). \quad . \quad . \quad . \quad . \quad (3)$$

If

$$\mu(n, \nu)=\left(\frac{\partial E}{\partial n}\right)_\nu, \quad . \quad . \quad . \quad . \quad . \quad . \quad . \quad . \quad (4)$$

and

$$x\Delta E(n, \nu)=E(n, \nu)-E(n, \nu-1), \quad . \quad . \quad . \quad . \quad . \quad (5)$$

the conditions (2) and (3) can be written, when x is small, as

$$\Delta E(n_0, \nu_0+1)>\mu(n_0-\tfrac{1}{2}x, \nu_0+1), \quad . \quad . \quad . \quad . \quad . \quad (6)$$

and

$$\mu(n_0+\tfrac{1}{2}x, \nu_0)>\Delta E(n_0, \nu_0), \quad . \quad . \quad . \quad . \quad . \quad . \quad (7)$$

where $n_0=N-x\nu_0$ is the number of conduction electrons per atom when $\nu=\nu_0$.

The quantity $\mu(n, \nu)$ is equal to the energy required to remove an electron from the top of the conduction band, and this, according to a well-known theorem of the Hartree–Fock theory, is equal to the eigenvalue of the highest occupied level (Wilson 1936, p. 28). $\Delta E(n, \nu)$ is equal to the energy required to take away one d-electron from an atom when ν are there originally. Since the d-levels are localized $\Delta E(n, \nu)$ is not exactly equal to the eigenvalue of the d-state, but is approximately so (Slater 1951, p. 142). Now let $\epsilon_0(n, \nu)$ be the lowest eigenvalue of the conduction band and let

$$\zeta(n, \nu) = \mu(n, \nu) - \epsilon_0(n, \nu),$$

and

$$\epsilon(n, \nu) = \Delta E(n, \nu) - \epsilon_0(n, \nu).$$

We can speak of ζ as the height of the Fermi level, and $\epsilon(n, \nu)$ as the height of the d-level for ν electrons relative to the bottom of the conduction band. In the case of very low atomic concentrations, i.e. as x tends to zero, ζ becomes independent of ν and (6) and (7) can be written

$$\epsilon(n_0, \nu_0+1) > \zeta(n_0) > \epsilon(n_0, \nu_0).$$

Fig. 1

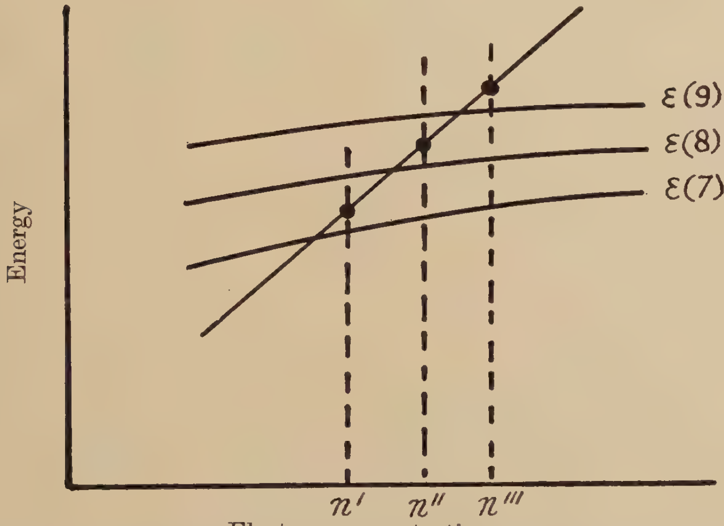

Diagram to show how the valency of a transition metal atom varies with electron concentration in the conduction band. The sloping line is the plot of ζ against n.

This shows that there are ν_0 electrons in the d-states if ζ lies between the d-levels with ν_0+1 and ν_0 electrons.

We now consider what happens when we alter the total electron concentration by changing the nature of the alloy. Figure 1 shows what might be expected in alloys containing small percentages of Fe. If the electron concentration in the conduction band is n' the Fe atoms, which have 8 electrons outside the 3p shell, will appear to have a valency +1; at n'' a valency 0, and at n''' a valency −1.

The change in n is brought about in practice, in ternary systems, by changing the composition of the solvent alloy, for example, by changing the Cu to Zn ratio in the system Cu–Zn–Fe. In cases where we have the same transition element in quite different alloys, for example Cu–Zn–Fe and Fe_5Zn_{21}, the relative positions of the d-level and the bottom of the conduction band may be different. It appears, however, that this difference may not be very great for the following reason: When a single foreign atom is dissolved substitutionally in another metal the wave function of the lowest state of the conduction band must be made continuous throughout the metal and the solute atom. If the two metals, the solvent A and the solute B, have approximately the same atomic volume, and if ϵ_A is the eigenvalue of the bottom of the conduction band in A, and ϵ_B that in B, then if we change the electrostatic potential of the whole neighbourhood of the single atom B in metal A by an amount $(\epsilon_A-\epsilon_B)$, the Wigner–Seitz wave functions around B and its neighbours A will join smoothly together. This is, in fact, what happens when solid solutions of this kind are formed. The change in the electrostatic potential of amount $(\epsilon_A-\epsilon_B)$ is brought about by a change in the density of the conduction electrons in the neighbourhood of the solute atom (Mott 1936, Arafa 1948, Huang 1948). Since any change in the potential of the whole neighbourhood of an atom does not affect the relative positions of the stationary states, we should not expect the $\epsilon(n, \nu)$ to differ greatly from one alloy system to another provided that the density of the conduction electrons is the same in each. We should, however, expect the $\epsilon(n, \nu)$ to increase with the electron concentration in any alloy, because the greater n the greater must be the negative charge density between the nucleus and the d-shell and this screening must raise each $\epsilon(n, \nu)$.

In alloys such as $CrAl_7$, in which the electron concentration is high, it is possible that the difference between successive d-levels, i.e. $\epsilon(n, \nu+1)-\epsilon(n, \nu)$, may be smaller than when n is low. This is because when n is large, decreased screening by the conduction electrons can compensate for the addition of an electron to the d-shell. In these alloys negative valencies as high as -4 do not seem impossible. If they do occur we should expect the density of the conduction electrons in the neighbourhood of the Cr atom to be greatly reduced, and as this density is approximately two electrons per atom, the excess negative charge near a Cr atom should be in the neighbourhood of 2 not 4 (cf. Douglas 1948).

§ 3. QUANTITATIVE ESTIMATES AND SPECIAL CASES

We consider first the transition element Co and try to estimate the energy differences in the d-levels. From the observed atomic spectra we obtain the following data:

Configuration	Term	Wave number	Electron volts
$4s^2 3d^7$	$^4F_{9/2}$	0	0
$4s\ 3d^8$	$^4F_{9/2}$	3,483	0·43
$3d^9$	$^2D_{5/2}$	27,497	3·40

We shall assume that these numbers give approximately the relative positions of the d-levels in the alloy, and in this rough estimate we shall neglect the effect of the electron concentration in the conduction band. The levels are, therefore, represented in fig. 2 (*a*) by horizontal lines.

The value of the lowest d-level $\epsilon(7)$ has been estimated as follows: Since the atomic states $4s^2 3d^7$ and $4s3d^8$ lie so close together it follows that the Fock eigenvalues of the s- and d-wave functions must also lie close together. Now the change in the s eigenvalue as the atoms are brought together arises mainly from the change in the boundary conditions which are applied. If the d-level remains discrete the boundary conditions applied to this wave function will not change very greatly, and thus in the metal the separation between the d-level and the bottom of the conduction band will be given very approximately by the lowering of this latter level in the process of reducing the interatomic distance. In fig. 2 (*b*) the lower curve represents the bottom of the conduction band as a function of the radius of the atomic sphere r_s; the higher curve is obtained by adding the mean Fermi energy w_F. If s' denotes the part of the cohesive energy due to the conduction electrons then we see that $\epsilon(7)=w_F+s'$. Assuming 0·71 conduction electrons per atom in pure Co we find $w_F=3{\cdot}5$ ev. The observed cohesive energy amounts to 4·5 ev per atom. Remembering that ϵ_0 is defined as the Fock eigenvalue, we have not to subtract an exchange energy to obtain the total cohesive energy but only the correlation term. According to Wigner's formula for free electrons this would amount to 1·0 ev. If we allow one electron volt per atom for the contribution to the cohesive energy from the d-band in pure Co we get $\epsilon(7)=6$ electron volts, which is the value assumed in fig. 2 (*a*).

Fig. 2

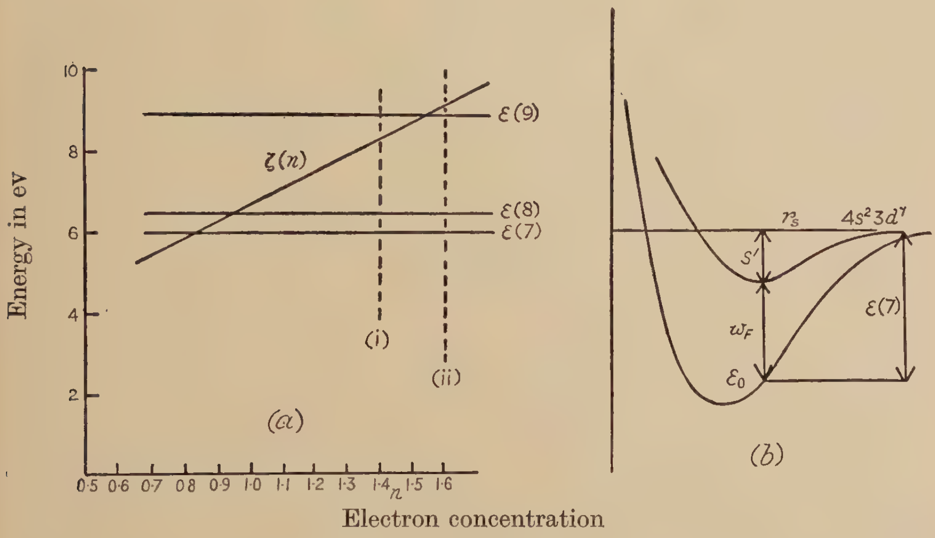

(*a*) Diagram showing the variation of the valency of cobalt in alloys with different electron concentrations in the conduction band. Line (i) electron concentration in the β-phase, line (ii) in the γ brass structure.

(*b*) Method of estimating the height of the first d-level above the bottom of the conduction band.

The general position of the line $\zeta(n)$ can be estimated by assuming that the conduction electrons may be regarded as free in the alloys we are considering. Then $\zeta=36{\cdot}1\, v_e^{-2/3}$ electron volts, where v_e is the volume per electron expressed in cubic A.U. The atomic volume of β-brass is $12{\cdot}77\times10^{-24}$ cm^3, and the electron–atom ratio is 1·41. Thus in the neighbourhood of this electron–atom ratio we can write

$$\zeta=8{\cdot}31+3{\cdot}93(n-1{\cdot}4) \text{ ev},$$

and this is the line plotted in fig. 2 (*a*).

The electron–atom ratios for the β-phase and the γ-brass structures are indicated, and show that the observed valencies of 1 and 0 respectively are consistent with the present theory. Strictly, the different atomic volume of the γ structure should be taken into account, but as the estimated energies are so approximate it does not appear worth while to do this. These numerical estimates do show, however, that the explanation of the varying valencies suggested here is not ruled out by such quantitative considerations as can be made at present.

The Cu–Al–Ni system examined by Haworth and Hume-Rothery (1952) shows some interesting features. At the $\alpha/\alpha+\beta$ boundary, where $n=1{\cdot}38$, the apparent valency of Ni is 1·75, and at the $\beta/\alpha+\beta$ boundary, where $n=1{\cdot}45$ the valency of Ni is zero. This behaviour might be the result of the ζ line crossing the $\epsilon(10)$ d-level in the neighbourhood of $n=1{\cdot}4$. It is to be noticed that in Ni the $\epsilon(8)$ and $\epsilon(9)$ levels are probably very close together, since the atomic states $3d^84s^2$, $^3F_4$ and $3d^94s$, $^3D_3$ are separated by only 0·025 ev. When two d-levels are as close together as this, differences in the surrounding atoms, for example, whether a Ni has an Al neighbour or not, may be sufficient to cause some Ni atoms to act with valency 1 and some with valency 2, leading to a fractional average valency.

A similar effect may occur in the Cu–Zn–Ni system where Ni has an apparent valency of 0·6, because this alloy is probably ordered since β-brass, even when quenched, takes up the ordered structure. If this is so there would be two quite different sites for the Ni atoms ; one in which a Ni is surrounded by Zn atoms, and the other in which it is surrounded by Cu atoms. The difference in the electron density, and therefore in the screening, might be sufficient to split the ϵ levels and lead to one set of Ni atoms having a valency 1 and the other set a valency zero.

REFERENCES

ARAFA, M. K. I., 1949, *Proc. Phys. Soc.* B, **62**, 238.
DOUGLAS, A. M. B., 1948, *Nature, Lond.*, **162**, 566.
HAWORTH, J. B., and HUME-ROTHERY, W., 1952, *Phil. Mag.*, **43**, 613.
HUANG, K., 1948, *Proc. Phys. Soc.* **60**, 161.
MOTT, N. F., 1936, *Proc. Camb. Phil. Soc.*, **32**, 281.
RAYNOR, G. V., 1949, *Prog. Met. Phys.*, **1**, 1.
SLATER, J. C., 1951, *Quantum Theory of Matter* (New York and London : McGraw-Hill Book Company).
WILSON, A. M., 1936, *The Theory of Metals* (Cambridge : University Press).

XCVI. CORRESPONDENCE

The Release of the Energy Stored in Deformed Nickel

By L. M. Clarebrough, M. E. Hargreaves and G. W. West
Division of Tribophysics, C.S.I.R.O., Melbourne, Australia

[Received April 29, 1953]

The energy stored during the deformation of pure copper has been measured recently (Clarebrough, Hargreaves, Michell and West 1952). The values obtained for the stored energy and the recrystallization temperatures were lower than those observed by Quinney and Taylor (1937) for impure copper. This suggested that portion of the energy stored might be released at room temperature and in fact Borelius (1952) has shown that energy is released from deformed pure copper at 24°c. For these reasons measurements of energy stored during deformation have now been made on nickel and correlated with measurements of hardness and electrical resistivity.

All measurements were made on bars of nickel of commercial purity $\frac{3}{4}$ in. in diameter and with a gauge length of 8 in. deformed in torsion 25 turns. The specimens for the determination of hardness were cut from the same deformed bar as those for the measurement of stored energy. The measurements of resistivity were made, by means of a Kelvin double bridge, on an identical deformed bar. In all experiments a heating rate of 6°c per minute was used. The specimens for the determination of hardness were quenched from various temperatures but the measurements of resistivity were made during heating. A second heating enabled the values of resistivity for the annealed material to be obtained.

The results are shown in the figure. The most striking aspect of these results is the observation that approximately 40% of the energy stored during deformation, area A, is released before any reduction in hardness occurs and that this release of stored energy is associated with the disappearance of the majority of the increase in resistivity due to deformation (c.f. Wilson and Thomassen, Tammann and Moritz). These facts are of interest in relation to recent suggestions by Mott (1951) and Seitz (1952) that vacancies which are generated during deformation are the main cause of the accompanying increase in electrical resistivity. Further they are consistent with Seitz's conception that an appreciable part of the stored energy resides in the form of vacancies.

If it is assumed that the initial release of energy is due to the disappearance of vacancies and that the energy associated with a vacancy is half the activation energy for self-diffusion, the density of vacancies in the deformed specimen can be calculated. No value of the activation energy for self-diffusion in nickel has been found in the literature, but a value of 70,000 calories/mole may be estimated using the approximately linear relationship between the activation energy for self-diffusion and melting point. The energy associated with the first peak is 0·21 calories/g which corresponds to a density of vacancies of approximately 3×10^{-4}. Preliminary measurements of macroscopic density show that there is an increase in density of this order of magnitude on heating to 325°c. Further measurements of density and lattice parameter are in progress.

A further 20% of the stored energy, area B, is released gradually in the temperature range in which a small decrease in hardness occurs, but microscopic and x-ray observations give no indication of recrystallization.

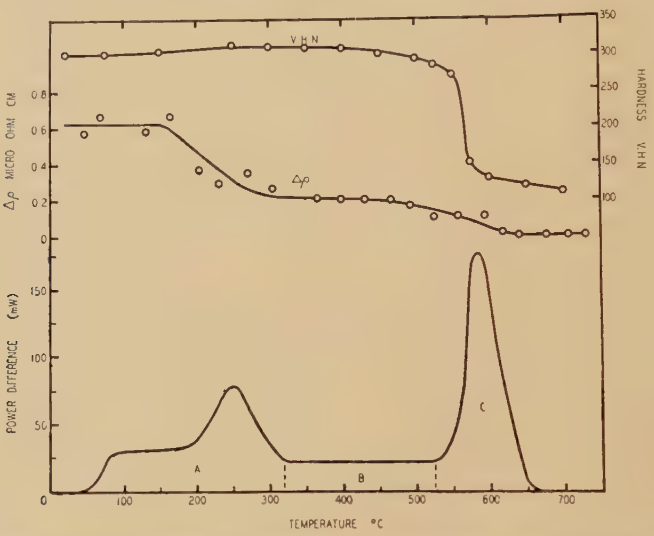

The release of stored energy, increment in resistivity and hardness plotted against temperature.

However, in contrast to the results of Suzuki (1949), the rapid release of the remaining 40% of the stored energy is associated with a large and sudden decrease in hardness and the disappearance of the remainder of the increment in resistivity. Microscopic and x-ray examination show that this release of energy and these changes in properties are concurrent with recrystallization. Thus, under the conditions of these experiments, recrystallization is accompanied by a sudden release of stored energy and takes place in a lattice in which considerable work hardening remains, contrary to the suggestions made by Beck (1952).

These experiments suggest one reason why the values of stored energy observed by Taylor and Quinney for impure copper were higher than those obtained with the present apparatus on pure copper, in which no peak corresponding to area A was observed. Thus, if the first peak in the present experiments is due to the disappearance of vacancies, its absence in the previous experiments indicates that this process takes place at room temperature in pure copper. Further this view is consistent with the results of Molenaar and Aarts (1950) who found that a considerable proportion of the increment in resistivity, produced in copper by deformation at the temperature of liquid air, disappeared on annealing at room temperature.

A more detailed account of these and other experiments will be published in the near future.

References

Beck, P. A., 1952, *J. of Metals*, **4,** 979.
Borelius, G., 1952, *L'Etat Solide, Institut International de Physique Solvay*, 427.
Clarebrough, L. M., Hargreaves, M. E., Michell, D., and West, G. W., 1952, *Proc. Roy. Soc.* A, **215,** 507.
Molenaar, J., and Aarts, W. H., 1950, *Nature, Lond.*, **166,** 690.
Mott, N. F., 1951, *Proc. Phys. Soc.* B, **64,** 929.
Quinney, H., and Taylor, G. I., 1937, *Proc. Roy. Soc.* A, **163,** 157.
Seitz, F., 1952, *Advances in Physics*, **1,** 43.
Suzuki, T., 1949, *Sci. Rep. RITU A*, **1,** 55.
Tammann, G., and Moritz, G., 1933, *Ann. d. Phys.*, **16,** 667.
Wilson, J. E., and Thomassen, L., 1934, *Trans. A.S.M.*, **22,** 769.

The Electronic Structure of Transition Metals in Alloys

By B. R. Coles
Department of Physics, Imperial College

[Received June 22, 1953]

In the current number of this journal, Jones (1953) shows that the stable electronic configuration of a transition metal atom in a metal or alloy should depend on the electron concentration of the solvent metal or alloy, and he interprets on this basis the results of Hume-Rothery and Haworth (1952) on the effect of transition metals on the α/β brass equilibrium. Other data, allowing of an even more direct interpretation, are the magnetic properties of alloys containing small amounts of transition metals. Results are available for the susceptibilities of dilute solid solutions in copper, silver, and gold of manganese, iron, cobalt, and nickel, and Schramm (1938) has examined the magnetic properties of the binary alloys of zinc with iron, cobalt, and nickel. Where the temperature-dependence shows a Curie–Weiss behaviour, effective magneton numbers (p_{eff}) for the transition metal atoms can be derived, and if the orbital contribution to the moment can be regarded as quenched by the crystalline field these numbers should be equal to $\sqrt{[4S(S+1)]}$, where S is the total spin quantum number of the atom in question. In some systems, however, the susceptibility decreases less rapidly, or even increases, with temperature at high temperatures and p_{eff} values cannot be derived.

Schramm's work shows that the γ-phase in the Ni–Zn system (15% Ni) is, like that in the Cu–Zn system, strongly diamagnetic, and the nickel is evidently present as $3d^{10}$ ions, while it seems clear (Coles 1952) that nickel enters copper with some empty d levels. Even stronger evidence is provided by the Co–Zn system. There the ζ-phase (7% Co) is more diamagnetic than zinc, whereas the γ-phase (14% Co) is markedly paramagnetic, the magneton number derived from the temperature-dependence being about 1·9. (For $3d^9$, spin only, p_{eff} is 1·73.) Thus the change from an electron concentration of 1·79 to one of 1·61 seems to result in a change of configuration of the cobalt atoms from $3d^{10}$ to $3d^9$. In the Fe–Zn system all intermediate phases are paramagnetic, and p_{eff} for the δ-phase (11% Fe) is 2·6 ; $3d^8$, spin only, would give 2·83. The γ-phase gives values of about 5·0, but the concentration of iron (25%) is probably too high for the model of isolated ions to be appropriate. Small concentrations of iron in gold (Kauffmann, Pan and Clark 1945) give rise to p_{eff} values of 3·6, that for $3d^7$, the configuration for iron in Cu–Zn alloys suggested by the work of Hume-Rothery and Haworth, being 3·87.

In Jones' theory the dependence on electron concentration arises from dependence on the band breadth of the conduction electrons, and it is of interest to note that the p_{eff} values for dilute solutions of manganese in copper (band breadth 7 ev) and silver or gold (band breadth 5·5 ev) are 4·8 and 5·5 respectively (Gustafsson 1936).

Magnetic investigations of this type are being extended to dilute solid solutions of transition metals in the various phases of the copper–zinc and copper–aluminium alloy systems.

REFERENCES

COLES, B. R., 1952, *Proc. Phys. Soc.* B, **65,** 221.
GUSTAFSSON, G., 1936, *Ann. Phys., Lpz.*, **25,** 545.
HUME-ROTHERY, W., and HAWORTH, J. B., 1952, *Phil. Mag.*, **43,** 613.
JONES, H., 1953, *Phil. Mag.*, **44,** 907.
KAUFFMANN, A. R., PAN, S. T., and CLARK, J. R., 1945, *Rev. Mod. Phys.*, **17,** 87
SCHRAMM, J., 1938, *Z. Metallkunde*, **30,** 327.

Resistance-Independent Absorption of Light Waves by Metals, and the Properties of Ideal Conductors

By J. LINDHARD
Institute for Theoretical Physics, Copenhagen*

[Received May 2, 1953]

THE theory of the optical properties of metals developed by Zener (1933) and Kronig (1934) gives in the first approximation a good account of the phenomena of transmission, absorption and reflection of a light wave incident on a metallic surface, at least for alkalies. This theory is based on a simple classical picture of the metallic electrons, the main assumption being that they are able to move around freely. The dielectric constant of the free electron gas is assumed to be, then,

---

* Communicated by Professor C. Møller.

$$\epsilon = 1 - \frac{\omega_0^2}{\omega(\omega + i/\tau)}, \quad . \quad . \quad . \quad . \quad . \quad . \quad . \quad . \quad . \quad (1)$$

for a transverse field of cyclic frequency ω. The system of electrons is thus characterized by two frequencies. First, the classical resonance frequency of the gas, $\omega_0 = (4\pi e^2 \rho/m)^{1/2}$, where ρ is the electron density, and second, the collision frequency $1/\tau$ representing in a crude manner the damping of motion due to collisions with the lattice. The solution of the field equation given by (1) is a wave proportional to exp $(\omega/c\ \epsilon^{1/2}x)$. As is well known, a wave with normal incidence on a plane surface is transmitted partially if the frequency is higher than the resonance frequency, while for $\omega < \omega_0$ the wave penetrates to a depth $\sim c/\omega_0$, and is reflected. In the latter instance the absorption due to resistance is $1 - R = 2/\tau\omega_0$. Here, and in the following, we consider only frequencies of collision $1/\tau$, small compared with the field frequency in question.

On the basis of equations similar to (1) many authors have discussed a so-called ideal conductor, i.e. a free gas where $1/\tau$ vanishes, the treatments being concerned with the case where the frequency of the field tends to zero. In the limit of static fields one then finds a freezing-in of the magnetic field, with a curious lack of uniqueness of the solution, and external changes in the field penetrate only to a depth c/ω_0. For reasons of this kind it is often suggested that superconductors have many properties in common with ideal conductors—as is indicated by the name superconductor— only that in a superconductor the frozen field is always zero (London 1950).

The treatment leading to (1) is deficient in the respect that it applies only for the field components of long wave length. As to a more detailed comparison with experiments it turns out, e.g., that the absorption resulting from (1) is several times smaller than the observed values for the absorption, in the near infra-red. Further, the theory fails to describe the anomalous skin effect.

For an improvement of the theory one should take into account the velocities of the free electrons. This will be done in some detail in two forthcoming papers. In the present note we shall use a qualitative description. Consider, then, the phenomenon of absorption. Usually, a direct absorption of an electromagnetic wave by an electron will not occur, since it would violate conservation of energy and momentum ; but the collisions of the electrons with the lattice can allow such processes. In each of the collisions, occurring at time intervals τ, the electron may be imagined to be scattered in a random manner, and it can then analyse the field only with a corresponding latitude $1/\tau$ in frequency. This circumstance directly leads to the imaginary term in the dielectric constant (1). When now we take into account the velocities v of the electrons, it is seen that a similar effect results if the field has a finite extension in space. For instance, when the field penetrates to a distance d from the surface of the gas, one finds an uncertainty $1/T = v/d$ in the frequency of the electronic reaction, due to the short time spent by the individual electron in the field. Instead of having only the damping term i/τ in the denominator in (1) we get the additional latitude in frequency iv/d.

Now, in the case of ω small compared to ω_0 the penetration depth is $d = c/\omega_0$, if the Zener–Kronig theory is assumed to hold as a first approximation, and we find $1/T = \omega_0 v_0/c$, where v_0 is the maximum velocity in the Fermi distribution. Since the absorption by resistance is $2/\tau\omega_0$, it may be concluded that an additional absorption, of magnitude about v_0/c, will take place. For a typical good conductor, Ag, the ratio v_0/c is close to 1/200, while $1/\tau\omega_0$ will be about 1/500 at normal temperature. Therefore the direct assumption by the gas is often dominating. Its inclusion in the absorption leads to an improved, but not complete, agreement with measurements in the near infra-red. Of course, in a proper treatment of a metal one must include the contributions from the more strongly bound electrons.

In view of the circumstance that the absorption by resistance does not account for the momentum taken up by the system when the wave is reflected at the surface, the presence of the additional absorption term is not surprising. Indeed, this term just serves to give momentum balance. As it is independent of the frequency of the field in the frequency region considered it has all the appearance of an increased resistance at the surface of the gas.

The above constant value of $1/T$ indicates the presence of a third characteristic frequency, $\omega_1 = \omega_0 v_0/c$. For frequencies below ω_1 the penetration and absorption of the wave is again changed. The behaviour in this region can be found when replacing $1/\tau$ in (1) by v_0/d, and assuming that ω is small compared with this quantity. The connection between penetration depth and dielectric constant then shows that d is of the order $\delta = (v_0/\omega)^{1/3} \,.\, (c/\omega_0)^{2/3}$, and the absorption about $(\omega/\omega_0)^{2/3} \,.\, (v_0/c)^{1/3}$. This phenomenon is the anomalous skin effect, discovered and explained by Pippard some years ago, and later investigated extensively by the same author (1949). The anomalous skin effect appears only for temperatures so low that $1/\tau < \omega_1$.

Reconsidering then the case of an ideal conductor we find that for ω tending to zero an external field will completely penetrate the medium, and no ambiguities arise in the solution of the field equations. The only magnetic property remaining in static fields is the weak susceptibility due to the Landau diamagnetism and the spin paramagnetism. Accordingly, the properties of an ideal conductor are not at all similar to those of a superconductor. Thus, if we are concerned with, e.g., a massive spherical ideal conductor of volume Ω, in an external magnetic field, the field will penetrate through the system within a time $(\omega_0{}^2\Omega/c^2 v_0)$, as determined by the above value of δ.

The ideal conductor, admittedly, is a rather artificial model, but it can serve to show the significance of the zero-point velocities of the electrons. The circumstance that for static fields the well-known equilibrium properties of the gas are attained—and the finite absorption effects—shows that the gas, including its field, will by itself tend towards statistical equilibrium. This trend is a result of taking the retarded solutions of the equations of motion. An analogous case is a gas of neutral particles where the particle collisions bring about equilibrium, and where background friction or surface scattering can be disregarded. It is apparent that the anomalous skin effect is intimately connected with other normal properties of an electron gas, and that it expresses the simultaneous conservation of energy and momentum. Therefore, it seems hardly profitable to use the eqn. (1), as it stands, as a guidance when discussing semi-empirical electromagnetic field equations for superconductors at low frequencies.

A quantitative treatment is given in the two mentioned papers, to be published in the *Kgl. Danske Vid. Selsk. Mat.-Fys. Medd.*, where the transverse and longitudinal field equations are deduced, and the self-consistency of the free electron picture discussed. There it is found that only the non-symmetric energy-momentum tensor of Minkowski applies. Indeed, it is obvious—if the absorption and reflection can be described by field equations—that the energy-momentum tensor can not be symmetric, because the momentum and energy lost by a reflected wave does not show any symmetry.

REFERENCES

KRONIG, R. DE L., 1934, *Nature, Lond.*, **133,** 211.
LONDON, F., 1950, *Superfluids*, Vol. I. (New York).
PIPPARD, A. B., 1947, *Proc. Roy. Soc.* A, **191,** 370, 385, 399; 1949, *Physica*, **15,** 45. See also REUTER, G. E., and SONDHEIMER, E. H., 1948, *Proc. Roy. Soc.* A, **195,** 336.
ZENER, C., 1933, *Nature, Lond.*, **132,** 968.

A Stripping Reaction at Low Bombarding Energy

By L. L. GREEN, J. P. SCANLON and J. C. WILLMOTT
Nuclear Physics Research Laboratory, University of Liverpool*

[Received June 23, 1953]

SEVERAL authors have briefly reported that a stripping mechanism may be important in deuteron reactions at relatively low bombarding energies (Risser and Burke 1952, Pruitt *et al.* 1952). We have recently determined the angular distributions of the neutron groups emitted in the reaction ^{9}Be(d, n)^{10}B at a bombarding energy of 860 kev, using the nuclear emulsion method. The angular distribution of the neutrons emitted in transitions to the excited state at 3·58 MEV in ^{10}B show a pronounced maximum at angles near fifty degrees to the forward direction, and this result indicates that, for this neutron group, the reaction proceeds mainly by a stripping mechanism.

---

* Communicated by Professor H. W. B. Skinner.

The experimental results are shown in fig. 1. The continuous curves are calculated from the Butler theory (Butler 1951) of stripping reactions and the curves for the three l values, $l=0, 1, 2$ are drawn. The $l=1$ curve gives the best fit to the experimental points and a radius of $5{\cdot}7\times10^{-13}$ cm is required for ^{9}Be. This radius value is in agreement with the large value required by Holt and Marsham (1953) to fit their results for the ^{9}Be(d, p)^{10}Be reaction at higher bombarding energies. The formula of Bhatia *et al.* (1952) for stripping angular distributions also gives good agreement with the experimental results if a value of $6{\cdot}7\times10^{-13}$ cm is taken for the radius. At higher bombarding energies this latter formula also requires a radius larger by one unit than the Butler formula.

Fig. 1

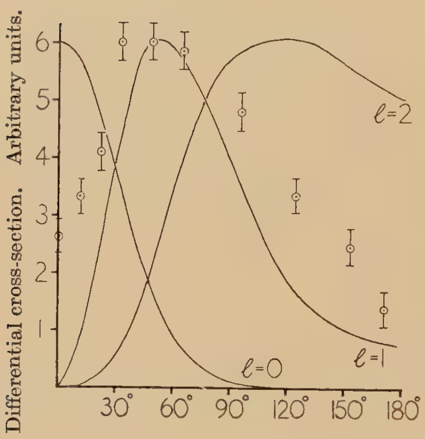

Fig. 2

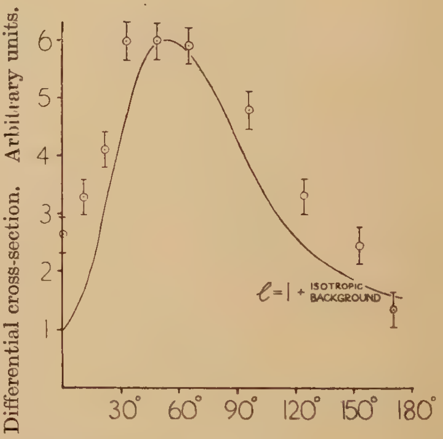

Angle of emission in C.M. system.

The deviations of the experimental points from the theoretical curve may be accounted for in part by a small compound nuclear contribution. In particular the assumption of an isotropic background of $\frac{1}{6}$ of the peak intensity is shown in fig. 2. This represents an upper limit to a compound nuclear contribution of this form. The experimental peak is broader than that predicted by the theory, and this may be due to Coulomb effects which are ignored in the theories of stripping.

We are grateful to Professor H. W. B. Skinner for helpful discussions, and one of us (J. P. S.) is indebted to the Department of Scientific and Industrial Research for the award of a Maintenance Grant.

References

Bhatia, A. B., Huang, K., Huby, R., and Newns, H. C., 1952, *Phil. Mag.*, **43,** 485.
Butler, S. T., 1951, *Proc. Roy. Soc.* A, **208,** 559.
Holt, J. R., and Marsham, T. N., 1953, *Proc. Phys. Soc.* (to be published).
Pruitt, J. S., Hanna, S. S., and Swartz, C. D., 1952, *Phys. Rev.*, **87,** 534.
Risser, J. R., and Burke, W. H., 1952, *Phys. Rev.*, **85,** 742.

Angular Correlations in the Reaction ^{23}Na(p, $\alpha\gamma$)^{20}Ne

By J. Seed
Cavendish Laboratory, Cambridge

[Received June 17, 1953]

The gamma ray yield from the proton bombardment of sodium-23 exhibits many resonances, as has been demonstrated by the work of Curran and Strothers (1939), Burling (1941), Freeman (1951), and Stelson, Preston and Goodman (1952). The last workers have shown that much of the radiation has a quantum energy of 1·63 Mev and probably corresponds to the de-excitation of the first level of ^{20}Ne. This would happen if the reaction scheme were

$$^{23}\mathrm{Na}+\mathrm{p} \rightarrow {}^{24}\mathrm{Mg}^*,$$
$$^{24}\mathrm{Mg}^* \rightarrow {}^{20}\mathrm{Ne}^*+\alpha,$$
$$^{20}\mathrm{Ne}^* \rightarrow {}^{20}\mathrm{Ne}+\gamma.$$

The occurrence of low energy alpha particles corresponding to the above scheme was established in the early stages of the present work, and their existence has been confirmed by the independent work of Donahue (1952).

The aim of the present work was to study angular correlations between the alpha particles and the 1·63 Mev gamma rays, and so to infer the spin of the first excited state of ^{20}Ne. Sodium targets were prepared by evaporating thin films of sodium chloride ($\sim$ 10 kev thick for 1000 kev protons) on to 0·004 in. copper foil. They were bombarded by a 3 μA beam of protons from the Cavendish Van de Graaff accelerator. Alpha particles emitted at 90° to the incident proton beam were separated from the scattered protons by a magnetic analyser having an energy resolution of 4% and a solid angle of 1/2000 sphere. The particles were detected by a thin ZnS screen and photomultiplier. Gamma rays were detected by a sodium iodide scintillation counter having an acceptance angle of 1/30 sphere and an intrinsic detection efficiency of about 50% for 1·63 Mev gamma rays.

By rotating the gamma counter about the target, (α, γ) correlations could be observed over the angular range 90° to 180°, and the arrangement was such that an angular correlation could be studied in a plane either perpendicular to or containing the proton beam direction.

A more complete account of the apparatus is given by Seed and French (1952 a, b).

Since there was a wide choice of ^{24}Mg resonant states accessible for correlation measurements, it was desirable to plan a definite way of attacking the problem. One aim was to find, if possible, a resonance formed by s-wave protons. The reason for this is as follows: the ^{1}H and ^{23}Na nuclei can collide with parallel or antiparallel spin configurations ($j=2$ or 1) and in general a given ^{24}Mg state (J) can be formed from both these substates. A ^{24}Mg state that is formed by s-wave protons can, however, derive from only one spin substate, since $J=j$ necessarily, and this permits a much simpler analysis of correlation results. One can further restrict ambiguities with the help of selection rules on angular

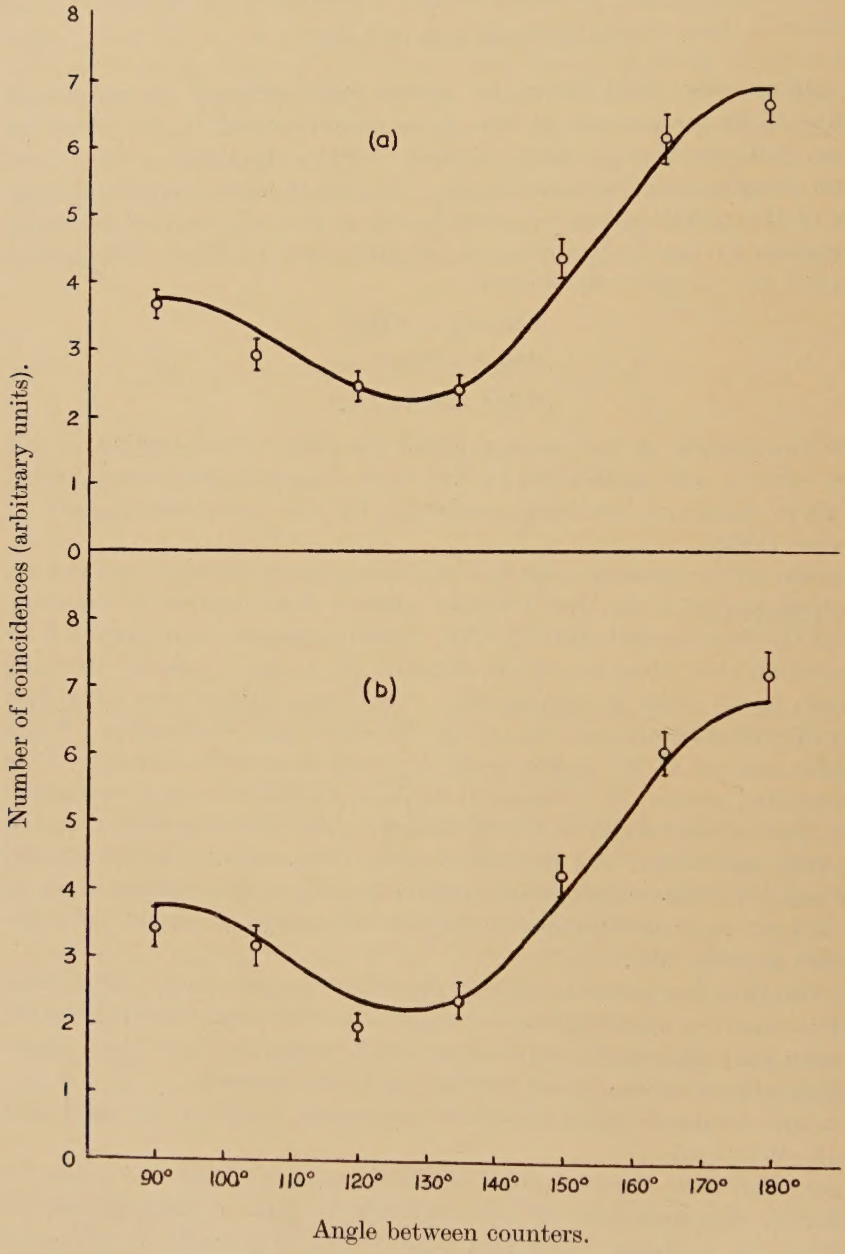

(α, γ) angular correlations in ^{23}Na(p, $\alpha\gamma$)^{20}Ne at 1255 kev: (*a*) in plane containing proton beam; (*b*) in plane perpendicular to beam.
The alpha particles were observed at 90° to the beam in each case.

momentum and parity, by finding whether or not a given ^{24}Mg state also decays by alpha particle emission to the ground state of ^{20}Ne.

A preliminary survey of resonances in the proton energy range 900–1300 kev was undertaken with the above considerations in mind, and it became clear that the 1255 kev resonance was particularly suitable for detailed study. This is a resonance at which alpha particles to the ground state of ^{20}Ne are absent, and it can therefore be assumed that the ^{24}Mg state belongs to the sequence

$$(0-),\quad (1+),\quad (2-),\quad (3+),\ldots.$$

(α, γ) correlation measurements were carried out at the 1255 kev resonance and the experimental points are shown in the figure. It is seen that the correlations in the two planes are identical within the limits of experimental error, and both contain a large $\cos^4\theta$ component. The full curves of the figure represent

$$I(\theta)=1-3\cos^2\theta+4\cos^4\theta$$

when corrected for the finite geometry of the detectors. This pattern, common to both planes, can arise only if the 1255 kev resonance is a (1+) state formed by s-wave protons, and if the ^{20}Ne excited state at 1·63 Mev is (2+). (This state would be formed by emission of d-wave alpha particles from the ^{24}Mg state, and would decay to the ^{20}Ne ground state by electric quadrupole radiation.)

The (2+) assignment to the first excited level of ^{20}Ne is the same as that found for the first excited states of most other even–even nuclei. The assignment is also predicted by the alpha particle model (Teller and Wheeler 1938), in which the ^{20}Ne nucleus is regarded as an assembly of five alpha groups, one at each corner of a trigonal bipyramid.

The result of the experiment is of relevance to the radiative capture process occurring at 669 kev in the ^{19}F+p reaction. It is known that the gamma radiation cascades via the first excited state of ^{20}Ne rather than occurring directly to the ground state (Rae *et al.* 1950, Carver and Wilkinson 1951, Jones and Wilkinson 1952). Since the 669 kev resonance is known to be (1+) (Seed and French 1952 a), the competition must be between magnetic dipole radiation and a mixture of magnetic dipole and electric quadrupole radiation, and the absence of the former transition remains yet to be explained.

I am indebted to Mr. E. S. Shire for the use of the Van de Graaff generator for this work, to Dr. A. P. French for helpful discussion, and to Mr. G. Dearnaley for assistance in the early stages of the experiments. I am also indebted to the Department of Scientific and Industrial Research for a Senior Research Award.

References

Burling, R. L., 1941, *Phys. Rev.*, **60,** 340.
Carver, J. H., and Wilkinson, D. H., 1951, *Proc. Phys. Soc.* A, **64,** 199.
Curran, S. C., and Strothers, J. E., 1939, *Proc Roy. Soc.* A, **172,** 72.
Donahue, D. J., 1952 (see Ajzenberg and Lauritsen, 1952, *Rev. Mod. Phys.*, **24,** 393).

Freeman, J. M., 1951, private communication.
Jones, G. A., and Wilkinson, D. H., 1952, *Proc. Phys. Soc.* A, **65**, 1055.
Rae, E. R., Rutherglen, J. G., and Smith, R. D., 1950, *Proc. Phys. Soc.* A, **63**, 775.
Seed, J., and French, A. P., 1952 a, *Phys. Rev.*, **88**, 1007 ; 1952 b, *Phil. Mag.*, **43**, 1214.
Stelson, P. H., Preston, W. M., and Goodman, C., 1952, *Phys. Rev.*, **86**, 629.
Teller, E., and Wheeler, J. A., 1938, *Phys. Rev.*, **53**, 778.

XCVII. *Notices of New Books and Periodicals received*

Elements of Nuclear Reactor Theory. By S. Glasstone and M. C. Edlund. (London: Macmillan and Co., Ltd.) [Pp. 416.] Price 35*s*.

A lucid introduction to the theory of nuclear reactors is indeed welcome. This book will serve an invaluable purpose as part of the training of physicists and engineers who plan to enter the expanding field of reactor design and operation. It begins with four chapters dealing briefly with the basic physical processes : although there are minor inaccuracies, these chapters give the newcomer enough background material to enable him to follow the book without further reference. The main part of the book is devoted to the diffusion of neutrons and the continuous slowing down model. These theories are applied to many standard problems such as the homogeneous reactor with and without reflector, and the heterogeneous reactor. There are excellent chapters on time-dependent solutions and reactor control. The book ends with a brief account of perturbation theory and an investigation of the validity of the diffusion approximation from the point of view of transport theory. The mathematical treatment is always elementary, if sometimes involved (as in the chapter on heterogeneous systems, for example). Unfortunately, presentation is sometimes obscured by a curious habit of stating what approximations are involved only at the end of a calculation, so throwing the reader into unnecessary confusion. A most valuable part of the work is the collection of realistic and useful examples presented to the reader for solution. B. H. F.

Reports on Progress in Physics, Vol. XVI. Executive Editor A. C. Stickland. (London : The Physical Society, 1953.) Price (to non-Fellows) £2 10*s*. 0*d*.

The Council of the Physical Society is to be congratulated on its continued success in persuading scientists, outstanding in their own fields, to write reviews about the subjects in which they are expert. Such reviews are extraordinarily useful, and are really the only way in which a research worker can find his way about those subjects on which he is not working himself. Among so many excellent articles it seems invidious to pick any out ; but the present reviewer was particularly interested in McCrea's article on Cosmology, with its impartial description of rival theories, and in the article by G. E. Bacon and Kathleen Lonsdale on Neutron Diffraction, which gives for the first time a comprehensive account of the results achieved with this technique, especially in the field of magnetism. The volume ends with an authoritative account by Rochester and Butler, of the University of Manchester, of the new unstable particles found in the Cosmic Rays. N. F. M.

[*The Editors do not hold themselves responsible for the views expressed by their correspondents.*]